Technische Universität München

Fakultät für Medizin

Hypercaloric diet induces a molecular, spatial, and transient rearrangement of astrocytes in the arcuate nucleus of the hypothalamus

Luiza Maria Lutomska

Vollständiger Abdruck der von der Fakultät für Medizin der Technischen Universität München zur Erlangung des akademischen Grades einer Doktorin der Naturwissenschaften genehmigten Dissertation.

Vorsitz: Prof. Dr. Mikael Simons

Prüfer*innen der Dissertation: 1. Prof. Dr. Paul Th. Pfluger

2. Prof. Dr. Jovica Ninkovic

Die Dissertation wurde am **15.06.2022** bei der Technischen Universität München eingereicht und durch die Fakultät für Medizin am **03.01.2023** angenommen.

Abstract

Hypothalamic astrocytes have recently emerged as a specialized glial cell population in the neuroendocrine control of metabolism, particularly affected in diet-induced obesity. Therefore, I here investigated their distinctive molecular responses over other brain region-derived astrocyte sources, as well as their individual and spatial alterations in the arcuate nucleus of the hypothalamus (ARC), following the exposure to a high-fat high-sugar (HFHS) diet. Using bulk-RNA sequencing and proteomic studies, I here showed that astrocytes are strongly influenced by their anatomical origin, which encodes HFHS diet-induced transcriptomic modifications, with a major proteomic switch in hypothalamic astrocytes. By sequencing ARC RNA at a single-cell resolution, I observed that astrocytes represent the cell type with the most affected transcriptomic response to a HFHS diet, compared to neurons and other ARC cells. Furthermore, astrocytes expressing Glial Fibrillary Acidic Protein (GFAP) and Aldehyde Dehydrogenase 1 Family Member L1 (Aldh1L1) increase in their number, and change their spatial distribution in the ARC in response to a HFHS diet. Finally, I revealed that calcium signaling and astrocyte-specific Sonic Hedgehog (Shh) molecular pathway play a role in the HFHS diet-induced increased number of GFAP positive cells within the ARC, as well as in the short-term body weight gain. Overall, these results highlight region-dependent molecular distinctions of hypothalamic astrocytes in response to a HFHS diet, which might define their selective vulnerability and contribution to the development of diet-induced obesity.

Zusammenfassung

Astrozyten des Hypothalamus sind besonders betroffen bei Diät-induziertem Adipositas und ihre Relevanz als speziallisierte Glia Population für die neuroendokrine Kontrolle des Stoffwechsels wird zunehmend erkannt. Daher habe ich ihre charakteristischen molekularen Antworten im Vergleich mit Astrozyten aus anderen Hirnregionen, sowie ihre individuellen und regionsspezifischen Veränderungen im Nucleus arcuatus des Hypothalamus (ARC) nach Immission einer Hochfett-Hochzucker (HFHZ) Diät untersucht. Mit Hilfe von Standard RNA Sequenzierung und Proteom Studien habe ich dargestellt, dass Astrozyten stark von ihrem anatomischen Ursprung beeinflusst sind, der ihre HFHZ Diät induzierten Modifikationen des Transkriptoms definiert und in hypothalamischen Astrozyten mit einem Umbau des Proteoms einher geht. Durch die Sequenzierung von RNA aus dem ARC auf Einzel-Zell Ebene konnte ich feststellen, dass Astrozyten, im Verglich zu anderen Zelltypen wie Neuronen und anderen ARC Zellen, die stärkste transkriptionelle Antwort auf die HFHZ Diät zeigen. Außerdem erhöht sich die Zahl an Glial Fibrillary Acidic Protein (GFAP) und Aldehyde Dehydrogenase 1 Family Member L1 (Aldh1L1) exprimierenden Astrozyten und ihre regionale Verteilung im ARC ändert sich. Zuletzt habe ich aufgedeckt, dass astrozytäre Calcium Signale und ein Astrozyten-spezifischer Sonic Hedgehog (Shh) Molekularweg bei der durch die HFHZ-Diät induzierte Erhöhung der GFAP positiven Zellen im ARC und einem kurzfristigen Körpergewichtszuwachs eine Rolle spielt. Zusammengefasst unterstreichen diese Ergebnisse die regionsabhängigen molekularen Charakteristika von hypothalamischen Astrozyten als Antwort auf eine HFHZ Diät, was ihre selektive Verletzbarkeit und ihren Beitrag zur Entwicklung von Diät-induziertem Adipositas bestimmen könnte.

Table of Contents

1. Introduction

1.1. Astrocytes: a heterogeneous population in the brain

1.1.1. Discovery and initial classification of glial cells

The discovery of the existence of glial cells starts in 1846, when Rudolf Virchow used for the first time the term "neuroglia" to name the connective tissue he observed to embed the neural elements of the brain (Virchow, 1846). Its role was thought to be merely structural, a "cement" in the brain holding the functionally relevant "nerve" together. Between the end of the 19th century and the beginning of the 20th century, Otto Deiters (Deiters and Schultze, 1865), Gustaf Retzius (Retzius, 1894; Savtchouk and Volterra, 2018; Srinivasan *et al.*, 2015), Camillo Golgi (Golgi, 1903), and others started to classify glia diversity depending on their form and size. The first glia classification was established by Albert Kölliker (Kölliker and Ebner, 1889; Rakers and Petzold, 2017; Petravicz, Boyt and McCarthy, 2014) and William Lloyd Andriezen (Andriezen, 1893), who divided those cells in "fibrous glia" and "protoplasmic glia" based on their morphology features. In 1893, Michael von Lenhossék described a subtype of neuroglial cell characterized by a star-like shape, and named as "astrocyte" (Lenhossék, 1893). This term was successively used by Ramón y Cajal to refer to both fibrous and protoplasmic glia (Ramón y Cajal, 1909) until he developed the sublimated gold chloride staining (y Cajal, 1913) to visualize both astrocytic types. This technique allowed Ramón y Cajal to confirm Golgi's previous observations, revealing the intimate association of astrocytes with blood vessels and neurons in the brain. The following years were characterized by a meaningful technological progress in the brain study, but only neuronal research benefited from it, while glial cells were considered less relevant and thus essentially ignored. Despite Ramon y Cajal pioneered several studies, most of the research was focused on solely examining the role of neurons for understanding brain physiology and function, while the study of glial cells remained in the shadows for many years. In the last past decades, the simplistic "neurocentric" view gradually disappeared in favor of a concept where neuronal and non-neuronal cells (astrocytes, tanycytes, oligodendrocytes, endothelial cells, pericytes, microglia) connect together forming fully integrated functional circuits for the homeostatic regulation of brain function (Garcia-Caceres *et al.*, 2019).

1.1.2. Origin and anatomical organization of astrocytes in healthy brain

Astrocytes are specialized glial cells with an ectodermal, neuroepithelial origin. During brain development astrocytes are generated -astrogliogenesis- from radial glial cells in the neonatal ventricular wall (Kriegstein and Alvarez-Buylla, 2009). In particular, the asymmetric division of radial glia occurs during early embryogenesis, producing specific intermediate progenitors which ultimately differentiate to diverse cell types including astrocytes, neurons, and oligodendrocytes (Ge *et al.*, 2012). Interestingly, a consistent part of astrogliogenesis continues in the early postnatal stage, where astrocytes derive directly from radial glial cells, or from proliferation of differentiated astrocytes, or from NG2 glial cells (Nishiyama *et al.*, 2016). This intricate and not fully understood process is thought to reside the foundations of astrocyte heterogeneity. In a healthy brain, astrocytes form functional domains in a non-overlapping manner, with only the very distal processes weaved together with one another (Ogata and Kosaka, 2002). Therefore, astrocyte arrangement in the brain appears to be exquisitely regulated and organized, and dictated by a finely-tuned distancing among them (Chan-Ling and Stone, 1991). Interestingly, it has been reported that the branched processes from a single astrocyte in the hippocampus and in the cortex can contact 100,000 or more synapses derived from multiple neurons in mice (Halassa *et al.*, 2007), which support that these glial cells regulate the exchange and processing of a big amount of synaptic information.

1.1.3. The diversity of astrocyte morphology

As mentioned above, astrocytes have been initially divided into two main subtypes: protoplasmic and fibrous. This distinction was based on the astrocyte diversity depending on their morphology and anatomical distribution (Sofroniew and Vinters, 2010; Ramón y Cajal, 1909). Particularly, the pioneer studies on protoplasmic astrocytes indicated that they were primarily observed in the grey matter, and characterized by short and highly branched fine processes, while fibrous astrocytes were mainly found in the white matter and exhibited many long poor-branched fiber-like extensions (Ramón y Cajal, 1909). Such morphological differences between subtypes were thought to be correlated with the functions of the diverse brain areas (Miller and Raff, 1984; Chaboub and Deneen, 2012; Oberheim, Goldman and Nedergaard, 2012). Indeed, protoplasmic astrocytes are considered the ones to form the "neurovascular unit" together with neurons and endothelial cells, while the function of fibrous astrocytes is less clear, suggesting to be related to the myelination process (Miller and Raff, 1984). Moreover, these two subsets of astrocytes also differ in the expression of specific

molecular markers, with protoplasmic astrocytes expressing mostly (but not exclusively) calcium binding proteins, such as S100β, whereas fibrous astrocytes express high levels of glial fibrillary acidic protein (GFAP) (Miller and Raff, 1984; Aberg and Kozlova, 2000; Chaboub and Deneen, 2012). These differences are thought to derive from local adaptations to the surrounding environment and thus to a region-specific functional heterogeneity. Accordingly, the existence of diverse astrocytic phenotypes also seems to be partly linked to the migration of astroglial precursors from a specific ventricular zone position into different brain compartments, where they acquire regional specificity and help to coordinate neural circuit refinements (Tsai *et al.*, 2012; Molofsky *et al.*, 2014). As matter of fact, astrocytes exhibit not only an inter-regional, but also an intra-regional diversity (Ben Haim and Rowitch, 2017; Yang and Jackson, 2019). In the hippocampus, different shapes of protoplasmic astrocytes have been found, such as spherical, fusiform and elongated (Bushong *et al.*, 2002), and two different subtypes of astrocytes based on the presence or absence of glutamate receptors and/or transporters (Matthias *et al.*, 2003). The same is observed for fibrous astrocytes, which have been divided into longitudinal, random and transverse, based on the orientation of their processes in the optic nerve (Butt *et al.*, 1994). However, the new advances in single cell (sc) RNA sequencing have revealed more extensive molecular heterogeneity in astrocytes than described in this initial poorly characterized classification, which considered morphology- and function-based subtypes of astrocytes, that was obsolete and underdeveloped. We know now that astrocytes are highly diverse depending on morphology, anatomical distribution, microenvironment embedding, and developmental stage (Barres, 2008). Emerging studies have shown that astrocytes possess regional and subregional molecular and functional distinctions (Köhler, Winkler and Hirrlinger, 2021; Matias, Morgado and Gomes, 2019).

1.1.4. Identification of astrocytes by specific molecular markers

One of the biggest challenges in astrocyte research is the full visualization and identification of these glial cells, not only because of their high morphological heterogeneity, but also because of the absence of a universal marker. Over the years, the gradual technological advancements in molecular biology have allowed the identification of several astrocyte-specific molecular markers, highlighting between them:

(a) Glial fibrillary acidic protein (GFAP): Hitherto, the most common marker for immunochemical identification of astrocytes, which belongs to a family of intermediate filaments, important to maintain the structure of the astrocyte cytoskeleton (Pekny and Pekna, 2004). The limitation of this marker consists in the fact that it is not expressed in

immunostaining detectable levels in many mature astrocytes in the healthy Central Nervous System (CNS) (Walz and Lang, 1998). Furthermore, the classical GFAP immunohistochemistry only labels the primary processes of an astrocyte, which leads to underestimate the complete astrocytic territory and branching. However, it represents a very reliable marker to label reactive astrocytes, thus it is typically considered a hallmark of healing processes and neurodegeneration (Eng and Ghirnikar, 1994).

(b) S100β glycoprotein: Ca^{2+}-binding protein, involved in the regulation of cell proliferation, differentiation, apoptosis, and energy metabolism through the interaction with several target proteins (Donato *et al.*, 2013). Such as GFAP, S100β expression increases in response to pathological conditions (Gonçalves, Leite and Nardin, 2008), and it seems to participate in the process which leads to activate astrocytes in response to brain injuries (Brozzi *et al.*, 2009).

(c) Glutamine Synthetase (GS): Similarly to S100β, GS has been found to be expressed in a higher number of astrocytes than GFAP, and thus considered as the most comprehensive astrocyte marker known so far (Anlauf and Derouiche, 2013). GS plays an important role in the physiology of the CNS, as it converts the excitotoxic glutamate into glutamine in the cytoplasm of astrocytes (Norenberg and Martinez-Hernandez, 1979). Abnormalities in this enzyme function have been associated to neurological disorders, such as epilepsy (Coulter and Steinhäuser, 2015).

(d) Glutamate Transporters: described to be involved in the glutamate turnover in the CNS. They are glutamate/aspartate transporter (**GLAST**) and glutamate transporter 1 (**GLT-1**) (Williams *et al.*, 2005; Parpura *et al.*, 2012; Schousboe *et al.*, 2014) which are used by astrocytes to protect the brain from a neuronal over-excitation damage induced by aberrant high glutamate levels. One of the main differences between those transporters relies on the rate of the glutamate turnover, with GLT-1 being considered more efficient than GLAST (Arriza *et al.*, 1994). The critical role of those transporters is supported by the fact that the lack of both of them induces severe neurological effects followed by the death of animals (Rothstein *et al.*, 1996; Matsugami *et al.*, 2006).

(e) Aldehyde Dehydrogenase 1 family member L1 (Aldh1L1): Folate enzyme identified by transcriptional profiling (Cahoy *et al.*, 2008) involved in many important processes, such as *de novo* nucleotide biosynthesis, with a subsequent major role in cell division and growth (Krupenko, 2009). Aldh1L1 seems to be a reliable marker for astrocytes, given its diffuse expression in both protoplasmic and fibrous subtypes, and the minor expression in other cell types. So far, very little is known about the role of this enzyme; interestingly, some studies reported that the silencing of Aldh1L1 in human cancers is correlated with an uncontrollable

cell proliferation and aggressive tumor phenotype (Chen, He and Wang, 2012) (Rodriguez *et al.*, 2008).

(f) Water Channel Aquaporin 4 (AQP4): Water channel present in both astrocytes and ependymal cells, and expressed mainly in their endfeet in contact with the cerebrospinal fluid (CSF), which suggests a role in the exchange of fluids in the brain (Hubbard *et al.*, 2015). This role was further confirmed by the observation that mice lacking AQP4 showed a significantly reduced brain edema after ischemic stroke (Manley *et al.*, 2000).

(g) Connexins (Cx): Gap junction proteins, in particular Cx30 and Cx43 have been observed to be expressed specifically by astrocytic endfeets in a regional different manner, with Cx30 being expressed especially in grey matter astrocytes, and Cx43 mainly in white matter astrocytes (Nagy *et al.*, 1999). The expression of connexins is essential to allow the establishment of an interconnected network between astrocytes, which seems to be important for the control of the synaptic plasticity, extracellular ion levels adjustment, and propagation of the calcium waves (Li, Giaume and Xiao, 2014; Lapato and Tiwari-Woodruff, 2018). Moreover, Cx30 and Cx43 expression in astrocytes have been shown to contribute to hypothalamic glucose sensing, through the transfer of glucose between astrocytes forming a connexin-based network (Allard *et al.*, 2014).

(h) SRY-Box Transcription Factor 9 (Sox9): transcription factor highly enriched in astrocytes, but also in neural progenitor cells found in neurogenic regions. Unlike all the previous markers here described, the immunolabeling of Sox9 reveals only the nuclei of astrocytes and its expression increases in reactive astrocytes during different neuropathological processes (Sun *et al.*, 2017).

For many years, the research on astrocytes was conducted by taking advantage of some of those molecular markers, but considering them basically interchangeable, with a scarce attention to the heterogeneity of their expression throughout the brain. In 1997, the first astrocyte-specific transgenic mouse model was characterized by the presence of astrocytes expressing the green fluorescent protein (GFP) under the human GFAP promoter (hGFAP) (Zhuo *et al.*, 1997). Nowadays, more and more astroglial promoters are becoming available, and different fluorescent proteins with diverse light spectra are used (Livet *et al.*, 2007). For example, astrocytic reporter mouse lines allow to selectively visualize the Cre-inducible expression of GFP in Aldh1L1-, GLAST-, or hGFAP -expressing astrocytes, which are diversely distributed throughout the brain (**Figure 1**).

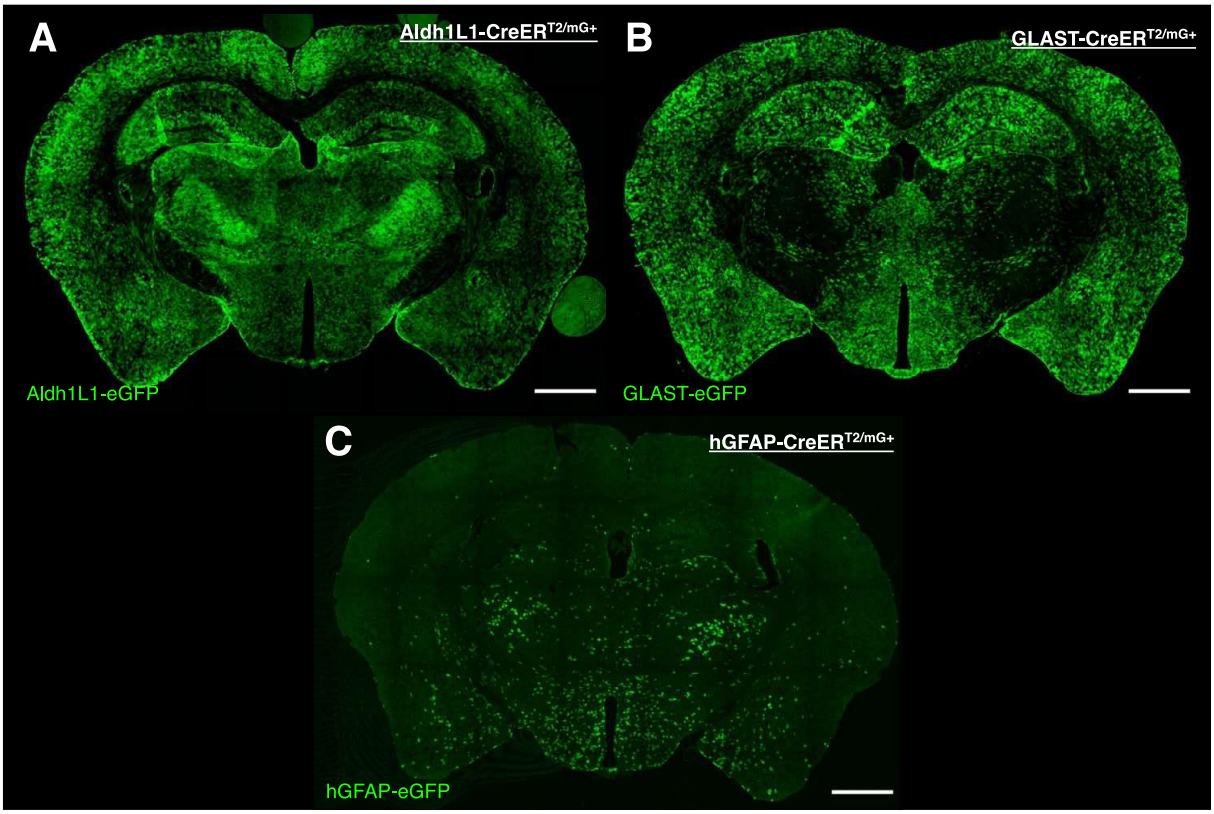

Figure 1: Coronal sections of astrocytic reporter mouse lines displaying the expression pattern of different astrocyte-specific markers. The tamoxifen-induced Cre-dependent expression of GFP in recombined cells under the Aldh1L1 (A), GLAST (B) and hGFAP (C) promoters allows the visualization of the targeted cells in coronal sections of the mouse brain. The expression pattern of these astrocyte-specific markers differs from each other, with Aldh1L1 distributed uniformly throughout the section (A), GLAST densely expressed in the majority of the section, aside from the thalamus (B), and hGFAP present particularly in the thalamus, hypothalamus, olfactory cortex, and amygdala (C). eGFP: enhanced green fluorescence protein; mG: cell membrane localized eGFP. Scale bars: 1000 µm.

These findings support the unequivocal observation of their different inter- and intra- regional expression patterns in the CNS. In particular, different molecular markers label diverse number of astrocytes, with potentially distinctive functions. Therefore, to target the function of one of those astrocyte molecular markers should not be generalized to the totality of astrocytes in the brain. Further studies, using different loss or gain of function models for targeting distinct astrocyte markers in different brain areas and combine with sorting techniques, such as fluorescent-activated cell sorting (FACS), might represent an important starting point to correctly describe the molecular signature of diverse astrocyte subtypes, but also to explore the functional meaning of such astrocytic molecular heterogeneity.

1.1.5. Astrocyte physiology: secretory cells

The concept of astrocytes as "secretory cells" has been postulated at the beginning of 1900 by Held, who observed the presence of granular inclusions in astrocyte processes, suggesting the presence of a secretory mechanism in these astrocytic compartments (Held, 1909). However, astrocytes, unlike neurons, are electrically non-excitable cells *i.e.*, do not trigger action potential firing despite the expression of voltage-gated sodium channels at the cell membrane surface (Pappalardo, Black and Waxman, 2016). They exhibit a marked potassium leak conductance predominantly established by the activity of potassium inwardly rectifying channels subtype 4.1, which sets a highly hyperpolarized resting membrane potential close to the potassium equilibrium potential, at around -80 mV, and a low membrane input resistance (Nwaobi *et al.*, 2016). Besides, astrocytes express a variety of transporters and receptors at the cell membrane surface, permitting the monitoring and response to ions, neurotransmitters, and energy-related molecules in the extracellular milieu (Verkhratsky and Nedergaard, 2018). They are capable to release signaling molecules to influence the activity of neighboring cells (Sofroniew, 2015) by increased intracellular calcium concentrations (Cornell-Bell *et al.*, 1990), a phenomenon considered the trademark of astrocyte communication (Rusakov, 2015; Volterra and Meldolesi, 2005). The astrocytic calcium activity is mediated by several pathways including the most well-known inositol triphosphate type 2 receptor (IP_3R2)-mediated signaling cascade (Verkhratsky, Rodríguez and Parpura, 2012) (more details in **Box 1**). By intracellular calcium rises, astrocytes can release molecules (ATP, GABA, glycine, glutamate) (Dowell, Johnson and Li, 2009) named as "gliotransmitters" (Araque *et al.*, 2014) via different mechanisms such as calcium-dependent SNARE-mediated vesicle exocytosis, diffusion through channels/pores, and extrusion by membrane transporters (Harada, Kamiya and Tsuboi, 2016). This process, also known as gliotransmission, have been shown to play important roles for the regulation of neurovascular tone, neuronal excitability, synaptic transmission, and behavior (Zorec *et al.*, 2012; Volterra and Meldolesi, 2005). Notably, astrocytes also form an extensive network through gap junctions, particularly comprised by connexins 30 and 43 (Rash *et al.*, 2001), thus endowing astrocytes with an intercellular communication via a continuous syncytium for the passage of ions, metabolites, and signaling molecules (Giaume *et al.*, 2010).

Box 1. Inositol triphosphate type 2 receptor (IP_3R2)

The major calcium signaling pathway in astrocytes is mediated by IP_3Rs. In particular, the stimulation of various astrocytic G-protein coupled receptors (GPCRs) by hormones, neurotransmitters, growth factors, etc., activates the phospholipase C (PLC), which in turn mediates the release of IP_3 and the release of calcium from the endoplasmic reticulum (ER) internal stores (Verkhratsky, Rodríguez and Parpura, 2012). The main IP_3R isoform highly enriched in astrocytes is IP_3R2 (Zhang *et al.*, 2014). Indeed, a transgenic mouse model lacking globally IP_3R2 has been generated (Li *et al.*, 2005), and widely used in order to investigate the importance of calcium activity in astrocytes (Petravicz, Fiacco and McCarthy, 2008; Srinivasan *et al.*, 2015; Li *et al.*, 2015a; Savtchouk and Volterra, 2018). However, the results of the different studies using $IP_3R2^{-/-}$ animals are controversial, some indicating effects on neuronal and vascular functions (Takata *et al.*, 2011; Navarrete *et al.*, 2012; Perez-Alvarez *et al.*, 2014; Verkhratsky, Rodríguez and Parpura, 2012; Mountjoy, 2015) or involvement in pathophysiological phenotypes (Kanemaru *et al.*, 2013; Saito *et al.*, 2018), and others describing a totally negative phenotype (Petravicz, Fiacco and McCarthy, 2008; Agulhon, Fiacco and McCarthy, 2010; Agulhon *et al.*, 2013; Fuccillo, Joyner and Fishell, 2006). Likewise, it is noted to mention that calcium activity in astrocytes have been also observed in $IP_3R2^{-/-}$ animals, suggesting that a calcium signaling IP_3R2-independent component exists in astrocytes, which is thought to be confined to processes, as well as the role of other IP_3R isoforms and/or different calcium storage origins (Kanemaru *et al.*, 2014; Srinivasan *et al.*, 2015; Rungta *et al.*, 2016; Bindocci *et al.*, 2017; Sherwood *et al.*, 2017).

1.1.6. The function of astrocytes in physiological conditions

For many decades, the role attributed to astrocytes was of a merely passive structural support to neurons in the CNS. However, we now know that astrocytes play a broad number of active roles in the brain, including the regulation of all biochemical and physiological processes required for a correct neuronal function. Indeed, astrocytes are often intimately associated with synapses forming an unique functional unit for the control of neuronal activity, coined as "tripartite synapse", which entails a tight connection between pre- and post-synaptic terminals and adjacent astroglial cells (Araque *et al.*, 1999). Astrocytes can be found located close to the synaptic clefts, assuring a proper neuronal transmission and function by providing signaling cues (such as ATP, lactate) to ultimately modulate the synaptic metabolism, plasticity and transmission (Piet *et al.*, 2004; Pascual *et al.*, 2005). The concept of "tripartite synapse" evolved

over time to “multipartite synapse”, as increasing evidences indicated the involvement of more cellular compartments in the regulation of the synaptic activity (Verkhratsky and Nedergaard, 2014; Verkhratsky and Nedergaard, 2016). In addition to astrocytic processes, pre-, and post-synaptic terminals, the presence of the surrounding extracellular matrix (ECM) as regulator of receptor trafficking and membrane excitability (Dityatev and Rusakov, 2011), as well as the neighboring microglial processes, as synapse pruners (Verkhratsky and Nedergaard, 2014), are involved in the fine-tuned regulation of the synapse. Likewise, other roles have been also assigned to astrocytes to maintain CNS homeostasis such as: (a) regulation of neurotransmitters turnover through their inactivation and removal from synapses (Santello and Volterra, 2009); (b) control of water fluxes through aquaporins and membrane transporters, which contributes to the regulation of the extracellular volume (Nagelhus and Ottersen, 2013); (c) ion homeostasis, essential to control signaling processes and the overall excitability, which is mediated by several astrocytic ion transporters, such as potassium and calcium channels (Walz, 2000; Rusakov and Fine, 2003); (d) removal of reactive oxygen species (ROS) derived from neuronal energy metabolism by the astrocytic antioxidant system primarily based on glutathione and ascorbic acid (Makar *et al.*, 1994). Besides, astrocyte role in the CNS is not only limited to the preservation of the functional integrity of all basic synaptic operations, but it also includes the regulation of additional important physiological processes, by interacting with other non-neuronal cells. In particular, astrocytes are involved in the control of the brain microcirculation through the interaction with endothelial cells, and, together with pericytes, constitute the “neurovascular unit” to govern the cerebral blood brain barrier (BBB) properties (*e.g.*, flow, permeability, constraints) by interacting and exchanging signaling cues with the ECM (Muoio, Persson and Sendeski, 2014). Lastly, astrocytes also cooperate with the meningeal lymphatic system for the clearance of the brain from potential neurotoxic products, as part of the so-called “glymphatic system”, which works in a similar way as the peripheral lymphatic system, and it is supported by astrocytic aquaporin channels (Iliff *et al.*, 2012). For a very detailed and complete overview on astrocyte physiology and function, refer to Verkhratsky and Nedergaard review “Physiology of astroglia” (Verkhratsky and Nedergaard, 2018).

1.1.7. The function of astrocytes in pathological conditions: reactive astrogliosis

Considering the high amount of essential functions played by astrocytes in a healthy CNS, it is not surprising the fact that their dysfunction is linked to a variety of brain pathologies. Indeed,

astrocytes undergo a dramatic transformation in response to different types of CNS injury, a mechanism recently consensually coined with "reactive astrogliosis", "astrocyte reactivity", or "reactive astrocytes" (Escartin *et al.*, 2021). This process entails morphological, molecular and/or functional changes observed in astrocytes responding to healing processes or pathophysiology (Hamby and Sofroniew, 2010). The variety of these changes differs depending on the grade and/or nature of the stimulus (Sofroniew, 2014). In general, reactive astrogliosis is referred to the acquisition of a characteristic hypertrophic phenotype, which is accompanied with proliferation in the most severe cases of brain atrophy. Notably, a hallmark of reactive astrogliosis is the upregulation of intermediate filaments GFAP and vimentin (Pekny and Pekna, 2014). Interestingly, reactive astrocytes have been reported to alter their homeostatic functions, such as calcium signaling and excitatory neurotransmitters uptake, but also to adopt a pre-inflammatory profile characterized by the production and release of inflammatory cytokines, ROS, and upregulation of AQP4 water channels (Sofroniew, 2009). Sometimes a continuum of progressive molecular and cellular alterations in astrocytes ends in the formation of a physical barrier, so-called "glial scar", as a result of severe cases of brain injuries. The glial scar is composed by local hypertrophic astrocytes which lost their classical domain organization (showing overlapping astrocytic domains), and its formation is accompanied by the ECM and the interaction with other cell types, such as fibromeningeal cells (Sofroniew and Vinters, 2010). It is still under discussion whether the formation of a glial scar and the presence of reactive astrogliosis might have a beneficial or a detrimental role. For many years, reactive astrocytes have been considered as a basically harmful element, blocking the normal functional neuronal recovery. Indeed, some evidences indicate for example that reactive astrogliosis can exacerbate inflammation (Brambilla *et al.*, 2005; Spence *et al.*, 2011) and inhibit axon regeneration (Silver and Miller, 2004). However, other studies showed that reactive astrocytosis, and in particular the glial scar formation, exhibits a neuroprotective role, by physically limiting the diffusion of inflammatory factors and preventing the extension of tissue damage (Macauley, Pekny and Sands, 2011; Wanner *et al.*, 2013). Other studies have further identified Sonic Hedgehog (Shh) signaling pathway as a mechanism involved in the initiation of brain injury-induced proliferation and reactive astrogliosis, the activation of which leads to reduce brain edema following stroke or neurodegenerative diseases (Sirko *et al.*, 2013) (see more details in **Box 2**). In 2017, Liddelow and colleagues identified two types of reactive astrocytes, named as "A1" and "A2" astrocytes, in neuroinflammation and in ischemic stroke (Liddelow *et al.*, 2017). The A1 astrocytes have been proposed to be harmful, as exhibiting high expression of many complement cascade genes known to be involved in damaging

synapses, whereas the A2 astrocytes are referred as having a neuroprotective role because of up-regulation of neurotrophic factors (Zamanian *et al.*, 2012; Liddelow *et al.*, 2017). However, this classification is not accepted by all scientific community so far. Therefore, the functional relevance of reactive astrogliosis is still unclear and it can vary depending on many factors including the type and origin of disease and its stage, as well as the health status and age of the animal. Diverse types of CNS insult are capable of inducing reactive astrogliosis, such as mechanical (*e.g.*, wound, trauma, stroke) or neurodegenerative diseases (*e.g.*, Alzheimer, Parkinson, Huntington, multiple sclerosis), and it occurs in combination with responses of multiple types of cells, including microglia, endothelial cells, neurons, and cells deriving from the blood circulation, such as platelets and leukocytes, capable of secreting molecular signals which influence surrounding astrocytes (Burda and Sofroniew, 2014). Thus, the response to CNS insults is a very complex event, which not only includes astrogliosis, but also the participation and co-interaction of multiple types of cells (Burda and Sofroniew, 2014). Thence, the interpretation of results obtained when studying reactive astrogliosis should take under consideration the presence of all those variables, which might lead to a different regulation of specific molecular pathways in reactive astrocytes with a subsequent diversity in the functional implications.

Box 2. The Shh signaling pathway

One of the molecular pathways described to be involved in brain injury-induced astrogliosis is the Shh signaling pathway (Sirko *et al.*, 2013). The Shh pathway is known to have an important role in the embryo neurodevelopment (Fuccillo, Joyner and Fishell, 2006), but it also persists in the adult life, acting in progenitor cells, neurons and astrocytes (Garcia *et al.*, 2010; Traiffort, Angot and Ruat, 2010). The signaling cascade initiates after Shh binding to and activation of the complex formed by Patched (Ptc) and Smoothened (Smo), which in turn triggers different transcription factors, such as Gli (Chen and Struhl, 1998; Kandel *et al.*, 2000). The involvement of Shh pathway in reactive astrogliosis following a brain injury became clear when the astrocyte-specific deletion of Smo blocked astrocytes from gaining a pro-proliferative profile in the site of injury (Sirko *et al.*, 2013). Moreover, Shh pathway activation in astrocytes has been linked to the reduction of brain edema following stroke or neurodegenerative diseases (Xia *et al.*, 2013; Pitter *et al.*, 2014). However, up to date, the involvement of Shh signaling pathway in astrogliosis induced by different types of neuropathological events remains unclear.

1.1.8. Inter- and intra- regional heterogeneity of astrocytes in health and disease

The astrocyte heterogeneity concept has been introduced previously above, while describing different classifications of astroglia based on their morphology and molecular markers. Furthermore, recent evidence indicate that astrocytes are characterized by extensive inter- and intra-regional differences in their developmental origin, morphology, molecular phenotype, physiology and function (Zhang and Barres, 2010; Ben Haim and Rowitch, 2017), as well as their response to brain pathology (Pestana *et al.*, 2020; Moulson *et al.*, 2021).

(a) Inter-regional heterogeneity. The introduction of the translating ribosome affinity purification (TRAP) technique was fundamental to provide the first insights into astroglia diversity. Indeed, it revealed heterogenous transcriptome in astrocytes collected from cortex, cerebellum and hypothalamus, finding substantial differences in their molecular profiles between brain areas, as well as age-related changes (Doyle *et al.*, 2008; Boisvert *et al.*, 2018). A similar study performed by Morel and colleagues based on sorted astrocytes derived from different brain regions (including thalamus, hypothalamus, hippocampus, cortex, nucleus accumbens, caudate putamen) showed that astrocytes isolated from different areas express sets of unique genes, which support again the high diversity of astrocytes within the brain (Morel *et al.*, 2017). Likewise, the transcriptome and proteome of astrocytes derived from hippocampus and striatum also revealed morphological, molecular and functional differences between them (Chai *et al.*, 2017). Specifically, they observed that striatum-derived astrocytes showed a greater size in their domain, contacting more neurons than hippocampal astrocytes, whereas a higher number of astrocytes were found interacting with excitatory synapses in the hippocampus (Chai *et al.*, 2017). Furthermore, the authors reported differences in the astrocyte physiology, as indicated by the diverse gap-junctions mediated interactions and calcium signaling mechanisms (Chai *et al.*, 2017). Consistently, Lin and colleagues described five diverse subtypes of astrocytes among the Aldh1L1-expressing cells isolated from different CNS areas, with differences in their molecular phenotype and functions (John Lin *et al.*, 2017). Particularly, they claimed that the origin of those differences resided on their capability to modulate synaptogenesis and on their contribution to human glioma onset (John Lin *et al.*, 2017).

(b) Intra-regional heterogeneity. The most extensive knowledge on astrocyte diversity within the same brain area concerns the cortex. Indeed, few recent studies demonstrated that molecular differences exist between astrocytes isolated from the upper and the deeper cortical layers, remarking genes involved in synaptogenesis and destruction (Lanjakornsiripan *et al.*, 2018;

Bayraktar *et al.*, 2020). Furthermore, the expression in the cortex of specific molecular markers is thought to define different astrocytic subpopulations, as described by Morel and colleagues, observed when they used a double astrocyte specific reporter line (GLT-1-TdTomato: Aldh1L1-eGFP) (Morel *et al.*, 2019). Specifically, they identified three diverse subtypes of cortical astrocytes, which presented differences in their location, molecular profile and physiology (Morel *et al.*, 2019). Another study based on astrocyte calcium recordings in different cortex layers showed striking differences between astrocytes located in the layer 1 and the layers 2/3 (Takata and Hirase, 2008). Molecular heterogeneity within the same brain area was also observed in the spinal cord, where unique transcripts between astrocytes sitting in the ventral or the dorsal horns were found (Molofsky *et al.*, 2014).

The concept of astrocyte heterogeneity in physiological conditions is nowadays a hot topic and drains a lot of attention from the scientific community, which invests many efforts to discover the extension and the nature of all the different astrocytic subpopulations. However, the impact of such a cellular heterogeneity in pathological states is largely unexplored. Might a particular subtype of astrocytes promote or prevent the disease pathogenesis? The characterization of specific astrocytic subtypes and their spatial localization corresponding to particular synaptic circuits might be helpful to define the functional role of such a circuitry, and to use it as potential target for new therapeutic approaches. As previously mentioned, some astrocytes can respond to brain insults with hypertrophy, GFAP up-regulation and the release of inflammatory molecules, but the functional meaning of this event is still unknown. Likewise, such particular changes in the astrocytic phenotype can vary depending on the pathology. For example, epilepsy is characterized by the down-regulation of astrocyte specific glutamate transporters (GLT-1), ion channels (Kir4.1), and water channels (AQP4), which is thought to be linked to the incorrect functioning of the glutamate and potassium reuptake at the synaptic cleft (Ohno *et al.*, 2015; Dossi, Vasile and Rouach, 2018), resulting of an exacerbation of the pathological phenotype. In ischemia, a different impact on protoplasmic and fibrous astrocytes has been reported (Lukaszevicz *et al.*, 2002; Shannon, Salter and Fern, 2007). Overall, these findings suggest the relevance of understanding astrocyte heterogeneity as a crucial step towards the development of new potential therapies for specific CNS pathologies.

1.2. Hypothalamic astrocytes

1.2.1. Hypothalamus: main integrator of nutritional and hormonal cues in the brain

The first studies of the hypothalamic involvement as core of metabolic control date back to the middle of the 20th century, when applied lesions or presence of tumors into different hypothalamic nuclei elicited severe obesity or anorexia in rodents. The lesions of the arcuate nucleus (ARC), ventromedial hypothalamic nucleus (VMH) or the paraventricular nucleus of the hypothalamus (PVN) seemed to be linked to an increased appetite (Olney, 1969; Leibowitz, Hammer and Chang, 1981); whereas the ones applied to the lateral hypothalamus (LH) or the dorsomedial hypothalamus (DMH) were associated with starvation (Mayer and Thomas, 1967; Bernardis and Bellinger, 1998). These pioneer studies demonstrated the key role of the hypothalamus in the brain's control of systemic energy homeostasis, which integrates and processes nutritional and metabolic cues emanating from the bloodstream, translating them into physiological responses regulating feeding behavior and energy expenditure (Dafny and Feldman, 1970; Schneeberger, Gomis and Claret, 2014; Timper and Brüning, 2017). However, as mentioned above, the hypothalamus is structured and organized in different nuclei with distinct specialized neurons and circuits interconnected (Luiten, ter Horst and Steffens, 1987). Among the nuclei composing the hypothalamus, the ones which deserve particular attention due to their key role in the control of metabolism include the PVN, main regulator of the autonomous nervous system (*e.g.* cardiovascular functions, thermoregulation, circadian rhythm), and coordinator of physiological responses to changes in energy balance (Ferguson, Latchford and Samson, 2008; Hill, 2012); the VMH, with an important role in the modulation of metabolic-related functions (*e.g.* body weight, food intake, glucose homeostasis), but also in sexual behavior, thermogenesis, fear response, and cardiovascular function (McClellan, Parker and Tobet, 2006; Klöckener *et al.*, 2011); the DMH, which regulates not only feeding behavior and body weight homeostasis, but also brown adipose tissue (BAT) thermoregulation, blood pressure and behavioral circadian rhythms (Chou *et al.*, 2003; Dimicco and Zaretsky, 2007; Gao and Horvath, 2008; Simonds *et al.*, 2014); the LH, key player in precise motivated behaviors, such as hedonic feeding behavior and wakeful cycles, and regulator of the autonomic nervous system (Gerashchenko and Shiromani, 2004; Seoane-Collazo *et al.*, 2015; Petrovich, 2018); and the ARC, one of the most metabolically important and intensively studied nuclei of the hypothalamus, as critical sensor and responder to feeding-related peripheral signals (see next paragraph for a more detailed description) (**Figure 2**).

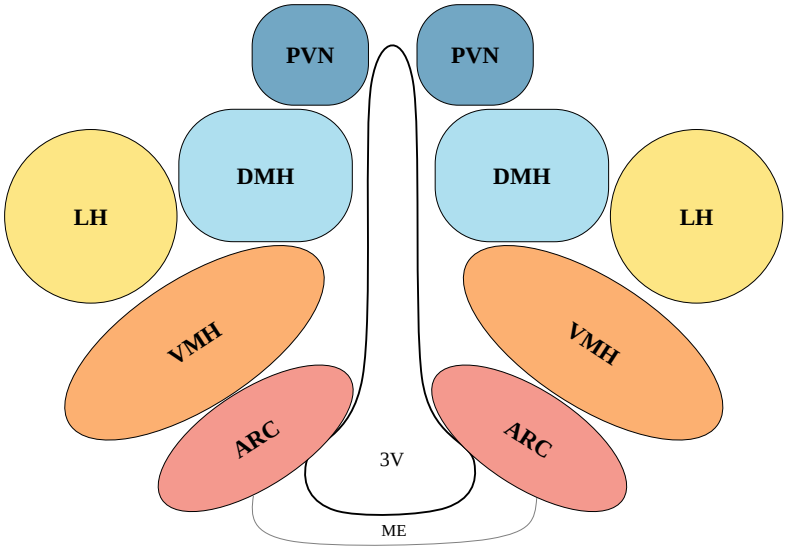

Figure 2: Schematic overview of the most metabolically relevant nuclei of the hypothalamus. The hypothalamus is composed by different nuclei located symmetrically in relation to the third ventricle (3V). ARC: arcuate nucleus of the hypothalamus; DMH: dorsomedial hypothalamus; LH: lateral hypothalamus; ME: median eminence; PVN: paraventricular nucleus of the hypothalamus; VMH: ventromedial nucleus of the hypothalamus.

1.2.2. The arcuate nucleus of the hypothalamus

The ARC is anatomically located at the ventral base of the hypothalamus adjacent to a circumventricular organ, the median eminence (ME). It is characterized by a particular angioarchitecture (*i.e.* fenestrated microvessels lacking BBB), positioning it strategically to rapidly sense and respond to circulating metabolic cues. The two most well-known functionally antagonistic neuronal populations in the control of metabolism are harbored in the ARC: the orexigenic neurons co-expressing neuropeptide Y and agouti-related protein (NPY/Agrp; hereafter indicated as Agrp neurons) (Hahn *et al.*, 1998; Krashes *et al.*, 2013), and the anorexigenic neurons co-expressing pro-opiomelanocortin and cocaine- and amphetamine-regulated transcript (POMC/CART; hereafter indicated as POMC neurons) (Elias *et al.*, 1998a; Balthasar *et al.*, 2004). These resident ARC neurons project and post-synaptically interact with neurons expressing melanocortin receptor 4 (MC4R) in the PVN ($MC4R^{PVN}$) with antagonistic effects, as part of the melanocortin system (see more details in **Box 3**). Specifically, POMC neurons activate $MC4R^{PVN}$ neurons stimulating energy expenditure and decreasing food intake, as opposed to Agrp neurons, which promotes hunger by inhibiting $MC4R^{PVN}$ neurons (Ollmann *et al.*, 1997). Moreover, Agrp neurons have been described to interact with POMC neurons to inhibit their activity by via neuropeptide Y receptor type 1 (Y1R) located on the membrane of

POMC neurons (Broberger *et al.*, 1999). The activity of these two populations of neurons is modulated by both centrally- (such as GABA, melanocortin, NPY) and peripherally- (hormone and nutritional inputs) derived stimuli, through the binding to specific receptors that they express along their membrane (Belgardt, Okamura and Brüning, 2009; Sohn, Elmquist and Williams, 2013; Paeger *et al.*, 2017; Gao and Horvath, 2007). The tight balance of these two neuronal subpopulations activity results in a fine-tuned control of food intake and energy expenditure to maintain stable body weight (**Figure 3**). Indeed, previous studies showed how abnormalities in the functioning of POMC or Agrp neurons in the ARC lead to obesity or starvation respectively (Yaswen *et al.*, 1999; Gropp *et al.*, 2005). Moreover, the optogenetic or the chemogenetic stimulation of Agrp neurons by using Designer Receptors exclusively activated by Designer Drugs (DREADD) is associated to a rapid increase in food intake and subsequent body weight gain (Alexander *et al.*, 2009; Aponte, Atasoy and Sternson, 2011; Krashes *et al.*, 2011); while POMC neurons activation with DREADD technology requires a chronic stimulus to induce suppression of food intake (Zhan *et al.*, 2013).

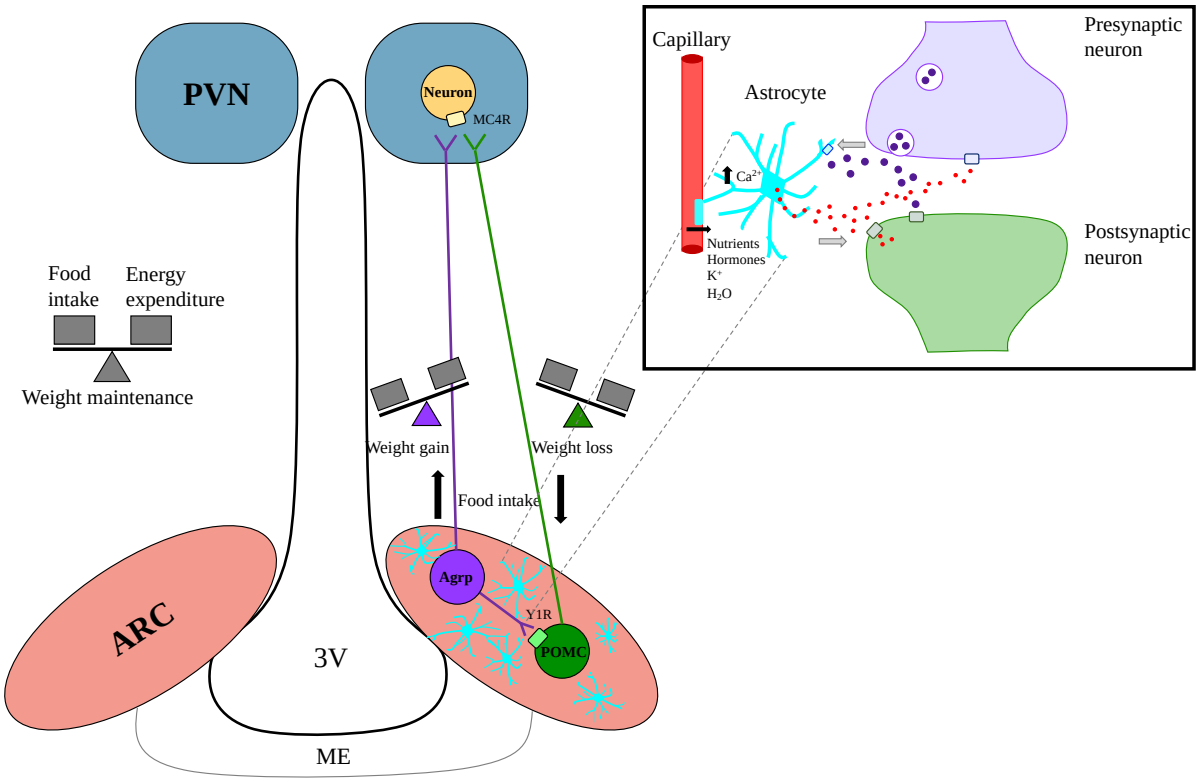

Figure 3: Schematic overview of the regulation of feeding behavior by hypothalamic ARC neurons and astrocytes. The ARC contains two major neuronal populations, the Agrp (purple) and the POMC (green) neurons, with antagonistic effects mediated by the interaction with second-order neurons (yellow) in the PVN. As represented in the upper right magnification, astrocytes (light blue) actively participate in the control of feeding behavior, by sensing nutrients and hormones from the capillaries,

neurotransmitters (violet) from the synaptic cleft, and releasing gliotransmitters (red), which in turn influence the synaptic activity. A disbalance between food intake and energy expenditure leads to the perturbation of the weight maintenance, resulting in a weight gain when the food intake exceeds the energy expenditure, and a weight loss in the opposite case. 3V: third ventricle; Agrp: Agouti-related protein; ARC: arcuate nucleus of the hypothalamus; MC4R: melanocortin receptor 4; ME: median eminence; POMC: proopiomelanocortin; PVN: paraventricular nucleus of the hypothalamus; Y1R: neuropeptide Y receptor Y1.

However, Agrp and POMC neurons represent only two of the neuronal populations sitting in the ARC. Indeed, other types of neurons have been identified in the ARC, such as tyrosine hydroxylase (TH) neurons, which activation induces an indirect increase in the food intake by stimulating Agrp neurons and inhibiting POMC neurons (Zhang and van den Pol, 2016); glutamate vesicular transporter 2 (VGluT2) neurons, which rapidly stimulates satiety (Fenselau *et al.*, 2017); kisspeptin (Kiss1) neurons, which regulate the reproductive mammalian axis, and interact with Agrp and POMC neurons (Nestor *et al.*, 2016; Padilla *et al.*, 2017). As previously mentioned, the ARC not only projects to the PVN, but also to other hypothalamic areas involved in the regulation of feeding behavior, such as DMH and LH (Elias *et al.*, 1998b; Bouret, Draper and Simerly, 2004), and extra-hypothalamic areas, such as nucleus tractus solitarius (NTS), subfornical organ (SFO), raphe nucleus (RN), and locus coeruleus (LC) (Elmquist, Elias and Saper, 1999). The correct regulation of systemic metabolism and feeding behavior is possible because of the reciprocal connection between those nuclei, some of which in turn project to the ARC (Sternson, Shepherd and Friedman, 2005; Krashes *et al.*, 2014).

Importantly, recent insights point out that the connectivity and efficiency of ARC circuits in adjusting energy balance require the cooperation of adjacent astroglial cells (Verkhratsky and Nedergaard, 2018; Garcia-Caceres *et al.*, 2019; Murat and García-Cáceres, 2021), which actively modulate the synaptic function by establishing physical interactions with the surrounding cells, and by releasing and sensing active transmitters (**Figure 3**).

Box 3. The melanocortin system

The best characterized neuronal circuit involved in the regulation of energy balance is the melanocortin system (MC), which includes neurons residing in the ARC that project to the PVN in order to regulate their activity through the release of specific neuropeptides binding to MC receptors (Cone, 2005). Melanocortins are the product of post-translational modifications of the prohormone POMC, and they act by binding to MCRs, among which MC4R isoform plays a main role in appetite regulation, and is predominantly located in the PVN, but also in the DMH and LH, areas well known for their role in controlling feeding behavior (Pritchard, Turnbull and White, 2002; Mountjoy *et al.*, 1994). MC3R is the second isoform expressed in the brain, including in the ARC, but its exact function is not completely understood, with evidences suggesting its involvement in obesity development, but not in hyperphagic behavior (Butler *et al.*, 2000). The peptides derived from POMC, such as α-, β-, and γ-melanocyte stimulating hormones (MSHs), β-endorphin, and adrenocorticotrophin (ACTH) act as natural ligands to MCRs, and their action in the brain is antagonized by Agrp (Morrison and Castro, 1997; Ollmann *et al.*, 1997; Verkhratsky, Rodríguez and Parpura, 2012; Harwell *et al.*, 2012). Therefore, a balanced action between agonists and antagonists of the MCRs is necessary to guarantee a homeostatic feeding regulation.

1.2.3. Hypothalamic astrocytes participate in energy regulation

In the last decade, increased evidences demonstrated the direct involvement of hypothalamic astrocytes in the regulation of neuronal circuits controlling energy metabolism (Zhou, 2018; Garcia-Caceres *et al.*, 2019; Chowen *et al.*, 2016). This type of response includes changes in the astrocyte morphology, in the transport of molecules, production of gliotransmitters, inflammatory signals, and growth factors, which in turn influence the surrounding microenvironment (Zhou, 2018; Garcia-Caceres *et al.*, 2019; Chowen *et al.*, 2016). In particular, the strategic location in the ARC allows to selectively control the access of circulating molecules in the brain by remodeling the local vasculature via astrocytes (Langlet, 2014; Gruber *et al.*, 2021). Moreover, the expression of specific receptors and transporters for hormones and nutrients, such as insulin (Garcia-Caceres *et al.*, 2016), leptin (Diano, Kalra and Horvath, 1998; Cheunsuang and Morris, 2005), ghrelin (Fuente-Martin *et al.*, 2016), insulin-like growth factor 1 (Cardona-Gómez, DonCarlos and Garcia-Segura, 2000), lipids (Gao et al., Diabetes 2014), glucose (Morgello *et al.*, 1995; Vannucci, Maher and Simpson, 1997) suggests

that astrocytes are capable to sense the whole-body metabolic status generating a cascade of responses to dynamically influence hypothalamic local neuronal circuitries (Pinto *et al.*, 2004; Gao *et al.*, 2007; Horvath *et al.*, 2010; Gyengesi *et al.*, 2010). Therefore, the correct signaling communication between the periphery and the hypothalamic astrocytes is essential to maintain energy homeostasis and a balanced body weight (Horvath *et al.*, 2010). Moreover, the use of DREADD in astrocytes have further demonstrated that these glial cells are key players in brain´s control of metabolism. Specifically, Yang and colleagues activated astrocytes in the medio-basal hypothalamus (MBH) and observed an anorectic-like phenotype, while astrocyte inactivation led to the opposite effect, with increased food intake (Yang, Qi and Yang, 2015). The mechanism mediating those effects has been described to be the adenosine release by astrocytes, responsible for the specific inactivation of Agrp neurons via adenosine A1 receptors binding, with consequent reduction of food intake (Yang, Qi and Yang, 2015). However, similar studies using different methodological parameters, found opposite feeding responses after DREADD-activated astrocytes in the ARC (Chen *et al.*, 2016). The reason of such a difference might rely on the fact that the synaptic activity of the hypothalamic neuronal circuitries and their connection to glial cells can be influenced by several factors, such as the age, sex and health status of the animal, the number of astrocytes targeted by DREADD, and the experimental settings. This suggests that the precise mechanisms adopted by astrocytes to control systemic metabolism need to be further investigated.

1.2.3.1. Glucose sensing

The brain is the organ with the highest glucose supply needs, requiring about 25% of the circulating glucose to maintain its physiological functions. Most brain energy is used for synaptic transmission and to maintain the right functioning of the Na/K pumps at the synaptic clefts, which allows the generation of electric potentials and the regulation of other ion types transport across the cell membrane. However, the brain glucose reservoir is limited and needs to be continuously replenished by the blood circulation. Brain microvessels are largely covered by astrocytic endfeets (Mathiisen *et al.*, 2010), that rapidly uptake glucose from the circulation, which can be metabolized to pyruvate or stored as glycogen in order to generate lactate to ultimately provide to neurons and sustain their activity in glucose deprivation conditions (Pellerin *et al.*, 1998; Chih and Roberts, 2003). Interestingly, the glucose accumulation as glycogen is a characteristic of astrocytes being essential for neurons in situations of hypoglycemia (Suh *et al.*, 2007) or high neuronal activity (Brown *et al.*, 2005). Glycogenolysis in astrocytes has also been demonstrated to be essential for learning and memory strengthening

(Drulis-Fajdasz *et al.*, 2015). It is noteworthy that cellular bioenergetics between astrocytes and neurons is different. Neurons mainly produce high ATP levels through oxidative metabolism (Boumezbeur *et al.*, 2010), while astrocytes use preferentially aerobic glycolysis to generate low quantities of ATP, but high amount of lactate (Pellerin and Magistretti, 1994; Bouzier-Sore *et al.*, 2006). The concept of lactate as essential substrate for neurons has been first introduced by Magistretti and Pellerin, who postulated the hypothesis of the so-called "Astrocyte-to-Neuron Lactate Shuttle" (ANLS) (Pellerin and Magistretti, 1994). This notion refers to the capability of neurons to use the lactate released by astrocytes in the extracellular space in a glutamate-mediated manner, after converting it to pyruvate (Pellerin and Magistretti, 1994). Furthermore, astrocytes are not only able to produce lactate via glycolysis, but they have been also reported to be capable of sensing and taking lactate up from the blood circulation, and provide it later on to neurons (Gandhi *et al.*, 2009).

The glucose sensing capability of astrocytes is mediated by the presence of glucose transporters (GLUTs), mainly GLUT -1 and -2, located at their endfeets, which cover microvessels (Morgello *et al.*, 1995; Vannucci, Maher and Simpson, 1997; Kacem *et al.*, 1998). In particular, the important role of glial GLUT-1 in mediating glucose sensing in the hypothalamus has been demonstrated by Chari and colleagues, who induced GLUT-1 overexpression specifically in hypothalamic GFAP-expressing cells of diabetic rats, observing a restoration of glucose levels in the plasma. Likewise, GLUT-2 in astrocytes has also been reported to play an important role in the regulation of systemic glucose levels, as indicated by the altered glucagon secretion in mice lacking this glucose transporter specifically in astrocytes, and restored after its re-activation (Marty *et al.*, 2005). A further proof of astrocyte involvement in whole-body glucose sensing derives from the evidence that the impairment of astrocytic network in the MBH by connexin 43 inhibition leads to a reduced hypothalamic glucose sensitivity in rats (Allard *et al.*, 2014).

1.2.3.2. Lipid sensing

Astrocytes are capable to use fatty acids, aside from glucose, to generate ATP (Auestad *et al.*, 1991). Indeed, astrocytes highly express the lipid transporter Apolipoprotein E (ApoE), which allows the entrance of lipidic substrates for successive fatty acids oxidation (Shen *et al.*, 2009). This lipid transporter has been revealed partly involved in the leptin-mediated control of food intake, acting as a satiety factor (Shen *et al.*, 2008; Shen *et al.*, 2009). Another important lipid transporter in the brain, which allows to sense and store lipids is the lipoprotein lipase (LPL), as demonstrated by Gao and colleagues, who observed a severe obese phenotype including a

marked insulin resistance in mice with a postnatal ablation of LPL specifically in astrocytes, accompanied by an accumulation of ceramides in ARC neurons (Gao *et al.*, 2017b).

1.2.3.3. Ketone bodies sensing

Astrocytes produce ketone bodies from fatty acids derived from the bloodstream, which are used by neurons as a metabolic substrate (Guzmán and Blázquez, 2004; Le Foll *et al.*, 2014). In particular, in situations of low blood glucose levels and/or excess of lipids derived from the diet, fatty acids are used by astrocytes to produce ketone bodies, which are then transported outside of the cell via the monocarboxylate transporter 1 (MCT1), and successively metabolized by the surrounding neurons to ATP and ROS (Auestad *et al.*, 1991; Le Foll *et al.*, 2014). The increase of ketone bodies production by astrocytes have been associated with an acute reduction of food intake in animals fed with a short-term high-fat diet, as the pharmacological inhibition of astrocyte-derived ketone bodies production specifically in the VMH correlated with a restored feeding behavior, in comparison to low-fat diet fed rats (Le Foll *et al.*, 2014). Therefore, astrocytes are specialized glial cells in sensing and producing lipids to regulate systemic energy metabolism.

1.2.3.4. Leptin sensing

Although most of the attention was focused on understanding the involvement of leptin-induced neuronal responses in the regulation of metabolic homeostasis, astrocytes have been described to change morphology, levels of expression of glucose and glutamate transporters (Garcia-Caceres *et al.*, 2011; Fuente-Martin *et al.*, 2012), and the ensheathment of surrounding neuronal synapses (Horvath *et al.*, 2010; Garcia-Caceres *et al.*, 2011; Kim *et al.*, 2014) in response to alterations of leptin circulating levels. One of the first studies postulating the capacity of leptin to regulate the synaptic rearrangements of the melanocortin neurons was published by Pinto and colleagues in 2004 (Pinto *et al.*, 2004). In this study, the authors observed that leptin-deficient mice exhibited alterations in the activity of Agrp and POMC neurons, which were associated with hyperphagia and obesity (Pinto *et al.*, 2004). Likewise, they reported that those mice treated with leptin showed a normalization of the synaptic density, which occurred before the leptin-mediated effects on food intake (Pinto *et al.*, 2004). Few years later, it was investigated whether astrocytes in the hypothalamus of obese mice might be also involved in the response to leptin, by using agouti viable yellow (Avy) mice, which present an adult-onset obese phenotype with the melanocortin receptors in the hypothalamus antagonized by the agouti signaling protein (Pan *et al.*, 2008; Hsuchou *et al.*, 2009; Pan *et al.*, 2011). Those studies

revealed that astrocytes may regulate the entry of leptin across the BBB through leptin receptor (LepR), which expression increases in obese animals, influencing leptin-induced calcium signaling in astrocytes (Pan *et al.*, 2008; Hsuchou *et al.*, 2009; Pan *et al.*, 2011). When astrocytic activity was inhibited, the uptake of leptin by neurons increased, demonstrating an opposite effect of leptin on neurons and astrocytes in obese mice (Pan *et al.*, 2011). Later on, it was demonstrated that astrocytes regulate the activation of POMC neurons in response to leptin, by using mice lacking LepR specifically in astrocytes (Kim *et al.*, 2014; Wang *et al.*, 2015). Moreover, the post-natal ablation of LepR from astrocytes induced a rearrangement in the interactions between astrocytes and neurons, which was accompanied with a synaptic reorganization of ARC residing neurons (Kim *et al.*, 2014). Furthermore, those mice exhibited a reduced response to leptin in inhibiting food intake; whereas exacerbated appetite in response to fasting or administration of ghrelin (Kim *et al.*, 2014). The importance of leptin signaling in astrocytes was also highlighted by Wang and colleagues, who observed an attenuated phosphorylated signal transducer and activator of transcription 3 (pSTAT3) signaling in the ARC of astrocyte-specific LepR knockout (ALKO) mice, concomitantly with the development of an obese phenotype (Wang *et al.*, 2015).

1.2.3.5. Insulin sensing

The ingestion of a carbohydrate-rich meal leads to the release of insulin from the pancreatic β-cells, which reaches peripheral tissues expressing Insulin Receptor (IR) (*i.e.* skeletal muscle, liver, adipose tissue), and where it acts balancing glucose homeostasis (Wilcox, 2005). For long time, the high expression of IR in the brain was correlated to other roles of insulin, unrelated to CNS glucose equilibrium maintenance, that was rather thought to be regulated independently from insulin (Banks, Owen and Erickson, 2012). However, the studies with mice postnatally lacking IR in astrocytes demonstrated that these glial cells regulate glucose entry into the brain via insulin signaling, which mediates the functional translocation of GLUT-1 onto the membrane (Garcia-Caceres *et al.*, 2016; Hernandez-Garzón *et al.*, 2016). Interestingly, these results were consistent when ablating IR specifically from GFAP- or from GLAST-expressing astrocytes, with both mouse models presenting perturbations in systemic glucose homeostasis and a delayed response to suppress food intake in presence of high peripheral glucose levels (Garcia-Caceres *et al.*, 2016; Cai *et al.*, 2018). Specifically, the disruption of astrocytic insulin signaling leads to alter the activation of ARC POMC neurons, which become less activated in response to elevated glucose levels (Garcia-Caceres *et al.*, 2016). This study provided the evidence that brain glucose homeostasis requires insulin astrocytic-mediated mechanisms.

1.3. Hypothalamic astrocytes in obesity

1.3.1. Obesity: a concerning modern epidemic

Nowadays the world is facing an incredibly fast rise in the incidence of obesity and related pathologies, which represents one of the biggest health care emergencies (Hales *et al.*, 2017). Over the last 45 years, the worldwide obesity incidence has nearly tripled, counting more than 39% of the adult global population overweight, and 13% obese in 2016 (WHO Obesity and Overweight, April 2020; https://www.who.int/news-room/fact-sheets/detail/obesity-and-overweight). Obesity arises when energy intake and energy expenditure are unbalanced, with a subsequent excessive accumulation of fat in the body. A dangerous consequence of obesity is the establishment of comorbidities caused by the impairment in systemic glucose and lipid metabolism, such as cardiovascular diseases, musculoskeletal disorders, cancer, and type 2 diabetes, which defines obesity as one of the major leading causes of death (Khaodhiar, McCowen and Blackburn, 1999). The onset of obesity can have genetic or environmental basis (Ravussin and Bogardus, 2000). Several genes involved in the monogenic and polygenic onset of obesity have been identified. The monogenic obesity is characterized by the presence of single nucleotide polymorphisms (SNPs) on specific genes involved in endocrine signaling and feeding behavior regulation, such as MC4R, leptin and LepR (Pigeyre *et al.*, 2016). The polygenic obesity instead relies on the presence of several modified genes, which alone would not produce any phenotype, but together cause the disease (Hinney and Hebebrand, 2008). However, environmental factors contribute in a higher extent to the origin of obesity cases, with cultural, socio-economic, psychological factors playing an important role (Wakefield, 2004). In particular, the positive energy balance leading to obesity can derive from the adoption of a more sedentary lifestyle, and the preference to consume affordable meals dense with calories (fast food, highly processed food) (Lee, Cardel and Donahoo, 2000). Obesity negatively affects not only the individual afflicted, but also the national healthcare system, which explains the urge of deeply unraveling obesity pathogenesis, and of developing new anti-obesity drugs. Despite the discovery of leptin (Zhang *et al.*, 1994) allowed great progresses in the obesity research field, the pathogenesis of this multifactorial disease is still unclear, and it might be partly due to the focus on targeting the classically described endocrine axes over a model of hypothalamic control.

1.3.2. Obesity: a brain disease

An important work published in *Nature* in 2015 explored the genetic phenotype of obese patients taking advantage of genome-wide association studies (GWAS), describing a strong correlation between candidate genes and molecular pathways with a higher body mass index (BMI) (Locke *et al.*, 2015). Those studies revealed that the greatest number of genetic variations associated with obesity susceptibility and metabolism control occurs in the brain, and more particularly in the hypothalamus (Locke *et al.*, 2015). Moreover, other clinical studies showed how obesity and BMI are associated with brain atrophy and white matter integrity reduction, which might influence the cognitive functions of an individual, independently from age and disease (Ward *et al.*, 2005; Gunstad *et al.*, 2008; Verstynen *et al.*, 2012). Furthermore, magnetic resonance imaging (MRI) indicated a correlation between obese patients, neuronal abnormalities, and astrogliosis specifically in the hypothalamus (Gazdzinski *et al.*, 2008; Thaler *et al.*, 2012). Consistently with the human studies, animal models of diet-induced obesity also showed hypothalamic gliosis, alterations in neuronal activity, dysfunction of circuitries regulating the food reward system, and angiopathy (Thaler *et al.*, 2012; Yi *et al.*, 2012; Berkseth *et al.*, 2014; Shin *et al.*, 2017; Kullmann *et al.*, 2020). In particular, it was observed that the hypothalamus was one of major brain sites involved in obesity-associated abnormalities, with the impairment of resident cells affecting systemic metabolism (García-Cáceres, Yi and Tschöp, 2013; Lee *et al.*, 2020).

1.3.3. Obesogenic diet consumption promotes hypothalamic inflammation

Interestingly, some evidences indicate that the hypothalamus of rodents exposed to an hypercaloric diet are characterized by an increase in inflammatory markers (De Souza *et al.*, 2005), similarly to what previously found in peripheral tissues, such as adipose tissue (Hotamisligil *et al.*, 1995) and liver (Park *et al.*, 2010). The mechanisms underlying high fat high sugar (HFHS) diet-induced central and peripheral inflammation were found to be similar, with the activation of inflammatory signaling intermediates: c-Jun N-terminal kinase (JNK), IkB kinase (IKK), and nuclear factor-kB (NF-kB), responsible for the production of several interleukins, and the inhibition of insulin and leptin pathways (De Souza *et al.*, 2005; Zhang *et al.*, 2008). Such a reduction in central hormone sensitivity is crucial for the development of obesity, in particular the insensitivity to leptin and insulin, that leads to an impaired energy balance (Zhang *et al.*, 2008). For this reason, hypothalamic and systemic inflammation have been highlighted as key events in the pathogenesis of obesity, although it is still unclear whether they play a role in promoting obesity, or they are a secondary phenomenon in the development

of obesity. Interestingly, some studies suggest that one single day of a HFHS feeding is enough to observe an increase in inflammatory markers and leptin resistance in the hypothalamus (Münzberg, Flier and Bjørbaek, 2004; Thaler *et al.*, 2012), and that the latter can be restored when using animals lacking the Toll-like Receptor (TLR) adaptor molecule MyD88 in the CNS, which are characterized by the impairment of the TLR4-mediated inflammatory pathway (Kleinridders *et al.*, 2009). Notably, such alterations in hormonal sensitivity occur prior to peripheral inflammation and significant body weight gain (De Souza *et al.*, 2005; Velloso, Araújo and de Souza, 2008; Thaler *et al.*, 2012). These observations support that hypothalamic inflammatory related patho-mechanisms might represent a main driver in obesity pathogenesis rather than a consequence. The initiation of HFHS diet-induced inflammatory process has been suggested to derive from the accumulation of different fatty acids species in the hypothalamus (Borg *et al.*, 2012). This hypothesis has been further confirmed by studies using acute intracerebroventricular (icv) infusion of lipids in the MBH, which demonstrated an increase in pro-inflammatory signals (Cheng *et al.*, 2015a; Cheng *et al.*, 2015b), endoplasmic reticulum (ER) stress (Zhang *et al.*, 2008), and apoptotic signals (Moraes *et al.*, 2009), with a concomitant insulin and leptin resistance (Posey *et al.*, 2009; Kleinridders *et al.*, 2009). Furthermore, dietary lipids might not be the only nutrient elements inducing hypothalamic inflammation, as the same result has been found in response to fructose-rich diets (Li *et al.*, 2015b), suggesting that the composition of diet is crucial for the development of an inflammatory environment in the hypothalamus. The fatty acids derived from the diet have been observed to be responsible for the activation of the IKK/NF-kB pathway upstream molecule TLR4 (Hayden and Ghosh, 2008), leading to the expression of several inflammatory cytokines, like TNFα, interleukins (ILs) -1β and -6 (Sartorius *et al.*, 2012; Milanski *et al.*, 2012) and to ER stress induction (Milanski *et al.*, 2009) in the hypothalamus. The stimulation of these pathways is thought to trigger the expression of a suppressant of insulin and leptin signaling, known as suppressor of cytokine signaling (SOCS)-3 (Zhang *et al.*, 2008), partially responsible for the resistance onset to these anorexic hormones (Howard *et al.*, 2004; Mori *et al.*, 2004).

1.3.4. Glial cells: main mediators of hypothalamic dysfunction associated with hypercaloric diet

CNS resident glial cells have been identified as the primary responders to a HFHS diet, and the main mediators of hypothalamic dysfunction associated with obesity, after several studies excluded the hypothesis that the first responders were circulating macrophages migrating into the brain in response to a HFHS diet (Yang *et al.*, 2013; Buckman *et al.*, 2014; Valdearcos *et*

al., 2014). Indeed, it has been observed that hypercaloric diet consumption induces reactive gliosis in the hypothalamus (Thaler *et al.*, 2012; Buckman *et al.*, 2013; Valdearcos *et al.*, 2014; Horvath *et al.*, 2010) (**Figure 4**).

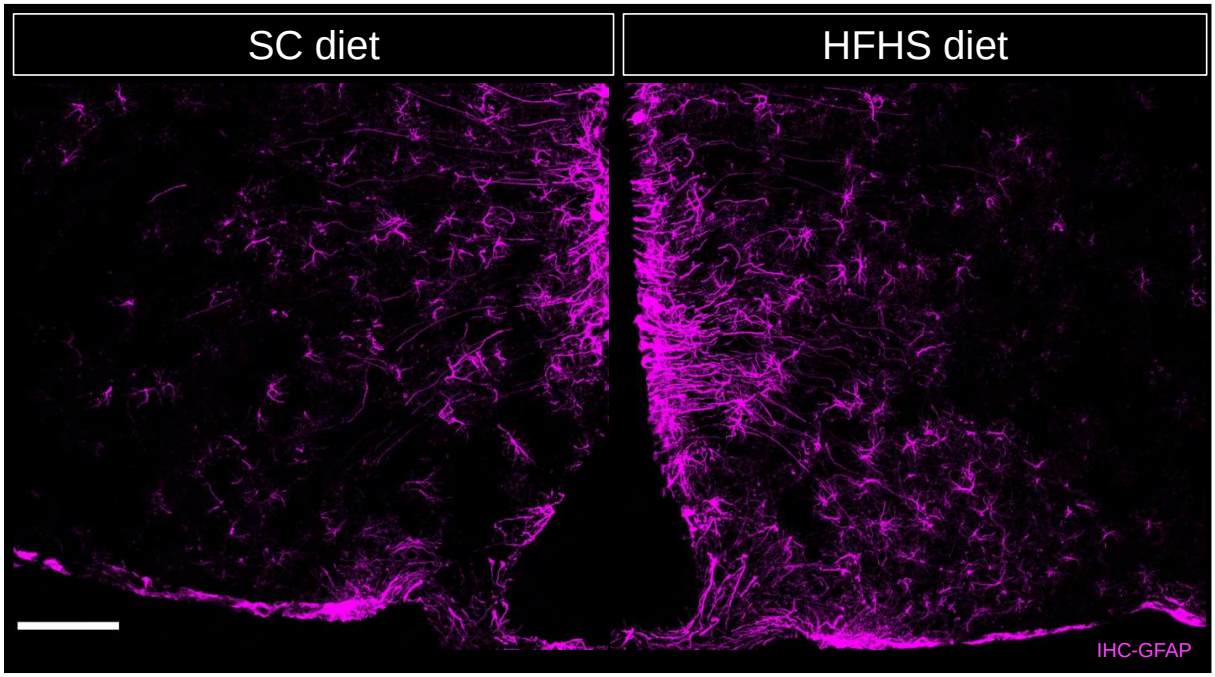

Figure 4: Representative images of astrogliosis in the MBH induced by 4 months HFHS diet feeding. Hypercaloric diet consumption induces an upregulation in GFAP immunolabeling (magenta) in the hypothalamus. In response to a HFHS diet exposure for four months, astrocytes exhibit an upregulation of GFAP, as well as a hypertrophic phenotype, features possible to visualize by using an antibody against the endogenous mouse GFAP. HFHS: high-fat high-sugar; IHC: immunohistochemistry; SC: standard chow. Scale bar: 100 µm.

Interestingly, HFHS diet-induced gliosis has a very early onset, as it can be found in the hypothalamus after only one day of an hypercaloric feeding, together with an increase in cytokines production, (Thaler *et al.*, 2012), and it persists after a long-term HFHS diet consumption (Thaler *et al.*, 2012; Valdearcos *et al.*, 2014). Interestingly, Berkseth and colleagues reported that HFHS diet-induced gliosis was largely reversible in the ARC of mice whose diet was switched back to chow, after being fed with a HFHS diet for 16 weeks; indeed, feeding those animals with chow diet in the 4 following weeks was sufficient to normalize their body weight, adiposity, and hypothalamic gliosis (Berkseth *et al.*, 2014). HFHS diet-induced astrogliosis correlates with endothelial and neuronal dysfunctions, resulting in an aberrant synaptic organization of hypothalamic circuits (Horvath *et al.*, 2010), which is associated with a late reduction in the number POMC neurons (Thaler *et al.*, 2012). Those findings highlight the importance of the HFHS diet-induced rapid response of glial cells, particularly astrocytes,

of the surrounding environment and the neuronal circuits, and the strong correlation with hypothalamic dysfunction promoted by an hypercaloric diet consumption.

1.3.5. Mechanisms involved in HFHS diet-induced hypothalamic astrogliosis

As previously mentioned, the hypercaloric diet-induced activation of the IKK/NF-kB pathway has been identified as one of the main mechanisms involved in hypothalamic dysfunction associated with the pathogenesis of obesity. In fact, several studies have been focused on the manipulation of this pathway, particularly in astrocytes, in order to understand its functional contribution to the development of hypothalamic inflammation and obese phenotype (Buckman *et al.*, 2015; Douglass *et al.*, 2017; Zhang *et al.*, 2017). Studies from Buckman and colleagues reported that hypothalamic HFHS diet-induced astrogliosis can be prevented by genetically blocking the NF-kB signaling specifically in GFAP-expressing astrocytes, resulting in an acute increase of food intake within the first 24 hours of a HFHS diet consumption (Buckman *et al.*, 2015). Furthermore, another similar study reported that astrocytes might be involved in the HFHS diet-induced chronic metabolic impairment via activation of the NF-kB pathway as well (Douglass *et al.*, 2017). Indeed, the authors could observe an attenuated hypothalamic astrogliosis, together with reduced food intake, body weight gain and improved glucose homeostasis in 6 weeks HFHS diet-fed mice, when the NF-kB signaling was genetically ablated in GFAP-expressing astrocytes (Douglass *et al.*, 2017). This observation was further supported by Zhang and colleagues, who found an increase in food intake and body weight gain when mice with a genetically overactivated NF-kB signaling in GFAP-expressing astrocytes were exposed to a HFHS diet (Zhang *et al.*, 2017). Other signaling pathways (STAT3, AKT and JNK signaling cascades) in astrocytes have been associated with astrogliosis and obesity; however, their direct involvement in diet-induced obesity is so far poorly understood.

1.3.6. Does obesogenic diet directly affect hypothalamic astrocytes?

Some studies indicate that the fast changes in the morphological, molecular and functional features of glial cells derive from the direct effect of specific components of the diet (Gao *et al.*, 2014; Gupta *et al.*, 2012; Gao *et al.*, 2017a). *In vitro* studies have reported that saturated fatty acids promote the release of inflammatory signals, such as IL-6 and TNF-α by astrocytes via the activation of TLR4 signaling (Gupta *et al.*, 2012). However, an *in vivo* study pointed out that the administration via oral gavage of saturated fatty acids in mice was not sufficient to induce astrogliosis in the MBH, where only microgliosis was observed (Valdearcos *et al.*, 2014). On the contrary, Gao and colleagues observed that the fat present in the diet was

sufficient to induce hypothalamic astrogliosis, while only the combination of dietary fat and sugar could lead to more complex pro-inflammatory aspects of hypothalamic gliosis, including microgliosis (Gao *et al.*, 2017a). This was confirmed by the loss of such pro-inflammatory effects when the animals were fed with a high-fat low-carbohydrate diet (Gao *et al.*, 2017a). Moreover, also aberrant peripheral hormone levels derived from a prolonged consumption of a HFHS diet have been observed to lead to changes in glia activity within the hypothalamus (Gao *et al.*, 2014). While obesity *per se* does not induce hypothalamic astrogliosis, as demonstrated by the absence of reactive astrogliosis in the hypothalamus of mice lacking leptin receptor (*db/db* mice) or leptin (*ob/ob* mice), which exhibit an obese phenotype on a standard chow diet, the treatment of *ob/ob* mice with exogenous leptin leads to modify the astroglia profile in parallel with a body weight loss (Gao *et al.*, 2014). Besides leptin, it was reported that the administration of ghrelin in chow fed rats induces an obese-like phenotype, with increase in the hypothalamic cytokine production, but not astrogliosis (Garcia-Caceres *et al.*, 2014). Together, all these variable outcomes suggest that hypothalamic glial cells respond differently to specific combinations of dietary nutrients (Gupta *et al.*, 2012; Gao *et al.*, 2017a), and that aberrant hormonal inputs occurring during the development of obesity might influence the HFHS diet-induced changes in the molecular profile of those cells (Garcia-Caceres *et al.*, 2011; Gao *et al.*, 2014).

Interestingly, sex has also been reported to be a determinant factor for the development of hypercaloric diet-induced hypothalamic astrogliosis and inflammation, as present in males and absent in females, when both sexes gained a significant body weight (Morselli *et al.*, 2014). Moreover, the levels of palmitic acid and pro-inflammatory cytokines (*e.g.* TNF-α, IL-6) were significantly increased in the hypothalamus of male, but not female, mice fed with an hypercaloric diet (Morselli *et al.*, 2014) The reason of such a difference might be found in the hypothalamic levels of estrogen receptor alpha (ERα), as its activation by estrogen protects females from HFHS diet-induced obesity and fatty acid-induced inflammatory responses (Morselli *et al.*, 2014; Heine *et al.*, 2000; Musatov *et al.*, 2007).

Lastly, age might also influence the onset of HFHS diet-induced astrogliosis, as the levels of GFAP expression in aged animals under physiological conditions is higher than in young ones (Lemus *et al.*, 2015). Moreover, the initial age at which animals are fed with a HFHS diet might be determinant for the development of hypothalamic gliosis, as reported by Freire-Regatillo and colleagues, who showed that juvenile, but not adult, mice put on a HFHS diet tend to be relatively resistant to the onset of hypothalamic gliosis (Freire-Regatillo *et al.*, 2020).

Therefore, considering all those evidences, many various factors may influence the molecular phenotype of hypothalamic astrocytes and their response to an hypercaloric diet, such as age, sex, and health status of the animal, the combination of diet components and hormonal inputs, as well as the condition of surrounding cells, with which astrocytes form intricated networks. For this reason, the outcomes obtained while assessing the role and the importance of HFHS diet-induced hypothalamic astrogliosis must be interpreted carefully.

2. Aim of the thesis

In the course of the thesis, I aimed to interrogate whether the molecular profile of astrocytes is determined by their anatomical distribution in the brain and/or the presence of specific astrocyte markers, such as GFAP and Aldh1L1, and to propose potential astrocytic signaling pathways mediating HFHS diet-induced GFAP up-regulation, and their impact on the body weight gain. In particular, I investigated:

(a) The inter-regional heterogeneity of astrocytes located in cortex, hypothalamus and hippocampus, in lean versus HFHS diet-obese mice, in order to understand if a HFHS diet induces specific molecular responses to the diet, depending on where astrocytes are located.

(b) The intra-regional heterogeneity of astrocytes within the ARC, with particular focus on the HFHS diet-induced effects on the molecular profile, numbers, and spatial distribution of Aldh1L1- and/or GFAP- expressing astrocytes.

(c) Potential molecular pathways that might correlate with the HFHS diet-induced GFAP up-regulation in the ARC.

3. Material and Methods

3.1. Material

3.1.1. Mouse strains and diets

Table 1: Mouse strains

Mouse strain	Strain name	Provided by:	References
Aldh1L1-CreER^{T2}	Tg(Aldh1l1-cre/ERT2)02Kan	Dr. Saher, Max Planck Institute, Göttingen	(Winchenbach *et al.*, 2016)
C57BL/6J	C57BL/6JRj	Janvier Lab, Saint-Berthevin Cedex, France	
GFAP KO	B6;129S-Gfap^{tm1Mes}	Prof. Pekny, University of Göteborg, Sweden	(Pekny *et al.*, 1995)
hGFAP-CreER^{T2}	B6.Cg-Tg(GFAP-cre/ERT2)505Fmv	Prof. Vaccarino, Yale University, Connecticut, USA	(Ganat *et al.*, 2006)
IP$_3$R2 KO	B6;Itpr2$^{tm1.1Chen}$	Prof. Araque, Cajal Institute, Madrid, Spain	(Li *et al.*, 2005) (Petravicz, Fiacco and McCarthy, 2008)
Smo$^{fl/fl}$	Smo^{tm2Amc}/J	Jackson Laboratory, Bar Harbor, ME, USA	(Long *et al.*, 2001)
Sun1-sfGFP	B6;129-Gt(ROSA)26Sor$^{tm5(CAGSun1/sfGFP)Nat}$/J	Jackson Laboratory, Bar Harbor, ME, USA	(Mo *et al.*, 2015)

Table 2: Mouse diets

Name	**Standard Chow (SC) diet**	**High-fat high-sugar (HFHS) diet**
Supplier	Harlan Teklad, Madison, USA	Research diets Inc., New Brunswick, NJ, USA
Reference number	LM-485	D12331
Carbohydrate (kcal%)	44.3	25
Fat (kcal%)	5.8	58
Protein (kcal%)	19.1	17
Energy density (kcal/g)	3.1	5.56

3.1.2. Genotyping

Table 3: Reagents for genotyping

Reagent	**Supplier**	**Product code**
5x Green GoTaq® flexi buffer	Promega Corporation, Madison, WI, USA	M891A
Betaine (5M)	Sigma-Aldrich Chemie GmbH, Taufkirchen, Germany	B0300
dNTPs (100 mM)	Life technologies/Thermo Fisher Scientific Inc., Waltham, MA, USA	10297018
Glycerol Standard Solution	Sigma-Aldrich Chemie GmbH, Taufkirchen, Germany	G7793
KAPA2G Fast Genotyping mix	Sigma-Aldrich Chemie GmbH, Taufkirchen, Germany	KK5121
$MgCl_2$ (25 mM)	Promega Corporation, Madison, WI, USA	A351B
GoTaq® G2 flexi DNA polymerase; 5 U/µl)	Promega Corporation, Madison, WI, USA	M7806

Table 4: Genotyping primers and product sizes for Aldh1L1-CreER^{T2} mice

Primer	Primer sequence	Product size (WT)	Product size (transgene)
20713	5'-CAACTCAGTCACCCTGTGCTC-3'	No band	590 bp
8250	5'-TTCTTGCGAACCTCATCACTCG-3'		

Table 5: Genotyping primers and product sizes for GFAP KO mice

Primer	Primer sequence	Product size (WT)	Product size (KO)
WT forward	5'-GTCCAGCCGCAGCCGCAG-3'	350 bp	/
WT reverse	5'-CTCCGAGACGGTGGTCAGG-3'		
KO forward	5'-TGTTCTCCTCTTCCTCATCTCC-3'	/	140 bp
KO reverse	5'-ATTGTCTGTTGTGCCCAGTC-3'		

Table 6: Genotyping primers and product sizes for hGFAP-CreER^{T2} mice

Primer	Primer sequence	Product size (WT)	Product size (transgene)
42 (control forward)	5'-CTAGGCCACAGAATTGAAAGATCT-3'	324 bp	/
43 (control reverse)	5'-GTAGGTGGAAATTCTAGCATCATCC-3'		
1084 (transgene forward)	5'-GCGGTCTGGCAGTAAAAACTATC-3'	/	100 bp
1085 (transgene reverse)	5'-GTGAAACAGCATTGCTGTCACTT-3'		

Table 7: Genotyping primers and product sizes for IP$_3$R2 KO mice

Primer	Primer sequence	Product size (WT)	Product size (KO)
WT forward	5'-ACCCTGATGAGGGAAGGTCT-3'	200 bp	/
WT reverse	5'-ATCGATTCATAGGGCACACC-3'		
KO forward	5'-AATGGGCTGACCGCTTCCTCGT-3'	/	300 bp

KO reverse	5'-TCTGAGAGTGCCTGGCTTTT-3'		

Table 8: Genotyping primers and product sizes for $Smo^{fl/fl}$ mice

Primer	Primer sequence	Product size (WT)	Product size (transgene)
oIMR0013	5'-CTTGGGTGGAGAGGCTATTC-3'	160 bp	280 bp
oIMR0014	5'-AGGTGAGATGACAGGAGATC-3'		
oIMR1834	5'-CCACTGCGAGCCTTTGCGCTAC-3'		
oIMR1835	5'-CCCATCACCTCCGCGTCGCA-3'		

Table 9: Genotyping primers and product sizes for Sun1-sfGFP mice

Primer	Primer sequence	Product size (WT)	Product size (transgene)
oIMR9020 (control forward)	5'-AAGGGAGCTGCAGTGGAGTA-3'	241 bp	/
24500 (control reverse)	5'-CAGGACAACGCCCACACA-3'		
36178 (transgene forward)	5'-ACACTTGCCTCTACCGGTTC-3'	/	225 bp
15020 (mutant reverse)	5'-CTGAACTTGTGGCCGTTTAC-3'		

All primers were purchased from Sigma-Aldrich Chemie GmbH, Taufkirchen, Germany.

3.1.3. Reagents and chemicals

Table 10: List of reagents and chemicals

Name	Supplier	Product code
2-Chloroacetamide (CAA)	Sigma-Aldrich Chemie GmbH, Taufkirchen, Germany	C0267

AccuGENE 0.5 M EDTA Lösung, pH 8.0	Biozym Scientific GmbH, Hessisch Oldendorf, Germany	Lonza 51201
β-mercaptoethanol	Carl Roth GmbH + CoKG, Karlsruhe, Germany	4227.3
BSA 0.4%	Sigma-Aldrich Chemie GmbH, Taufkirchen, Germany	A1595
Collagenase/dispase solution	Sigma-Aldrich Chemie GmbH, Taufkirchen, Germany	10269638001
Dabco® 33-LV	Sigma-Aldrich Chemie GmbH, Taufkirchen, Germany	290734
DMEM/F-12	Thermo Fisher Scientific Inc., Waltham, USA	11320033
D(+)Trehalose Dihydrate	Sigma-Aldrich Chemie GmbH, Taufkirchen, Germany	T0167-10G
Dulbecco's Phosphate Buffered Saline (D-PBS)	Sigma-Aldrich Chemie GmbH, Taufkirchen, Germany	D8537
Ethanol	Th. Geyer GmbH+CoKG, Renningen, Germany	1.00983.2500
Gelatin from porcine skin	VWR International GmbH, Darmstadt, Germany	SAFSG1890
HaltTM protease and phosphatase inhibitors (100x)	Thermo Fisher Scientific Inc., Waltham, USA	78446
MACS® BSA Stock Solution (10%)	Miltenyi BioTec, USA	130-091-376
Mowiol	Merck Group, Darmstadt, Germany	475904
NaCl	Thermo Fisher Scientific Inc., Waltham, USA	15023021
NaCl 0.9 % (injectable saline)	VWR International GmbH, Darmstadt, Germany	BRAU3570160
Natriumhydroxid	Carl Roth GmbH + CoKG, Karlsruhe, Germany	6771.1
Papain Dissociation System	Worthington Biochemical Corporation, Lakewood, NJ	LK003150
Paraformaldehyde (PFA)	Carl Roth GmbH + CoKG, Karlsruhe, Germany	0335.2

PBS (1X), liquid; pH:7.4	Thermo Fisher Scientific Inc., Waltham, USA	10010056
Pierce™ Trypsin/Lys-C Protease Mix	Thermo Fisher Scientific Inc., Waltham, USA	A40007
PMSF Solution	Santa Cruz Biotechnology, Heidelberg, Germany	sc-482875
RIPA buffer	Sigma-Aldrich Chemie GmbH, Taufkirchen, Germany	R0278-500
RNaseOUT	Thermo Fisher Scientific Inc., Waltham, USA	10-777-019
Sodium azide	Sigma-Aldrich Chemie GmbH, Taufkirchen, Germany	S2002
Sodium Deoxycholate Detergent	Thermo Fisher Scientific Inc., Waltham, USA	89904
Sodium Phosphate Dibasic (Na_2HPO_4)	Sigma-Aldrich Chemie GmbH, Taufkirchen, Germany	S5136
Sodium Phosphate Monobasic (NaH_2PO_4)	Sigma-Aldrich Chemie GmbH, Taufkirchen, Germany	S5011
Sucrose	Carl Roth GmbH + CoKG, Karlsruhe, Germany	4621.2
Sunflower seed oil	Sigma-Aldrich Chemie GmbH, Taufkirchen, Germany	S5007
Tamoxifen	Sigma-Aldrich Chemie GmbH, Taufkirchen, Germany	T5648-1g
Trypan Blue	Bio-Rad Laboratories GmbH, Feldkirchen, Germany	1450021
Tris(2-carboxyethyl)phosphine hydrochloride (TCEP)	Sigma-Aldrich Chemie GmbH, Taufkirchen, Germany	C4706
TRIS PUFFERAN®	Carl Roth GmbH + CoKG, Karlsruhe, Germany	4855.5
Triton X-100	Roche Diagnostics GmbH, Mannheim, Germany	11858620

3.1.4. Kits

Table 11: List of kits

Name	Supplier	Product code
Adult brain dissociation kit, mouse and rat	Miltenyi BioTec, USA	130-107-677
Anti-ACSA-2 MicroBead Kit, mouse	Miltenyi BioTec, USA	130-097-678
Chromium Single Cell 3′ Reagent Kits v3.1	10X Genomics, Pleasanton, USA	PN-1000121
Pierce BCA protein assay	Thermo Fisher Scientific Inc., Waltham, USA	23228
RNAscope® Multiplex Fluorescent Reagent Kit v2- Mm	Advanced Cell Diagnostic	323100
RNeasy Micro Kit	Qiagen, Hilden, Germany	74004
SMART-Seq® v4 Ultra® Low Input RNA Kit for Sequencing	Takara Bio Clontech USA, Inc.	634891

3.1.5. Antibodies and fluorescent dyes

Table 12: List of primary antibodies

Target	Host	Dilution	Supplier	Product code
ACSA2	rat	10 µl / 10^7 cells	Milteny, BioTec, USA	130-097-678
Aldh1L1	/	1/50	Advanced Cell Diagnostic	405891-C2
GFAP	rabbit	1/1000	Dako, USA	Z0334
GFP	chicken	1/500	OriGene Technologies, USA	AP31791PU-N
Ki67	rabbit	1/1000	Abcam, USA	Ab16667

Table 13: List of secondary antibodies

Target	Host	Conjugate	Dilution	Supplier	Product code
chicken IgG	goat	Alexa Fluor 488	1/1000	Invitrogen, USA	A11039
chicken IgG	rabbit	HRP	1/1000	Rockland Immunochemicals	603-4302
rabbit IgG	donkey	Alexa Fluor 647	1/1000	Invitrogen, USA	A31573
/	/	Opal 570	1/1000	Akoya Biosciences	
/		Opal 520	1/1000	Akoya Biosciences	

3.1.6. Instruments and tools

Table 14: List of instruments and tools

Name	Application	Supplier
3P Brain Puncher Tissue Set	ARC punch	Thermo Fisher Scientific Inc., Waltham, USA
Bürker chamber	Cell counting	VWR International GmbH, Darmstadt, Germany
Cell strainer 40 µm	Filters	Schubert&Weiss, Germany
EASY-nLC™ 1200 System	HPLC	Thermo Fisher Scientific Inc., Waltham, USA
Gentle MACS Octo Dissociator	Tissue dissociation	Miltenyi BioTec, USA
HybEZ oven	FISH	Advanced Cell Diagnostic
Leica TCS SP5	Confocal microscope for imaging	Leica Mikrosysteme Vetrieb GmbH, Wetzlar, Germany
LS columns	MACS	Miltenyi BioTec, USA
MACS separator	Magnetic cell isolation	Miltenyi BioTec, USA
Mastercycler ®	PCR	Eppendorf, Germany
Micro-Perfusion pump	Perfusion	Automate Scientific, USA
MS columns	MACS	Miltenyi BioTec, USA
Omnifix-f 1ml syringes	Tamoxifen injections	B.Braun, Melsungen, Germany
Pre-Separation Filters (70 µm)	MACS	Miltenyi BioTec, USA
Q Exactive HF-X hybrid quadrupole-Orbitrap	Mass spectometer	Thermo Fisher Scientific Inc., Waltham, USA
Qiaxcel Analysis system	PCR analysis	Qiagen N.V., Hilden, Germany
ReproSil-Pur C18	HPLC	Dr. Maisch GmbH, Germany
Rodent Brain Matrix	Brain slicing	ASI instruments, USA
SDB-RPS STAGE tips	Purification of peptides	3M Empore, USA
SuperFrost Plus Gold slides	IHC and FISH	Thermo Fisher Scientific Inc., Waltham, USA
Sterican Kanülen, 27 G	Tamoxifen injections	B.Braun, Melsungen, Germany

3.2. Methods

3.2.1. Animal experiments

3.2.1.1. Animals

The Animal Ethics Committee of the Upper Bavaria government (Germany) approved all animal experiments, which were successively conducted following the guidelines and regulations of the Institutional Animal Care and Use Committee of the Helmholtz Center München, Neuherberg, Germany. All mice were housed in groups in individually ventilated cages (IVC), under a 12-h light/12-h dark cycle at 22 ± 2°C and at constant 45-65% humidity, with free access to food and water. All studies were performed on male mice. The diet of C57BL/6JRj mice was either maintained on SC or switched to a HFHS diet at 8-10 weeks of age (OMICs studies and RNAscope®) or at 4 weeks of age (scRNA-Seq study). In order to generate a mouse line carrying the Sun1-GFP fusion sequence specifically under the Aldh1L1 promoter in a Cre-dependent inducible manner, Aldh1L1-CreER^{T2} line was crossed with Sun1-sfGFP mice. At 8-12 weeks of age, the resulting Aldh1L1-CreER^{T2}:Sun1-sfGFP animals received a SC or a HFHS diet for 5 or 15 days. In order to induce the expression of GFP in the nuclei of Aldh1L1-expressing cells, Aldh1L1-CreER^{T2}:Sun1-sfGFP littermates were injected with Tamoxifen (1 mg in 100 µl per day, *i.p.*) during the last two days of a HFHS diet exposure, and sacrificed three days after the last injection, during which they were maintained on the same experimental diet. Tamoxifen injectable solution was prepared by dissolving Tamoxifen in Ethanol 100% and sunflower seed oil (1:9 ratio), in a final concentration of 10 mg/ml, then filter sterilized and stored in aliquots at -20°C in the dark until the moment of use. GFAP KO and IP_3R2 KO mice were bred with a heterozygous *x* heterozygous strategy in order to produce WT and KO littermates, which were successively maintained at SC diet or switched to a HFHS diet at 8-12 weeks of age. In order to delete the sequences flanked by loxP sites specifically in GFAP-expressing astrocytes, the Smo$^{fl/fl}$ line was crossed with hGFAP-CreER^{T2} mice. At 6 weeks of age, the resulting Smo$^{fl/fl}$: hGFAP-CreER^{T2} littermates were injected with Tamoxifen (1 mg in 100 µl per day, *i.p.*) for 5 consecutive days, and stayed on a SC diet for the following 4 weeks, until the control diet was either maintained or changed to a HFHS diet. Mice were randomized and evenly distributed among test groups according to age and body weight.

3.2.1.2. Genotyping protocols

Genomic DNA was extracted from eartags of 3 weeks old mice, and successively used to genotype the different mouse lines following the respective protocol (see **Tables** below). The DNA isolation was performed by boiling the eartags in 200 µl of 50 mM NaOH solution for 30 min, and subsequently by adding 20 µl of 1 M Tris buffer. The DNA was stored in 4°C until the moment of use.

Table 15: Genotyping protocol for Aldh1L1-CreER^{T2} mice

Material	**Concentration**	**Volume (µl per well)**
MilliQ H2O		5
KAPA2G Fast Genotyping mix	1x	6.25
Primer 20713	20 µM	0.625
Primer 8250	20 µM	0.625
DNA		1

See **Table 4** for details on primers. In a PCR cycler, the samples underwent the following temperature profile: 95°C for 3 min, 40 repetitions of the sequence 95°C (15 sec)- 60°C (15 sec)- 72°C (15 sec), followed by 1 min at 72°C, and cooling down to 10°C.

Table 16: Genotyping protocol for GFAP KO mice

Material	**Concentration**	**Volume (µl per well)**
MilliQ H2O		3.75
KAPA2G Fast Genotyping mix	1x	6.25
WT forward	20 µM	0.625
WT reverse	20 µM	0.625
KO forward	20 µM	0.625
KO reverse	20 µM	0.625
DNA		1

See **Table 5** for details on primers. The temperature profile used corresponds to the same described under **Table 15**.

Table 17: Genotyping protocol for hGFAP-CreER^{T2} mice

Material	Concentration	Volume (µl per well)
5x Green GoTaq® flexi buffer	5x	2.5
dNTPs	10 mM	0.25
$MgCl_2$	25 mM	1
42 (control forward)	20 µM	0.25
43 (control reverse)	20 µM	0.25
1084 (transgene forward)	20 µM	0.25
1085 (transgene reverse)	20 µM	0.25
Betaine	5 M	2.5
GoTaq® G2 flexi DNA polymerase	5 U/µl	0.1
DNA		3

See **Table 6** for details on primers. The temperature profile used in the PCR cycler is: 94°C for 3 min, 36 repetitions of the sequence 94°C (45 sec)- 60°C (45 sec)- 72°C (1 min), followed by 2 min at 72°C, and cooling down to 4°C.

Table 18: Genotyping protocol for IP$_3$R2 KO mice

Material	Concentration	Volume (µl per well)
MilliQ H2O		3.9
5x Green GoTaq® flexi buffer	5x	2.5
dNTPs	10 mM	0.25
$MgCl_2$	25 mM	1
WT forward	20 µM	0.25
WT reverse	20 µM	0.25
KO forward	20 µM	0.25
KO reverse	20 µM	0.25
Betaine	5 M	2.5
GoTaq® G2 flexi DNA polymerase	5 U/µl	0.1
DNA		1

See **Table 7** for details on primers. The temperature program run in the PCR cycler is: 94°C for 4 min, 30 repetitions of the sequence 95°C (30 sec)- 55°C (1 min)- 72°C (1 min), followed by 7 min at 72°C, and cooling down to 4°C.

Table 19: Genotyping protocol for Smo$^{fl/fl}$ mice

Material	**Concentration**	**Volume (µl per well)**
5x Green GoTaq® flexi buffer	5x	5
dNTPs	10 mM	0.5
$MgCl_2$	25 mM	2
oIMR0013	20 µM	0.5
oIMR0014	20 µM	0.5
oIMR1834	20 µM	0.5
oIMR1835	20 µM	0.5
Betaine	5 M	5
GoTaq® G2 flexi DNA polymerase	5 U/µl	0.2
DNA		2

See **Table 8** for details on primers. The temperature profile run in the PCR cycler is: 94°C for 1 min, 35 repetitions of the sequence 94°C (1 min)- 63°C (1 min)- 72°C (1 min), followed by 2 min at 72°C, and cooling down to 4°C.

Table 20: Genotyping protocol for Sun1-sfGFP mice

Material	**Concentration**	**Volume (µl per well)**
MilliQ H2O		5.61
5x Green GoTaq® flexi buffer	5x	3.9
dNTPs	10 mM	0.39
$MgCl_2$	25 mM	1.56
oIMR9020 (control forward)	20 µM	0.38
24500 (control reverse)	20 µM	0.38
36178 (transgene forward)	20 µM	0.38
15020 (mutant reverse)	20 µM	0.38

Glycerol Standard Solution	50%	1.95
GoTaq® G2 flexi DNA polymerase	5 U/µl	0.09
DNA		2

See **Table 9** for details on primers. The temperature profile used corresponds to the same described under **Table 17**.

All the samples produced by following the above-described genotyping protocols were analyzed with a Qiaxcel Analysis system.

3.2.2. RNA and protein sequencing

3.2.2.1. Tissue dissociation and magnetic-activated cell sorting (MACS)

C57BL/6JRj mice exposed to a SC or a HFHS diet for 4 months were sacrificed by cervical dislocation and tissues rapidly dissected for downstream analysis. For transcriptomics, hypothalami, hippocampi, and half cortices from 2 animals were pooled together by brain region in distinct tubes prefilled with cold D-PBS; the same was done for proteomics, but with 4 mice in total. Cortices were chopped into smaller pieces with a scalpel. Tissue dissociation and debris removal were performed following manufacturer's instructions (Adult Brain Dissociation Kit, Miltenyi BioTec). In order to specifically separate astrocytes from other cell types, the resulting cell suspensions underwent magnetic-activated cell sorting (MACS) procedure, using the astrocyte-specific surface marker ACSA2 (Batiuk *et al.*, 2017) (Kantzer *et al.*, 2017). First, the total number of cells derived from the tissue dissociation was counted in order to define the correct reagent and buffer volumes and the type of MACS columns to use in the following steps. As the total number of cells derived from the cortices exceeded 10^7 cells, all reagents volumes were scaled up and LS columns used, according to the manufacturer's protocol (Anti-ACSA2 MicroBead Kit, Miltenyi BioTec). For hypothalamic and hippocampal samples instead, MS columns were used and standard procedure was followed (Anti-ACSA2 MicroBead Kit, Miltenyi BioTec), as the total number of cells counted was lower than 10^7. The unlabeled cellular fraction (flow-through) was collected to validate the correct separation of astrocytes from other cell types. Both the ACSA2 labeled and the unlabeled cellular fractions were collected in cold PBS and centrifuged for 10 min at 3,000 x g and 4°C. The so-pelleted cells were either directly stored at -20°C for successive protein extraction, or resuspended in 350 µl RLT buffer containing 3.5 µl of β-mercaptoethanol, and stored at -80°C until RNA extraction.

3.2.2.2. RNA isolation and sequencing

The RNA from sorted ACSA2^{+} astrocytes was extracted (RNeasy Micro Kit; Qiagen) according to the manufacturer's protocol. Afterwards, cDNA synthesis and amplification were performed (SMART-Seq® v4 Ultra® Low Input RNA Kit for Sequencing, Takara) following the user manual provided with the kit. The mRNA sequencing and transcriptomics data generation were conducted by Novogene Europe, United Kingdom.

3.2.2.3. Protein extraction and sequencing

To perform protein extraction from ACSA2^{+} astrocytes and ACSA2^{-} cells previously isolated via MACS, cells were washed one time in cold PBS by centrifugation (500 x g, 5 min, 4°C), resuspended in 80 µl of cold RIPA buffer (Sigma-Aldrich Chemie GmbH, Taufkirchen, Germany) containing 1% v/v of protease and phosphatase inhibitors mix (Thermo Fisher Scientific Inc., Waltham, USA), and sonicated with a glass homogenizer (Duran Wheaten Kimble, USA). The lysate was then centrifuged at 13,000 x g for 10 minutes at 4°C, the pellet containing cell debris discarded, and the supernatant protein concentration evaluated with Pierce BCA protein assay (Thermo Fisher Scientific Inc., Waltham, USA), according to the manufacturer's instructions.

The following sample preparation and mass spectrometry (MS) analysis were performed by Dr. Natalie Krahmer from the Institute for Diabetes and Obesity (Helmholtz Zentrum München). In particular, 2 µg of proteins were boiled for 5 min at 95 °C, and then sonicated (Branson probe sonifier output 3-4, 50% duty cycle, 3× 30s) in 4% SDC (sodium deoxycholate), 100 mM Tris pH 8.5. After alkylation and reduction with 10 mM tris-(2-carboxyethyl)-phosphin-hydrochlorid (TCEP), 40 mM 2-chloroacetamide (CAA), proteins were digested overnight with 1:50 (protein:enzyme) LysC and Trypsin at 37 °C. The resulting digested peptides were acidified to a final concentration of 1% trifluoroacetic acid (TFA), centrifuged for clearing, and loaded onto activated (30% methanol, 1% TFA) double layer styrenedivinylbenzene–reversed phase sulfonated STAGE tips (SDB-RPS; 3M Empore) (Kulak *et al.*, 2014). First, the STAGE tips were washed with 200 µl 0.2% TFA, then with 200 µl 0.2% TFA and 5% acetonitrile (ACN). The peptides were eluted with 60 µl SDB-RPS elution buffer (80% ACN, 5% NH_4OH) for single shot analysis. Samples were concentrated in a SpeedVac for 40min at 45 °C and dissolved in 10µl MS loading buffer (2% ACN, 0.1% TFA). For MS analysis, 1 µg of peptides was loaded onto a 50-cm column with a 75 µM inner diameter, packed in-house with 1.9 µM C18 ReproSil particles (Dr. Maisch GmbH) at 60°C. The peptides were separated by reversed-

phase chromatography on a 120 min gradient (5-30% buffer B over 95 min, 30-60% buffer B over 5 min followed by washout) using a binary buffer system consisting of 0.1% formic acid (buffer A) and 80% ACN in 0.1% formic acid (buffer B) at a flowrate of 350 nl on an EASY-nLC 1200 system (Thermo Fisher Scientific). A Quadrupole-Orbitrap instrument (Q Exactive HF-X, Thermo Scientific) was used to acquire MS data, utilizing data dependent top-15 method with maximum injection time of 20 ms, a scan range of 300–1650 Th, and an automatic gain control (AGC) target of 3e6. Higher-energy collisional dissociation (HCD) fragmentation with a target value of 1e5, and a window of 1.4 Th was used to perform protein sequencing. A resolution of 60,000 was used to acquire survey scans, while a resolution of 15,000 was used for HCD spectra, with maximum ion injection time of 28 ms and an underfill ratio of 20%. Dynamic exclusion was set to 30 s.

3.2.2.4. Bulk transcriptomics and proteomics analysis

Bulk transcriptomics and proteomics data were analyzed by Dr. Viktorian Miok from the Institute of Diabetes and Obesity (Helmholtz Zentrum München). FastQC (Andrews, 2010) was first used to evaluate the raw transcriptomics sequencing reads. The transcripts underwent first a quality control check, followed by alignment and quantification against the reference index, which was generated on the base of GRCm38 genome with Salmon (Patro *et al.*, 2017), and default parameters were set. Tixmeta (Love *et al.*, 2020) was then used to summarize the transcript abundances imported in R. The levels of gene expression were normalized following a median ratio method with DESeq2 (Love, Huber and Anders, 2014). The transformed counts were stabilized and principal components calculated on the variance. The comparison between SC diet and HFHS diet groups within each brain region allowed the identification of differentially expressed genes (DEGs), by using standard parameters and simple two-group comparison Wald test. For proteomics, raw mass spectrometry data were analyzed with MaxQuant software version 1.6.7.0. (Tyanova *et al.*, 2016). Perseus software's data imputation component (Max Planck Institute of Biochemistry, Munich, Germany) (Tyanova *et al.*, 2016) was used to replace the missing values from the normal distribution. Student t-test was performed to evaluate the statistically significant differences in protein levels between experimental groups for every brain region. R's ggplot2 package (Wickham, 2016) was used to produce data principal component analysis graphs, R's EnhancedVolcano (Blighe, Rana and Lewis, 2021) and VennDiagram (Chen and Boutros, 2011) packages were utilized to generate respectively Volcano plots and Venn diagrams. R Base package was used to perform the integration analysis between transcriptomics and proteomics data, and the calculation of

Spearman's rank correlation coefficient. The heatmaps illustrating the expression of DEGs over the groups were generated with R's pheatmap package (Kolde, 2015), while gene ontology (GO) enrichment analysis was performed and illustrated with R's clusterProfiler (Yu *et al.*, 2012) and ggplot2 (Wickham, 2016) packages.

3.2.2.5. Generation of single-cells suspension from the ARC

The brains of 5-6 weeks old C57BL/6JRj mice were rapidly extracted, cooled in ice-cold DMEM/F12 medium (Thermo Fisher Scientific Inc., Waltham, USA) and settled in a chilled rodent brain matrix (ASI-instruments) laying on their dorsal surface. 1 mm-thick coronal section containing the ARC was obtained by slicing the brain in the middle of the hypothalamus, approx. 1 mm from the optic chiasm. The ARC was then isolated from the slice by using a tissue puncher (1 mm diameter, Thermo Fisher Scientific Inc., Waltham, USA), and immediately transferred to ice-cold DMEM/F12 medium. Per each sample, 6 ARCs were pooled together before proceeding to enzymatic digestion. The tissue dissociation protocol was adapted from M.D. Claudia Doege's lab (Columbia University Medical Center). The pooled tissues were washed with ice-cold D-PBS supplemented with Trehalose (Sigma-Aldrich Chemie GmbH, Taufkirchen, Germany) (Saxena *et al.*, 2012) solution (5% w/v), and successively incubated for 16 min at 37°C in 200 µl of 4 mg/ml collagenase/dispase solution (Sigma-Aldrich Chemie GmbH, Taufkirchen, Germany) supplemented with 5% w/v Trehalose. After the incubation, the enzymatic solution was removed carefully without disturbing the tissue, and replaced with 200 µl of papain/DNAse solution (steps 2 and 3 from Worthington Biochemical Corporation catalogue) containing 5% w/v Trehalose, and incubated for 12 min at 37°C. The enzymatic solution was then removed and substituted with 200 µl of D-PBS supplemented with 5% w/v Trehalose and RNAseOUT (1/1000; Thermo Fisher Scientific Inc., Waltham, USA), in which the tissue was gently tritured. The resulting cell suspension was filtrated drop by drop through a 40 µm cell strainer, and centrifuged at 300 x g for 8 min at 4°C in a big volume of D-PBS supplemented with 2% bovine serum albumin (BSA) solution (Miltenyi BioTec). The pelleted cells were resuspended in D-PBS with 0.04% BSA and washed by centrifugation at 300 x g for 10 min at 4°C. The supernatant was carefully removed and cells resuspended in 40 µl of D-PBS with 0.04% BSA. The final cells concentration and vitality was estimated by hemacytometer after trypan blue staining, and the volume was subsequently adjusted to approx. 1000 cells/µl. Cells were kept on ice until further use.

3.2.2.6. Single-cell RNA sequencing analysis

Single-cell RNA-seq libraries were prepared by Dr. Michael Sterr from the Institute of Diabetes and Regeneration Research (Helmholtz Zentrum München), and pre-analyzed by Dr. Thomas Walzthoeni from the Core Facility Genomics/Bioinformatics Platform (Helmholtz Zentrum München). The cell suspensions were immediately used for single-cell RNA-seq library preparation with a target recovery of 10000 cells. Libraries were prepared using the Chromium Single Cell 3′ Reagent Kits v3.1 (10X Genomics, PN-1000121) according to the manufacturer's instructions. Illumina NovaSeq6000 system was used to pool and sequence the libraries (target read depth of 50000 reads/cell), following 10X Genomics' recommendations. The alignment of the reads was performed by using the sequence and annotation files for the mouse genome GRCm38 assembly and annotation release 100 from Ensembl. The index of the genome was generated with the command "cellranger mkref" in the Cell Ranger software (version 3.1.0, from 10X Genomics, Pleasanton, CA), while the command "cellranger count" was run to align the reads, generate quality control (QC) metrics, estimate the numbers of valid barcodes, and create the count matrices. Standard parameters were used when performing the analysis, except for the adjustment of expected cells' number. Python's Scanpy package (v1.4.4) (Wolf, Angerer and Theis, 2018) was used to generate an anndata object.

Single-cell RNA-seq data were analyzed by Dr. Viktorian Miok from the Institute of Diabetes and Obesity (Helmholtz Zentrum München), by using Python's Scanpy package (v1.7.1) (Wolf, Angerer and Theis, 2018). Cells were filtered using a minimum unique molecular identifier (UMI) count of 500. A total count of 1e4 remaining cell vectors was obtained by linear scaling when performing normalization in default settings. The top 50 principal components were used to generate a k-nearest neighbor (kNN) graph (k = 100, metho = umap), based on which a leiden clustering (resolution = 0.3, flavor = vtraag) was computed. The uniform manifold approximation and projection (UMAP) plot was generated to illustrate the assignment of cell identities to clusters, based on specific molecular markers expression. Further analyses were performed on the leiden cluster corresponding to astrocytes (cluster 0). Only cells with a minimum UMI count of 500 were further processed to 1e4 counts normalization, transformation log (x+1) and principal component analysis (PCA) with 50 PCs. A kNN graph (k = 100, method = umap) based on the PC space was generated. For each diet, a UMAP plot was developed and superimposed by Leiden clustering. The absolute number of cells per each cluster is shown by a barplot chart (matplotlib) (Hunter, 2007). The total number of DEGs (split in up- and down-regulated) per cell type was identified by comparing SC diet group with 5d and 15d HFHS diet groups with a Student's t-test. The scVelo phyton package (https://github.com/theislab/scvelo)

was implemented and utilized to analyze the RNA velocity (La Manno *et al.*, 2018) of single astrocytes. The pipeline velocyto (http://velocyto.org) was used to extract spliced and unspliced reads, after creating a loompy file. To further continue the analysis, the file was switched to an AnnData object by using Scanpy. After calculating the RNA velocities of each astrocyte using scvelo python pipeline, the resulting graph was combined to the low dimensional UMAP plots. Finally, for each diet, the potential driver genes of RNA velocity were identified by utilizing the same pipeline, considering they halve high likelihoods in the dynamic models, with a dynamic behavior.

3.2.3. Immunohistochemistry and imaging

3.2.3.1. Brain slicing and histology

Animals were transcardially perfused first with NaCl 0.9%, and then with a solution containing 4% PFA in 0.1 M PBS. Afterwards, brains were carefully extracted, post-fixed overnight at 4°C in the same fixative solution (4% PFA), which was then substituted by 30% sucrose in 0.1 M tris-buffered saline (TBS) with a pH of 7.2, in which brains were left to equilibrate for 24-48h at 4°C. Successively, brains were frozen at -20°C for 1h, and sliced into 30 μm coronal sections on a cryostat. All brain slices were collected into 1M TBS. Next, 3-4 sections of interest containing the medial ARC (Bregma between -1.58 mm and -1.82 mm) were selected, and blocked for 1h in a solution composed by 0.25% porcine gelatin and 0.2% Triton X 100 in 0.1M TBS (named SUMI). Afterwards, the brain slices were incubated with primary antibodies correctly diluted in SUMI overnight at 4°C. The successive day, sections were washed four times in 0.1M TBS, and incubated in the respective secondary antibodies diluted in SUMI for 2h at room temperature (RT). After four more rinses in 0.1M TBS, the penultimate of which containing 4′,6-diamidino-2-phenylindole (DAPI) (2 μg/ml), brain slices were mounted on microscope slides, and left to dry for 1h at RT, before storing them at 4°C.

3.2.3.2. Confocal imaging

Between 1 and 20 days from immunohistochemistry, mounted sections were imaged. All images were acquired using a confocal microscope (Leica TCS SP5) at 20x magnification with an air-immersed objective. The final z-stack was composed by constant 2 μm step sizes for a total of 17-22 optical slices.

3.2.3.3. Analysis of number and spatial location of cells

Images were analyzed with ImageJ/Fiji software on maximum intensity z-stack projections. The assessment of cell numbers and spatial coordinates was performed within a defined region of interest (ROI) in the cortex, hippocampus and hypothalamus. The ROI in the somatory-sensory cortex was positioned consistently in an area including layers 4 and 5 (144334 μm^2), while the ROI in the hippocampus was defined in a region including stratum radiatum, stratum lacunosum-moleculare and dentate gyrus (96138 μm^2). In the hypothalamus, only the ARC was analyzed, by positioning a ROI manually drawn as a right-angled triangle (approximately 105350 μm^2) on the basis of DAPI staining and Allen Mouse Brain Atlas (Lein *et al.*, 2007; Atlas, 2011). The lower cathetus of the ROI (490 μm) corresponded to the inferior border of the ARC and defined the x-axis, while the second cathetus (430 μm) was positioned at the edge of the third ventricle, defining the y-axis. The analysis was done manually and blindly. The x/y coordinates of each cell were defined roughly at the center of Aldh1L1+ nuclei, while for GFAP immunoreactive astrocytes, the converging point between main processes was considered as center of the cell. $GFAP^+$ cells located at the border of the third ventricle, and showing long and straight processes were excluded from the analysis, as they could possibly be tanycytes, rather than astrocytes. The analysis of the number of astrocytes in ARCs, cortices and hippocampi was performed on the same slices in a consistent manner. The same ARC slices were used to analyze the number and the spatial location of astrocytes.

3.2.3.4. Spatial distribution analysis

Spatial distribution of astrocytes in the ARC was analyzed by Dr. Viktorian Miok from the Institute of Diabetes and Obesity (Helmholtz Zentrum München). R's plotly (Sievert, 2020) and statspat (Baddeley and Turner, 2005) packages were utilized to create respectively 3D and 2D spatial point pattern density plots. The significance of the overall and local analysis of spatial point pattern densities was estimated with a generalized linear model to fit the data $y \sim \beta_0 + \beta_1 * diet + \beta_2 * mouse$ (*mouse*: random effect; *diet*: fixed effect), and with an asymptotic Wald test to calculate the p-values (R-package lme4). Moreover, the differences between the cells present in each square along the diet groups was calculated using the same statistical tests. R's randomForest (Liaw and Wiener, 2002), mlr3, mlr3learners, and mlr3viz (Lang *et al.*, 2019) packages were utilized to perform random forest classification. The Moran I values were calculated with spatial auto-correlation ape (Paradis and Schliep, 2019).

3.2.4. Fluorescence *in situ* hybridization (FISH)

To validate Aldh1L1 -RNA and -protein co-localization, and to assess Aldh1L1-RNA levels changes in the ARC in response to a HFHS diet, Aldh1L1-CreER^{T2}::Sun1-sfGFP and C57BL/6JRj mice were perfused with 0.9% w/v NaCl and a cold 4% solution of PFA in 0.1 M PBS (pH 7.4). Afterwards, the brains were kept in 4% PFA solution at 4°C overnight, and moved first to 10%, then 20%, and finally 30% sucrose in 0.1 M TBS solution each consecutive day. The brains were then sliced in 10 µm sections on a cryostat, after a period of 1-2h freezing in -20°C. The slices were immediately mounted on SuperFrost Plus Gold slides (Fisher Scientific) and kept in -80°C until further use. Within one month from the initial storage, slides were warmed up for 30 minutes at 60°C, then incubated in 4% PFA solution for 15 minutes. Next, the slides were treated with sequential 5 min-long steps of dehydration with 50%, 70%, and 100% ethanol. After few minutes of air-drying, RNAscope® Multiplex Fluorescent Reagent Kit v2- Mm (ACD, Advanced Cell Diagnostic, #323100) was applied to the slides following the manufacture's protocol. *M. musculus* Aldh1L1 mRNA was targeted by using the corresponding probe (RNAscope® Probe Mm-Aldh1l1; ACD, #405891-C2), and Opal 570 Fluorophore Reagent (1/1000; Akoya Biosciences) for visualization. As the treatment with proteases used in the protocol might weaken the GFP expression, a retrieval step was applied to the slides by incubating them for 2 hours at RT with chicken anti-GFP (1/500, OriGene, #AP31791PU-N) antibody diluted in 0.1% bovine serum albumin (BSA) in TBS, and then for 30 minutes with secondary rabbit HRP-conjugated anti-chicken IgG (H&L) antibody (1/1000 in 0.1% bovine serum albumin (BSA) in TBS, Rockland Immunochemicals, #603-4302), and finally 15 minutes with Opal 520 Fluorophore Reagent (1/1000; Akoya Biosciences) at RT. The slides were then mounted and stored at 4°C until imaging. Within 2 weeks, Z-stack pictures of the slides were taken under a confocal microscope (Leica TCS SP8) with glycerin oil-immersed 20X objective applying a 0.5 µm z-interval, and keeping the same acquisition parameters to all slides. Fiji software was used to analyze the pictures, on maximum intensity Z-stack projections, on which the same ROI used before for IHC analyses was utilized to define the ARC position. Within the ARC, the number of cells showing the highest density of Aldh1L1-RNA, which allowed to identify the cellular form, was counted manually. Areas showing low and sparse RNA expression were not considered for the quantification. All the analyses were done blindly.

3.2.5. Statistics

GraphPad Prism (v8.2.1), R (v4.0.3, R Core Team, 2019), Python (v3.9.2, http://www.python.org), and Perseus (v1.6.7.0, (Tyanova *et al.*, 2016) were utilized to perform all statistical and computational analyses. A generalized linear model combined to an asymptotic Wald test was applied to assess cell numbers in the ARC. Only p-values ≤ 0.05 were considered statistically significant. All results are shown as means ± SEMs.

4. Results

4.1. Hypercaloric diet consumption impacts the molecular inter-regional heterogeneity of astrocytes

4.1.1. The molecular profile of MACS-sorted astrocytes is influenced by their anatomical location rather than the diet

In order to unravel the impact of a long-term hypercaloric diet consumption on the molecular signature of astrocytes located in different brain areas, C57BL/6J male mice were exposed to a standard chow (SC) or a HFHS diet for 4 months, after which cortices, hypothalami, and hippocampi were rapidly dissected and dissociated into single-cell suspensions (**Figure 5A**). Astrocytes from the dissected brain areas were isolated via magnetic-activated cell sorting (MACS), by using the astrocyte cell surface antigen 2 (ACSA2) antibody, which targets the membrane protein ATPase Na^+/K^+ Transporting Subunit Beta 2 (ATP1B2), as previously described (Batiuk *et al.*, 2017; Kantzer *et al.*, 2017). Bulk RNA-seq and proteomics analyses were then performed on the samples obtained by MACS, using as negative control for proteomics the unlabeled fraction ($ACSA2^-$) of cells (**Figure 5A and B**). The evaluation of specific cell types enrichment in each fraction revealed that canonical astrocyte markers (*e.g. Aldh1l1*, *Aqp4*, *Gfap*, *Slc1a2*, *Slc1a3*) were highly enriched in $ACSA2^+$ cells, while almost undetectable in $ACSA2^-$ cells, as expected (**Figure 5B**). Conversely, neuronal (*e.g. Snap25*, *Syp*, *Syt1*, *Tubb3*), and microglia (*e.g. Aif1*, *Itgam*) specific molecular markers were highly enriched in $ACSA2^-$ cells, and almost absent in $ACSA2^+$ fractions (**Figure 5B**). Moreover, it was possible to observe that $ACSA2^+$ cells were also enriched with markers other than astrocyte-specific, such as oligodendrocyte- (*e.g. Mag*, *Mog*), and mural cells- (*e.g. Des*, *Mustn1*, *Pdgfrb*) specific, in transcriptome and proteome respectively (**Figure 5B**), in line with previous evidences reporting that the anti-ACSA2 antibody might also target neural stem cells and glial progenitors (Kantzer *et al.*, 2017). In order to define the degree of molecular similarity between $ACSA2^+$ astrocytes isolated from different brain areas of mice exposed to a SC or a HFHS diet, their transcriptome and proteome were analyzed by using principal component analysis (PCA) (**Figure 5C**). The PCA indicated that the anatomical location of $ACSA2^+$ astrocytes influences their expression profile in a higher degree than the exposure to different diets (**Figure 5C**). Therefore, the location of an astrocyte in the brain influences the expressional variance of its molecular phenotype.

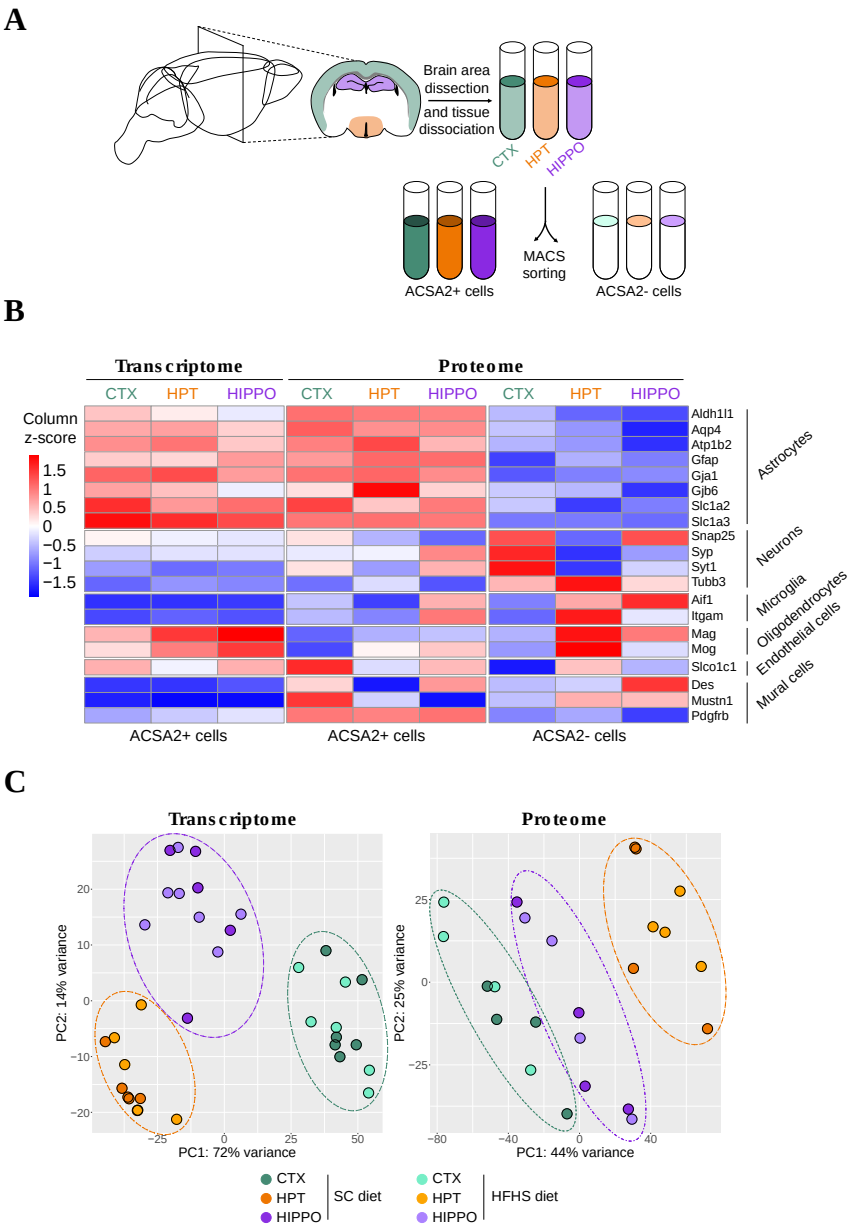

Figure 5: MACS-purified astrocytes show molecular similarities based on their anatomical location. (A) Schematic illustration summarizing the experimental procedure performed to selectively isolate ACSA2$^+$ astrocytes from cortex (CTX; jade-green), hypothalamus (HPT; orange), and hippocampus (HIPPO; purple) of mice fed with a SC or a HFHS diet for 4 months. After dissection and dissociation of the brain areas, the resulting cell suspensions were incubated with ACSA2 antibody, used to separate ACSA2$^+$ from ACSA2$^-$ cells via MACS. **(B)** Heatmap representing mean expression levels of canonical markers for CNS cell types in ACSA2$^+$ (transcriptomics and proteomics) and ACSA2$^-$ (proteomics) cells isolated from cortex, hypothalamus and hippocampus. Measurements are indicated as column z-scores. Per each condition, 4 (proteomics) or 5-7 (transcriptomics) samples were used, derived from mice fed with a SC or a HFHS diet for 4 months, and combined for the analysis. Per each sample, brain tissue derived from 2 (bulk RNA-Seq) or 4 (proteomics) mice was pooled together. **(C)** PCA plots of transcriptome and proteome datasets derived from ACSA2$^+$ astrocytes isolated from cortex, hypothalamus and hippocampus of mice fed with a SC or a HFHS diet for 4 months. Each sample is represented by one dot. All samples derived by one specific brain region are surrounded by a dashed circle. ACSA2: astrocyte cell surface antigen 2; *Aif1*: Allograft inflammatory factor 1; *Aldh1l1*: Aldehyde Dehydrogenase 1 family member L1; *Aqp4*: Aquaporin 4; *Atp1b2*: ATPase Na^+/K^+ Transporting Subunit Beta 2; CTX: cortex; *Des*: Desmin; *Gfap*: Glial Fibrillary Acidic Protein; *Gja1*: Gap Junction Protein Alpha 1; *Gjb6*: Gap Junction Protein Beta 6; HFHS: high-fat high-sugar; HIPPO:

hippocampus; HPT: hypothalamus; *Itgam*: Integrin Subunit Alpha M; MACS: magnetic-activated cell sorting; *Mag*: Myelin Associated Glycoprotein; *Mog*: Myelin Oligodendrocyte Glycoprotein; *Mustn1*: Musculoskeletal, Embryonic Nuclear Protein 1; PC: principal component; *Pdgfrb*: Platelet Derived Growth Factor Receptor Beta; SC: standard chow; *Slc1a2*: Solute Carrier Family 1 Member 2; *Slc1a3*: Solute Carrier Family 1 Member 3; *Slco1c1*: Solute Carrier Organic Anion Transporter Family Member 1 C1; *Snap25*: Synaptosome Associated Protein 25; *Syp*: Synaptophysin; *Syt1*: Synaptotagmin 1; *Tubb3*: Tubulin Beta 3 Class III.

4.1.2. MACS-sorted astrocytes from different brain areas display transcriptional heterogeneity in response to a HFHS diet

Considering the impact of the anatomical location of an astrocyte on its molecular signature, the next question was centered on exploring the extent to which an hypercaloric feeding could influence the transcriptional profile of astrocytes, and whether specific regions of the brain might be more affected than others. Therefore, the HFHS diet-induced transcriptional changes in ACSA2$^+$ astrocytes MACS-isolated from diverse brain regions were analyzed, and a total of 4727 differentially expressed genes (DEGs) between SC and HFHS diet groups was identified (**Figure 6A and B**; **Table 21**), 12 of which commonly expressed between cortex, hypothalamus and hippocampus (**Figure 6B**). Interestingly, HFHS diet had the major impact on the transcriptional signature of ACSA2$^+$ astrocytes located in the cortex (2514 non-overlapping DEGs), rather than in other brain regions (868 non-overlapping DEGs in the hypothalamus, and 563 in the hippocampus) (**Figure 6B**). Furthermore, the majority of the so-identified DEGs was down-regulated in cortex and hippocampus, and up-regulated in hypothalamus, following a HFHS diet exposure, in comparison to the control group (**Figure 6C**; **Table 21**).

Table 21: Total number of DEGs, divided between up- and down-regulated, identified comparing SC and HFHS diet groups in ACSA2$^+$ astrocytes isolated from different brain regions.

Brain Area	Total number of DEGs	Up-regulated	Down-regulated
CTX	2819	1309	1510
HPT	1150	581	569
HIPPO	758	270	488

In order to determine which molecular pathways in astrocytes located in diverse brain regions might be influenced by an hypercaloric diet, gene ontology (GO) enrichment analysis (**Figure 6D**) on the non-overlapping DEGs previously identified and hierarchically clustered (**Figure 6A-C**) was performed. Between the molecular pathways recognized with GO enrichment analysis, pathways of interest were selected and classified based on the biological roles they

are known to be involved in (**Figure 6D**). As previously mentioned, the majority of DEGs identified between SC and HFHS diet groups was down-regulated (**Figure 6C**; **Table 21**), such as cortices-derived astrocytic DEGs specifically involved in hormonal signaling regulation- ("*insulin receptor signaling pathway*," "*response to insulin*," and *"TOR signaling"*), metabolic stress- ("*response to endoplasmic reticulum stress*"), proliferation- ("*regulation of mitotic cell cycle*"), inflammation- ("*transforming growth factor beta receptor signaling pathway*," and "*I-kappaB kinase/NF-kappaB signaling*"), and microvasculature- ("*positive regulation of blood vessel endothelial cell migration*," and "*sprouting angiogenesis*") related pathways (**Figure 6D**). However, cortical DEGs involved in "*intracellular lipid transport*" pathway were mainly up-regulated (**Figure 6D**). Moreover, in hippocampal astrocytes, down-regulated DEGs were enriched in "*cell-matrix adhesion*," and *"regulation of angiogenesis"* pathways (**Figure 6D**). Finally, when analyzing the enrichment of DEGs identified in hypothalamic astrocytes, it was possible to observe that hypercaloric diet induced a remarkable up-regulation of glucose metabolism- ("*pyruvate metabolic process*"), lipid metabolism- ("*fatty acid metabolic process*," and "*fatty acid oxidation*"), and metabolic stress- ("*response to reactive oxygen species*") related pathways, while pathways involved in ECM and intercellular organization ("*regulation of cell junction assembly*"), neuronal and synaptic regulation ("*regulation of synapse structure or activity*," "*synaptic transmission, GABAergic*," and "*AMPA glutamate receptor clustering*") were majorly down-regulated (**Figure 6D**). Together, those data indicate a particular susceptibility of astrocytes to an hypercaloric diet, which differently influences the gene expression program of astrocytes located in specific brain areas.

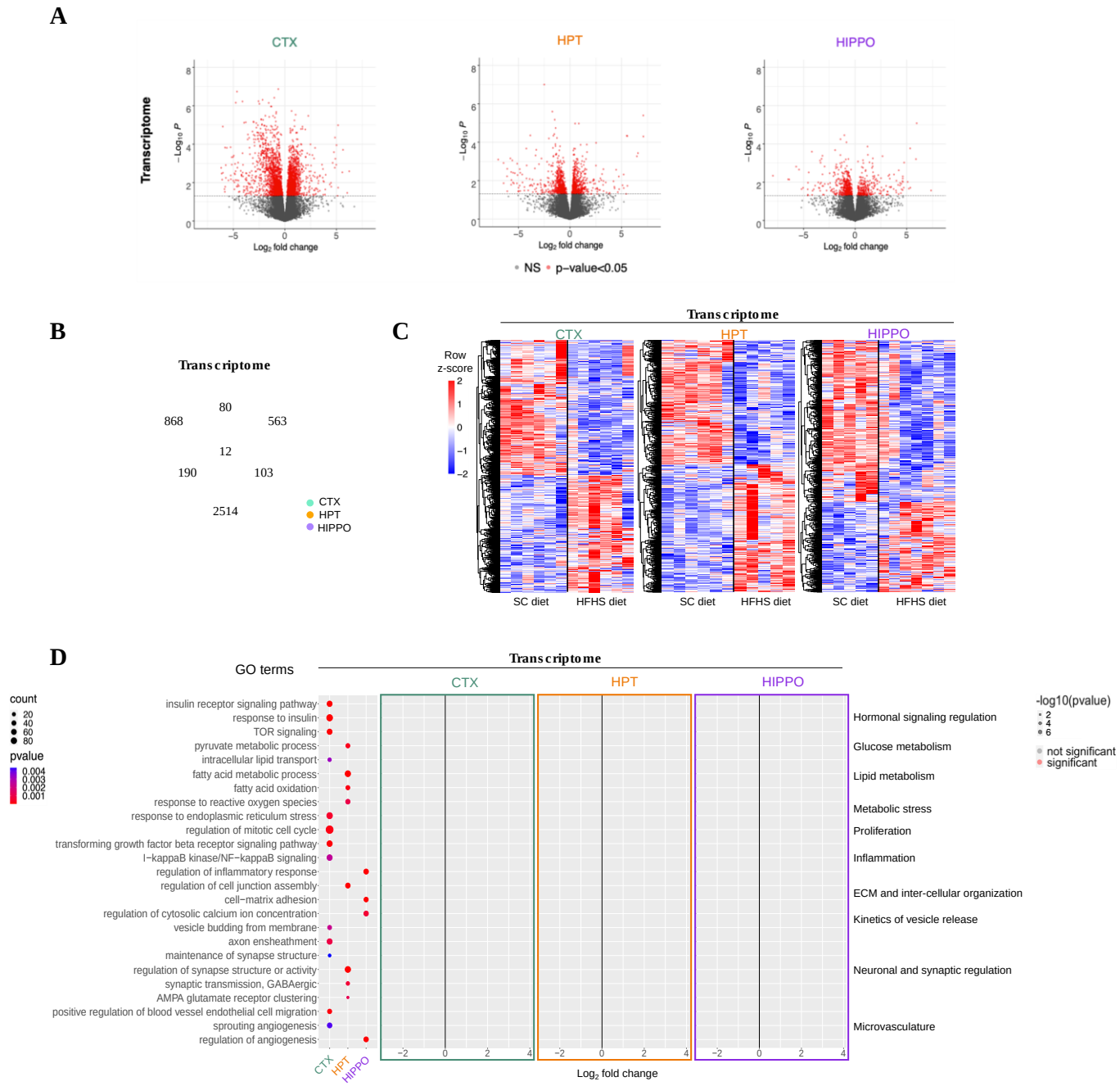

Figure 6: Hypercaloric diet induces transcriptional changes in MACS-sorted astrocytes from distinct brain regions. (A) Volcano plots indicate the differential expression of genes comparing ACSA2$^+$ astrocytes isolated from 4 months SC or HFHS diet fed mice, per each brain region. The $\log_2$ fold change (x-axis) is plotted against the -$\log_{10}$ p-value (y-axis). Genes are indicated in red when significant ($p < 0.05$), and in grey when not significant ($p > 0.05$). DEGs were identified with a two-group comparison Wald test. **(B)** Venn diagram indicates the number of DEGs ($p < 0.05$) identified in ACSA2$^+$ cells when comparing SC and HFHS diet groups in each brain area, and their unicity or overlap between cortex, hypothalamus and hippocampus. **(C)** Heatmaps depicting normalized counts derived from unsupervised clustering of DEGs ($p < 0.05$) identified per each brain region analyzed, when comparing the transcriptome of ACSA2$^+$ astrocytes isolated from SC or HFHS diet fed mice. Each column represents one sample, and SC or HFHS diet groups-derived samples are separated by a black line. Each replicate is formed by the combination of tissues derived from 2 mice. Row z-score normalized expression values are indicated in the color code. **(D)** Gene ontology (GO) enrichment analysis on DEGs identified in the comparison between SC and HFHS diet groups, per each brain area. Pathways of interest were manually selected. In the first panel on the left, the size of the dots represents

the number of DEGs enriched per each pathway, and the color the degree of statistical significance. The adjacent three panels on the right illustrate the significant ($p < 0.05$; in red) and not significant ($p > 0.05$; in grey) DEGs identified in each pathway. The x-axis corresponds to log_2 fold change. Each panel corresponds to one brain region. ACSA2: astrocyte cell surface antigen 2; CTX: cortex; DEGs: differentially expressed genes; ECM: extracellular matrix; GO: gene ontology; HFHS: high-fat high-sugar; HIPPO: hippocampus; HPT: hypothalamus; MACS: magnetic-activated cell sorting; NS: not significant; SC: standard chow.

4.1.3. Hypercaloric diet remarkably affects hypothalamic astrocytes at post-transcriptional level

Considering that the transcriptome levels not always precisely reflect the protein amount in a cell, and its associated biological functions (Liu, Beyer and Aebersold, 2016; Buccitelli and Selbach, 2020), the effect of a calorie-rich diet on the post-transcriptional profile of astrocytes located in different brain regions was evaluated, in order to assess whether it mirrors the observed transcriptional gene regulation changes. For this reason, using a similar approach as described above, differentially expressed proteins (DEPs) between astrocytes derived from mice fed with a SC or a HFHS diet were identified and compared between diverse brain regions (**Figure 7A and B**). None of the so-identified DEPs were common between all three brain areas analyzed (0 of 689 DEPs; **Figure 7B**), while 447 unique DEPs in the hypothalamus, 92 in the cortex, and 124 in the hippocampus were detected (**Figure 7B**). In line with transcriptomics analysis, the majority of DEPs identified comparing the proteome of astrocytes derived from mice fed with a SC or a HFHS diet was down-regulated in all brain regions under analysis (**Figure 7C; Table 22**).

Table 22: Total number of DEPs, divided between up- and down-regulated, identified comparing SC and HFHS diet groups in $ACSA2^+$ astrocytes isolated from different brain regions.

Brain Area	Total number of DEPs	Up-regulated	Down-regulated
CTX	102	28	74
HPT	456	205	251
HIPPO	131	36	95

Successively, GO enrichment analysis was performed specifically on the non-overlapping DEPs previously identified, and metabolically relevant pathways manually selected (**Figure 7C and D**). The analysis showed that astrocytes derived from cortex were enriched with DEPs mostly up-regulated in glucose metabolism- ("*cellular response to glucose stimulus*") and metabolic stress- ("*response to reactive oxygen species*") related pathways, and mostly down-

regulated in "*positive regulation of G1/S transition of mitotic cell cycle*" pathway (**Figure 7D**). Furthermore, hypercaloric diet induced mainly a down-regulation of the DEPs identified in hippocampal astrocytes, which were enriched in pathways involved in glucose metabolism ("*cellular carbohydrate metabolic process*"), kinetics of vesicle release ("*calcium ion transport into cytosol*"), and neuronal and synaptic regulation ("*axon guidance*") (**Figure 7D**). Interestingly, HFHS diet exposure predominantly influenced hypothalamic astrocytes at proteome level, in comparison to astrocytes isolated from cortex or hippocampus, as shown by the number of DEPs identified, and their enrichment in several crucial pathways (**Figure 7B and D**). In particular, the DEPs in hypothalamic astrocytes were primarily up-regulated in pathways associated with hormonal signaling regulation ("*leptin-mediated signaling pathway,*" and "*response to leptin*"), lipid metabolism ("*fatty acid catabolic process*"), inflammation ("*positive regulation of inflammatory response*"), and mostly down-regulated in glucose metabolism- ("*glycogen metabolic process,*" and "*glucose transmembrane transport*"), kinetics of vesicle release- ("*calcium-mediated signaling*"), neuronal and synaptic regulation- ("*regulation of neurotransmitter levels,*" "*glutamate receptor signaling pathway,*" and "*regulation of neuronal synaptic plasticity*") related pathways (**Figure 7D**). Given the differences observed between HFHS diet-induced transcriptomic and proteomic expression changes in cortical, hippocampal, and hypothalamic astrocytes, a correlation analysis between the two datasets was performed (**Figure 7E**). However, it was not possible to detect a significant correlation between the transcripts and related proteins (**Figure 7E**), phenomenon which has been already described along the literature, and currently under debate (de Sousa Abreu *et al.*, 2009; Payne, 2015). Together, those findings indicate that long-term exposure to a HFHS diet affects the inter-regional molecular heterogeneity of astrocytes, with the most remarkable changes in the proteome of hypothalamic astrocytes, and particularly in pathways involved in the regulation of hormonal and nutritional signaling.

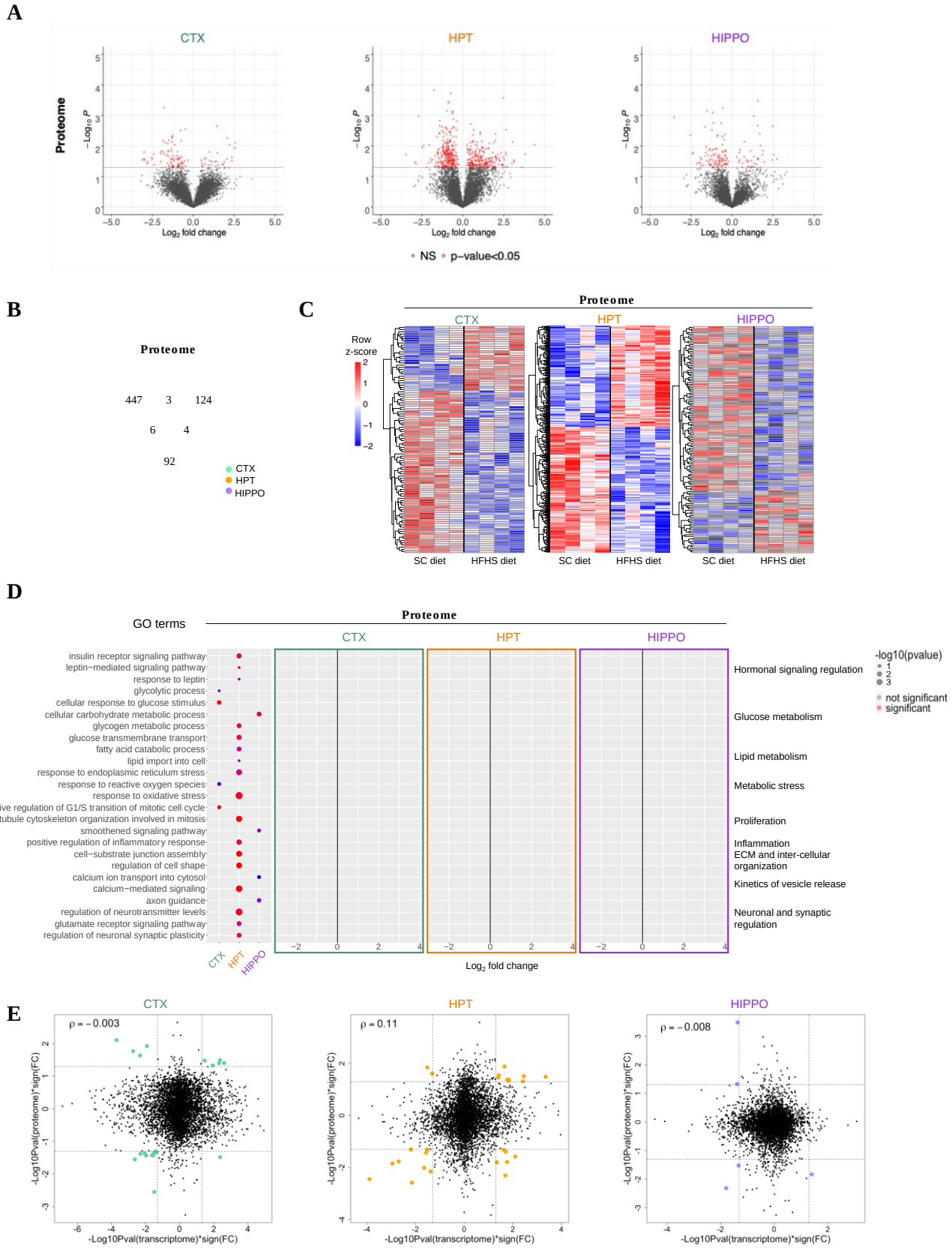

Figure 7: Hypercaloric diet induces post-transcriptional changes in MACS-sorted astrocytes from distinct brain regions. (A) Volcano plots indicate the DEPs identified comparing ACSA2^{+} astrocytes derived from 4 months SC or HFHS diet fed mice, per each brain region. The $\log_2$ fold change (x-axis) is plotted against the -$\log_{10}$ p-value (y-axis). Significant DEPs are indicated in red ($p < 0.05$), while not

significant DEPs are shown in grey ($p > 0.05$). P values for differential protein expression were analyzed by Student's *t*-test. **(B)** Venn diagram indicates the number of DEPs ($p < 0.05$) between SC and HFHS diet groups in cortical, hypothalamic and hippocampal astrocytes, and their overlap or unicity. **(C)** Heatmaps represent normalized proteome intensity values derived from unsupervised clustering of DEPs ($p < 0.05$) identified in cortex, hypothalamus, and hippocampus, when comparing the proteome of $ACSA2^+$ astrocytes from SC or HFHS diet fed animals. Each column indicates one sample, each one composed by $ACSA2^+$ astrocytes derived from 4 animals. The color code illustrates row z-score normalized expression values. A black line separates samples derived from SC or HFHS diet fed mice. **(D)** Gene ontology (GO) enrichment analysis on DEPs ($p < 0.05$) identified in the comparison between $ACSA2^+$ astrocytes derived from SC and HFHS diet groups. Pathways of interest were manually selected. In the first panel on the left, the size of the dots represents the number of DEPs, and the color the degree of significance. The adjacent three panels illustrate the significant ($p < 0.05$; in red) and not significant ($p > 0.05$; in grey) DEPs identified in each pathway. The x-axis corresponds to $\log_2$ fold change. Each panel corresponds to one brain region. **(E)** Correlation analysis between transcriptome and proteome derived from $ACSA2^+$ cells isolated from cortex, hypothalamus and hippocampus. The transcriptome is plotted against $-\log_{10}$(p-value) multiplied with sign of the fold change of proteins. The significant genes are represented in red ($p < 0.05$). The Spearman's rank correlation coefficient is indicated in the top left corner of each plot. ACSA2: astrocyte cell surface antigen 2; CTX: cortex; DEPs: differentially expressed proteins; ECM: extracellular matrix; FC: fold change; GO: gene ontology; HFHS: high-fat high-sugar; HIPPO: hippocampus; HPT: hypothalamus; MACS: magnetic-activated cell sorting; NS: not significant; SC: standard chow; ρ: Spearman correlation coefficient.

4.2. Hypercaloric diet consumption impacts the molecular and spatial profile of astrocytes located in the ARC

4.2.1. ARC astrocytes respond to hypercaloric diet in a fast, but transient manner

Given the above described evidences showing that astrocytes respond differently to a HFHS diet according to their location in the brain, with the most remarkable changes at proteome level in the hypothalamus, the question which arouse next is whether an hypercaloric diet might induce distinct molecular behaviors in astrocytes located within the same brain area. Considering that the ARC is a crucial player in the control of systemic energy metabolism, in which astrocytes play a main role (Jais and Brüning, 2021; González-García and García-Cáceres, 2021), the HFHS diet-induced transcriptomics changes over time in ARC-derived cells were investigated.

The selected timepoints for the analysis were 5 and 15 days (d) of a HFHS diet feeding, considering that the body weight (BW) of mice exposed to a HFHS diet for 15d significantly increases compared to SC diet fed animals (Gruber *et al.*, 2021), while a shorter exposure to an hypercaloric diet leads to the activation of hypothalamic inflammatory pathways and reactive gliosis before a substantial BW gain (Thaler *et al.*, 2012). For all those reasons, single-cell RNA sequencing (scRNA-Seq) was performed on the entirety of cells isolated from the ARC (19995

cells analyzed after filtering from initial 21143 cells, of which SC diet = 6741 cells; 5d HFHS diet = 5886 cells; 15d HFHS diet = 7368 cells; per each cell, a median of 1802 unique transcripts was found). Successively, the cells were mapped into 14 different clusters by unsupervised Leiden clustering (**Figure 8A**), and their identity was assessed based on the expression of brain cell type-specific molecular markers (**Figure 8A-C**). The so-identified clusters included neuronal (*Rbfox3, Snap25, Syp, Syt1, Tubb3*; 3322 cells; clusters 3 and 8), and non-neuronal cells (16673 cells). The last consisted of astrocytes (*Aldh1l1, Aqp4, Atp1b2, Gfap, Gja1, Gjb6, Slc1a2, Slc1a3*; 3921 cells; cluster 0), microglia (*Aif1, Csf1r, Cx3cr1, Itgam, P2ry12, Tmem119*; 2289 cells; clusters 6 and 9), oligodendrocytes (*Mag, Mog, Olig1*; 2360 cells; clusters 5, 7, 10, 13), mural cells (*Des, Mustn1, Pdgfrb*; 515 cells; cluster 11), endothelial cells (*Cldn5, Pecam1, Slco1c1*; 1466 cells; cluster 4), vascular and leptomeningeal cells (VLMCs; *Col1a1, Col3a1, Lum*; 109 cells; cluster 12), and ependymal cells (*Ccdc153, Hdc, Rarres2, Tm4sf1*; 4933 cells; clusters 1 and 2) of which tanycytes occupied cluster 1 (*Adm, Col23a1, Crym, Lhx2, Rax, Slc16a2*; 2547 cells) (**Figure 8A-C**). Interestingly, canonical astrocytic markers were enriched in clusters 0, 1, and 2, with the strongest expression in cluster 0; however, ependymal cells well-known molecular markers were not highly present in cluster 0, which was thence defined as "astrocyte specific" (**Figure 8B**). Next, the estimation of the number of DEGs per each ARC cell population after 5d or 15d of a HFHS diet exposure in comparison to the SC diet fed group identified astrocytes as the cell type with the highest number of DEGs after 5d HFHS diet feeding (mostly up-regulated), drastically reduced after 15d HFHS diet exposure (**Figure 8D and E**). Aside astrocytes, all ARC cell types showed the highest number of DEGs after 15d HFHS diet, which were mostly down-regulated (**Figure 8D and E**). However, hypercaloric diet did not particularly affect microglia and mural cells at the analyzed timepoints (**Figure 8D and E**). Interestingly, the two cell types with the highest number of DEGs after 5d HFHS diet exposure, astrocytes and neurons, exhibited a poor number of DEGs commonly expressed after exposure to both 5d (unique neuronal DEGs: 246 up-, 1 down- regulated; unique astrocytic DEGs: 643 up-, 9 down- regulated; common DEGs: 136 up-, 0 down- regulated) and 15d HFHS diet (unique neuronal DEGs: 5 up-, 1403 down- regulated; unique astrocytic DEGs: 25 up-, 21 down- regulated; common DEGs: 7 up-, 47 down-regulated) (**Figure 8F**). Together, those data indicate that hypercaloric diet differently influences the gene expression of specific ARC cell-types in a time-dependent manner, with astrocytes showing a distinct transcriptomic response, compared to the surrounding cells. In particular, 5d of exposure to a HFHS diet are sufficient to induce relevant, but transient,

transcriptomic modifications in ARC astrocytes, which are lost after a longer HFHS diet exposure time (15d).

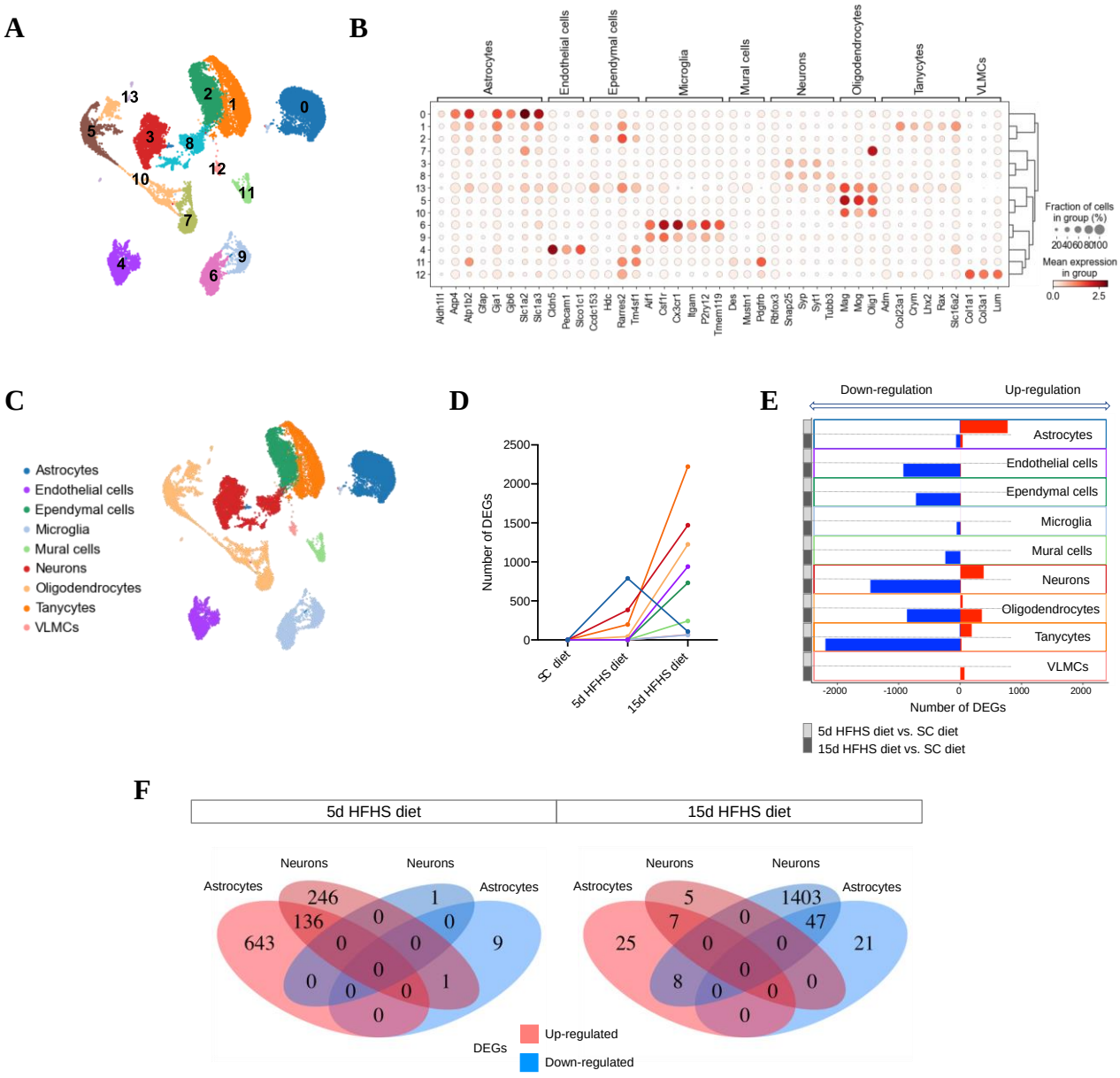

Figure 8: Hypercaloric diet induces time-dependent molecular changes in specific ARC cell types. **(A)** UMAP plot realized on the complete scRNA-Seq dataset, which includes all diet groups (19,995 cells analyzed, of which SC diet = 6741; 5d HFHS diet: 5886; 15d HFHS diet: 7368), with annotated Leiden clusters superimposed. Each diet group is composed by the cells obtained from the dissection of 6 ARCs. Per each cell, a median of 1802 unique transcripts was detected. P values for differential expression analysis were determined by two-tailed Student's t-test. **(B)** The 14 clusters identified in (A) are plotted against canonical markers for CNS-specific cell types. The color scale per each dot represents the mean expression degree of the gene of interest per cluster, and the size of each dot indicates the proportion of cells expressing the gene analyzed. **(C)** UMAP plot in (A) colored according to the cell types identified in (B). **(D)** Graph showing the number of DEGs (adjusted $p < 0.05$) identified comparing SC diet group with 5d or 15d HFHS diet groups per each cell type. **(E)** Plot describing the number of the DEGs identified in (D) which are up- (red) or down- (blue) regulated, per each cell type. The squares on the left are colored in light grey when indicating the DEGs identified comparing 5d HFHS diet and

SC diet groups, while in dark grey when the DEGs derive from the comparison between 15d HFHS diet and SC diet groups. **(F)** Venn diagrams indicating the number of common or unique up- (pink) and down- (light blue) regulated DEGs between SC diet and 5d or 15d HFHS diet groups, between astrocytes and neurons. 5d: 5 days; 15d: 15 days; *Adm*: Adrenomedullin; *Aif1*: Allograft inflammatory factor 1; *Aldh1l1*: Aldehyde Dehydrogenase 1 family member L1; *Aqp4*: Aquaporin 4; *Atp1b2*: ATPase Na^+/K^+ Transporting Subunit Beta 2*; Ccdc153*: Coiled-Coil Domain Containing 153; *Cldn5*: Claudin 5; *Col1a1*: Collagen Type I Alpha 1 Chain; *Col3a1*: Collagen Type III Alpha 1 Chain; *Col23a1*: Collagen Type XXIII Alpha 1 Chain; *Crym*: Crystallin Mu; *Csf1r*: Colony stimulating factor 1 receptor; *Cx3cr1*: C-X3-C Motif Chemokine Receptor 1; DEGs: differentially expressed genes; *Des*: Desmin; *Gfap*: Glial Fibrillary Acidic Protein; *Gja1*: Gap Junction Protein Alpha 1; *Gjb6*: Gap Junction Protein Beta 6; *Hdc*: Histidine Decarboxylase; HFHS: high-fat high-sugar; *Itgam*: Integrin Subunit Alpha M; *Lhx2*: LIM Homeobox 2; *Lum*: Lumican; *Mag*: Myelin Associated Glycoprotein; *Mog*: Myelin Oligodendrocyte Glycoprotein; *Mustn1*: Musculoskeletal, Embryonic Nuclear Protein 1; *Olig1*: Oligodendrocyte Transcription Factor 1; *P2ry12*: Purinergic Receptor P2Y12; *Pdgfrb*: Platelet Derived Growth Factor Receptor Beta; *Pecam1*: Platelet And Endothelial Cell Adhesion Molecule 1; *Rarres2*: Retinoic Acid Receptor Responder 2; *Rax*: Retina And Anterior Neural Fold Homeobox; *Rbfox3*: RNA Binding Fox-1 Homolog 3; SC: standard chow; *Slc1a2*: Solute Carrier Family 1 Member 2; *Slc1a3*: Solute Carrier Family 1 Member 3; *Slc16a2*: Solute Carrier Family 16 Member 2; *Slco1c1*: Solute Carrier Organic Anion Transporter Family Member 1 C1; *Snap25*: Synaptosome Associated Protein 25; *Syp*: Synaptophysin; *Syt1*: Synaptotagmin 1; *Tm4sf1*: Transmembrane 4 L Six Family Member 1; *Tmem119*: Transmembrane Protein 119; *Tubb3*: Tubulin Beta 3 Class III; UMAP: uniform manifold approximation and projection; VLMCs: vascular leptomeningeal cells.

4.2.2. HFHS diet impacts the transcriptional dynamics of ARC astrocytes in a time-dependent manner

Considering the dynamic changes in the transcriptome of ARC astrocytes in response to a 5d and a 15d HFHS diet exposure, the kinetics of gene expression in ARC astrocytes at the two selected timepoints were additionally investigated. In particular, the astrocyte cluster in each diet condition was further divided into sub-clusters by firstly applying uniform manifold approximation and projection (UMAP), and secondly Leiden clustering (**Figure 9A**). The so-identified astrocyte sub-clusters in SC diet group were four (named *a*, *b*, *c*, and *d*), such as in 15d HFHS diet group (named *0*, *1*, *2*, and *3*), while in 5d HFHS diet group three sub-clusters were found (named *0*, *1*, and *2*) (**Figure 9A**). However, in sub-cluster *3* only 15 cells were present, therefore it was not considered in the following analyses. The sub-clusters *0*, *1*, and *2* showed a considerable similarity between the two HFHS diet groups, and a clear difference with the sub-clusters *a*, *b*, *c*, and *d* in SC diet (**Figure 9A**). In particular, after the exposure to a HFHS diet, the sub-cluster *a* followed a division into sub-clusters *0* and *1*, whereas the three sub-clusters *b*, *c*, and *d* were merged into sub-cluster *2* (**Figure 9A**). Considering this intriguing observation, RNA velocity analysis (Bergen *et al.*, 2020; La Manno *et al.*, 2018) was performed on the above-identified astrocyte sub-clusters, in order to understand how the shift in the clustering between SC diet and HFHS diet groups takes place, and whether it might be explained by changes in the transcriptional activity of ARC astrocytes. Interestingly, the RNA

velocity in ARC astrocytes isolated from SC diet-fed mice was undirected and unsynchronized, similarly to ARC astrocytes derived from the 15d HFHS diet-fed group (**Figure 9A**). On the contrary, the RNA velocity was synchronized in ARC astrocytes isolated from 5d HFHS diet-fed mice, exhibiting several directed flows, the major of which with two origin points in sub-clusters *0* and *1*, terminating in two specific areas in sub-clusters *1* and *2* (**Figure 9A**). This was consistent with the transcriptional activity determined by the number of DEGs in astrocytes, which increased after the exposure to a 5d HFHS diet, and reversed to similar levels as in SC diet-fed mice after 15d HFHS diet feeding (**Figure 8D and E**). Of note, when comparing the relative number of cells between 5d and 15d HFHS diet-fed mice, it was possible to observe that it doubled in sub-cluster *1* (from 15.2% in 5d HFHS diet group to 31.3% in 15d HFHS diet group), and it almost halved in sub-cluster *0* (from 22.7% in 5d HFHS diet group to 12.2% in 15d HFHS diet group) (**Figure 9A**). Finally, the potential driver genes of these transcriptional dynamics were identified per each sub-cluster of ARC astrocytes, and then ordered by the inferred latent time (**Figure 9B**), as previously described (Bergen *et al.*, 2020). Among them, crucial genes for the function of astrocytes and for their role in the control of metabolism were further analyzed, by evaluating their sub-cluster-wise expression at the investigated timepoints (**Figure 9B and C**). For example, cells belonging to sub-cluster *a* in SC diet group actively expressed the driver genes *Aldoc* (critical for glucose metabolism) and *Pcsk1n* (involved in the regulation of hormonal signaling) (**Figure 9C**). Moreover, cells belonging to sub-clusters *0* and *1* in both HFHS diet groups actively expressed *ApoE*, *Clu* (crucial role in lipid metabolism), *Gfap* (astrocyte reactivity), *Ucp2* (involved in mitochondrial dynamics), *Vamp5* (vesicle dynamics), and *Ift43* (ciliary transport) (**Figure 9C**). Together, these data reveal that the transcriptional activation of ARC astrocytes depends on the time of a HFHS diet exposure, with a prominent response after 5d, which reverses to physiological-like levels after 15d of an hypercaloric feeding. Moreover, the transcriptional changes resulting from 5d HFHS diet feeding diversely affect specific subpopulations of ARC astrocytes, which actively express individual driver genes at different levels in a time-dependent manner.

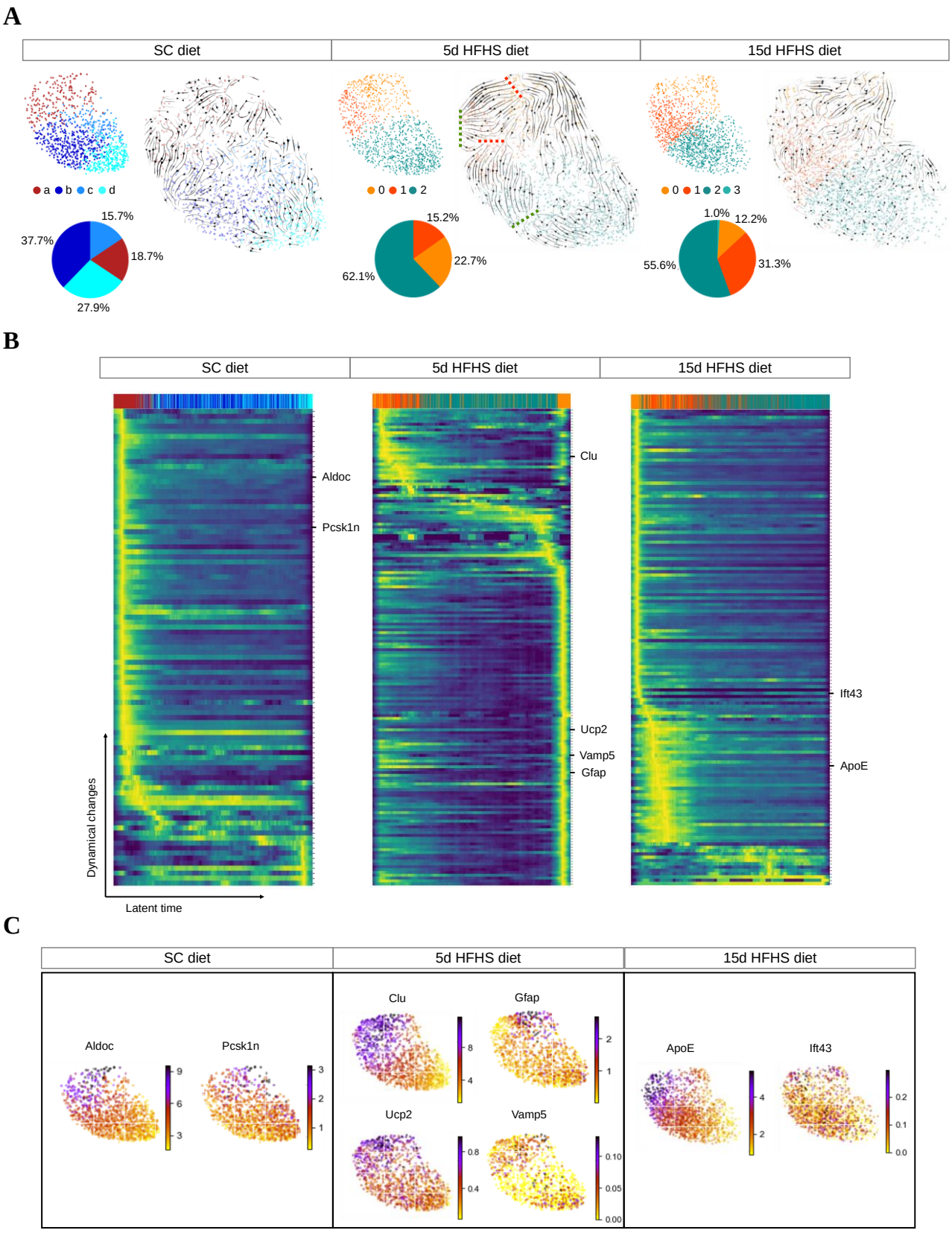

Figure 9: The HFHS diet-induced transcriptional activation of ARC astrocytes is time-dependent. **(A)** Per each diet group, the UMAP plot with Leiden clustering of astrocyte cluster is shown. RNA velocity analysis is superimposed on the UMAP plots, with the red dashed lines indicating the points of origin, and the green dashed lines the terminal areas of the RNA velocity flows. At the bottom left of each UMAP plot, a pie chart represents the relative number (in percentage) of cells belonging to each

sub-cluster, whose absolute numbers are as it follows: SC diet: *a* = 210; *b* = 424; *c* = 176; *d* = 314; 5d HFHS diet: *0* = 282; *1* = 189; *2* = 772; 15d HFHS diet: *0* = 189; *1* = 468; *2* = 864; *3* = 15. **(B)** Per each diet group, the expression of potential driver genes of RNA velocity is plotted against the inferred latent time and represented by a heatmap. The association between the driver genes expression and the relative sub-cluster identity is represented in the color code at the top of the heatmaps. The position on each heatmap of selected genes of interest involved in astrocyte function and in the metabolic control is highlighted on the right side of each plot. **(C)** The active expression of the potential driver genes selected in (B) is illustrated by UMAP plots, which are divided by the analyzed diet groups. 5d: 5 days; 15d: 15 days; *Aldoc*: Fructose-bisphosphate aldolase C; *ApoE*: Apolipoprotein E; *Clu*: Clusterin; *Gfap*: Glial Fibrillary Acidic Protein; HFHS: high-fat high-sugar; *Ift43*: Intraflagellar Transport 43; *Pcsk1n*: Proprotein Convertase Subtilisin/Kexin Type 1 Inhibitor; SC: standard chow; *Ucp2*: Uncoupling Protein 2; UMAP: uniform manifold approximation and projection; *Vamp5*: Vesicle Associated Membrane Protein 5.

4.2.3. The time of a HFHS diet exposure differently influences the expression pattern of Aldh1L1 and GFAP in the ARC

As widely explained in paragraph 1.1.4, astrocytes express a range of specific molecular markers, of which GFAP is the most well-known. Considering that GFAP expression has been reported to change in response to particular physiological or pathological states (Pekny and Pekna, 2014), the putative effect of a HFHS diet on the expression of astrocyte-specific molecular markers in the ARC has been investigated. In particular, the question was directed on unraveling whether the HFHS diet-induced modifications in the transcriptional activity of ARC astrocytes described above might also concern the expression of astrocyte canonical markers. Therefore, the HFHS diet-induced expression of selected astrocyte-specific molecular markers was analyzed at single-cell resolution in the astrocyte cluster, where no distinct sub-clusters were observed, indicating that the mere expression of astrocyte-enriched markers is not sufficient to determine individual subpopulations of cells (**Figure 10A**). Interestingly, although Aldh1L1 has been described as expressed in the majority of astrocytes (Cahoy *et al.*, 2008), its expression level along the astrocyte cluster in all three diet conditions was rather poor and similar to GFAP, compared to all the other markers selected (**Figure 10A**). Moreover, the exposure to 5d HFHS diet affected the number of cells expressing Aldh1L1 (36.3%) and GFAP (19.3%) in a higher amount than the other molecular markers, such as *Aqp4*, *Atp1b2*, *Gja1*, *Gja6*, *Slc1a2*, and *Slc1a3* (10-15%) (**Figure 10B**). On the contrary, the increase of the number of cells expressing Aldh1L1 (7%) and GFAP (1.5%) was lower than the other selected markers after 15d HFHS diet (25-30%) (**Figure 10B**).

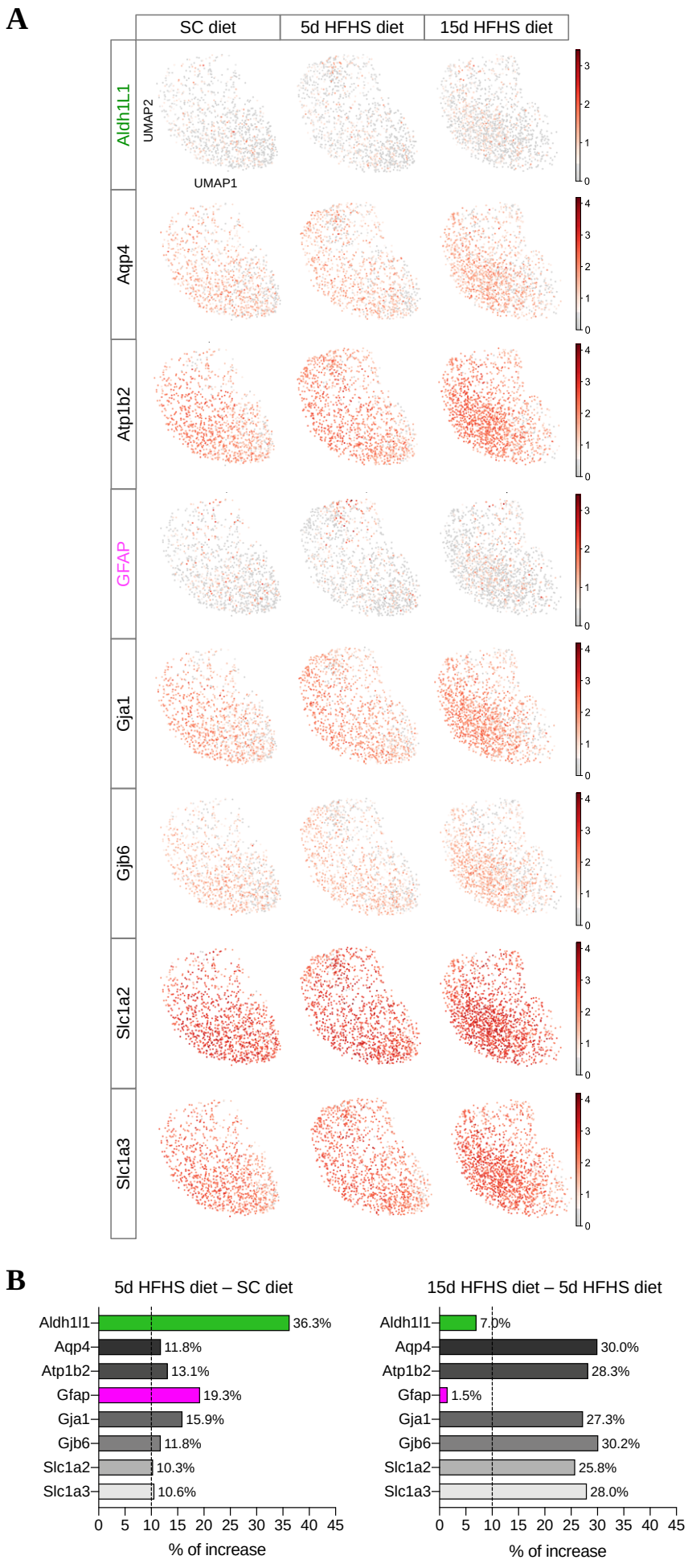
A
SC diet
5d HFHS diet
15d HFHS diet
Aldh1L1
Aqp4
Atp1b2
GFAP
Gja1
Gjb6
Slc1a2
Slc1a3
UMAP2
UMAP1
B
5d HFHS diet – SC diet
Aldh1l1 36.3%
Aqp4 11.8%
Atp1b2 13.1%
Gfap 19.3%
Gja1 15.9%
Gjb6 11.8%
Slc1a2 10.3%
Slc1a3 10.6%
0 5 10 15 20 25 30 35 40 45
% of increase
15d HFHS diet – 5d HFHS diet
Aldh1l1 7.0%
Aqp4 30.0%
Atp1b2 28.3%
Gfap 1.5%
Gja1 27.3%
Gjb6 30.2%
Slc1a2 25.8%
Slc1a3 28.0%
0 5 10 15 20 25 30 35 40 45
% of increase

Figure 10: Different times of exposure to a HFHS diet diversely influence the expression of astrocyte-specific molecular markers. (A) The UMAP plots show the expression of selected astrocyte-specific canonical markers along the cluster identified as "astrocyte" in scRNA-Seq dataset. The plots are divided per marker and per diet condition. **(B)** The bar plots indicate the increase (in percentage) of the number of cells expressing the astrocyte-specific molecular markers selected within the astrocyte cluster identified in the scRNA-Seq dataset. The graph on the left shows the percentage of increase of the number of cells after the exposure to a 5d HFHS diet, compared to a SC diet, while the plot on the right shows the percentage of increase of the number of cells after 15d HFHS diet feeding, in comparison to 5d HFHS diet. The minor percentage increase of the cell numbers observed in the first plot on the left is indicated by a dashed line (10%). The bars describing the percentage of increase of Aldh1L1- and GFAP- expressing cells are shown in green and magenta respectively, as they represent the molecular markers impacted the most and the least by a HFHS diet exposure for 5d and 15d respectively. 5d: 5 days; 15d: 15 days; *Aldh1l1*: Aldehyde Dehydrogenase 1 family member L1; *Aqp4*: Aquaporin 4; *Atp1b2*: ATPase Na^+/K^+ Transporting Subunit Beta 2; *Gfap*: Glial Fibrillary Acidic Protein; *Gja1*: Gap Junction Protein Alpha 1; *Gjb6*: Gap Junction Protein Beta 6; HFHS: high-fat high-sugar; SC: standard chow; *Slc1a2*: Solute Carrier Family 1 Member 2; *Slc1a3*: Solute Carrier Family 1 Member 3; UMAP: uniform manifold approximation and projection.

Considering the interesting difference in the HFHS diet-induced RNA level changes of Aldh1L1 and GFAP in comparison to the other astrocyte-specific molecular markers in the ARC, a confirmation of such a molecular response was further investigated at the protein level. In particular, the quantitative assessment of the HFHS diet-induced response of Aldh1L1- and GFAP- expressing astrocytes in the ARC was performed by using a transgenic mouse model, the Aldh1L1-CreER^{T2}::Sun1-sfGFP line, which derived from the crossing of Aldh1L1-CreER^{T2} mice (Winchenbach *et al.*, 2016) with Sun1-sfGFP tagged mice. The rationale behind the use of this particular mouse model consists in the fact that it allows to clearly identify Aldh1L1-expressing cells, as the green fluorescent protein (GFP) is expressed within their nucleus; the identification might otherwise be problematic because of the poor efficacy of the commercially available anti-Aldh1L1 antibodies for immunohistochemistry. Therefore, after feeding the animals with a SC or a HFHS diet, tamoxifen was injected to induce the Cre-dependent GFP expression specifically in the nuclei of Aldh1L1$^+$ cells, which number in the ARC was then quantified. Interestingly, the total number of astrocytes expressing Aldh1L1 in the ARC significantly increased after both 5d and 15d of exposure to a HFHS diet, in comparison to a SC diet (**Figure 11A and B**). However, the number of Aldh1L1$^+$ cells in the ARC significantly diminished from 5d to 15d of feeding with a HFHS diet (**Figure 11A and B**). A similar result was observed at the RNA level, as the number of cells positive for Aldh1L1-RNA in the ARC of wildtype mice increased after 5d HFHS diet feeding compared to SC diet fed animals, and decreased from 5d to 15d of exposure to a HFHS diet (**Figure 11C-E**). Nevertheless, the HFHS diet-induced increase in the number of Aldh1L1$^+$ cells in the ARC was not associated to a pro-

proliferative profile, as the number of Aldh1L1-expressing astrocytes in a mitotic stage was close to zero in all diet conditions (**Figure 11F and G**).

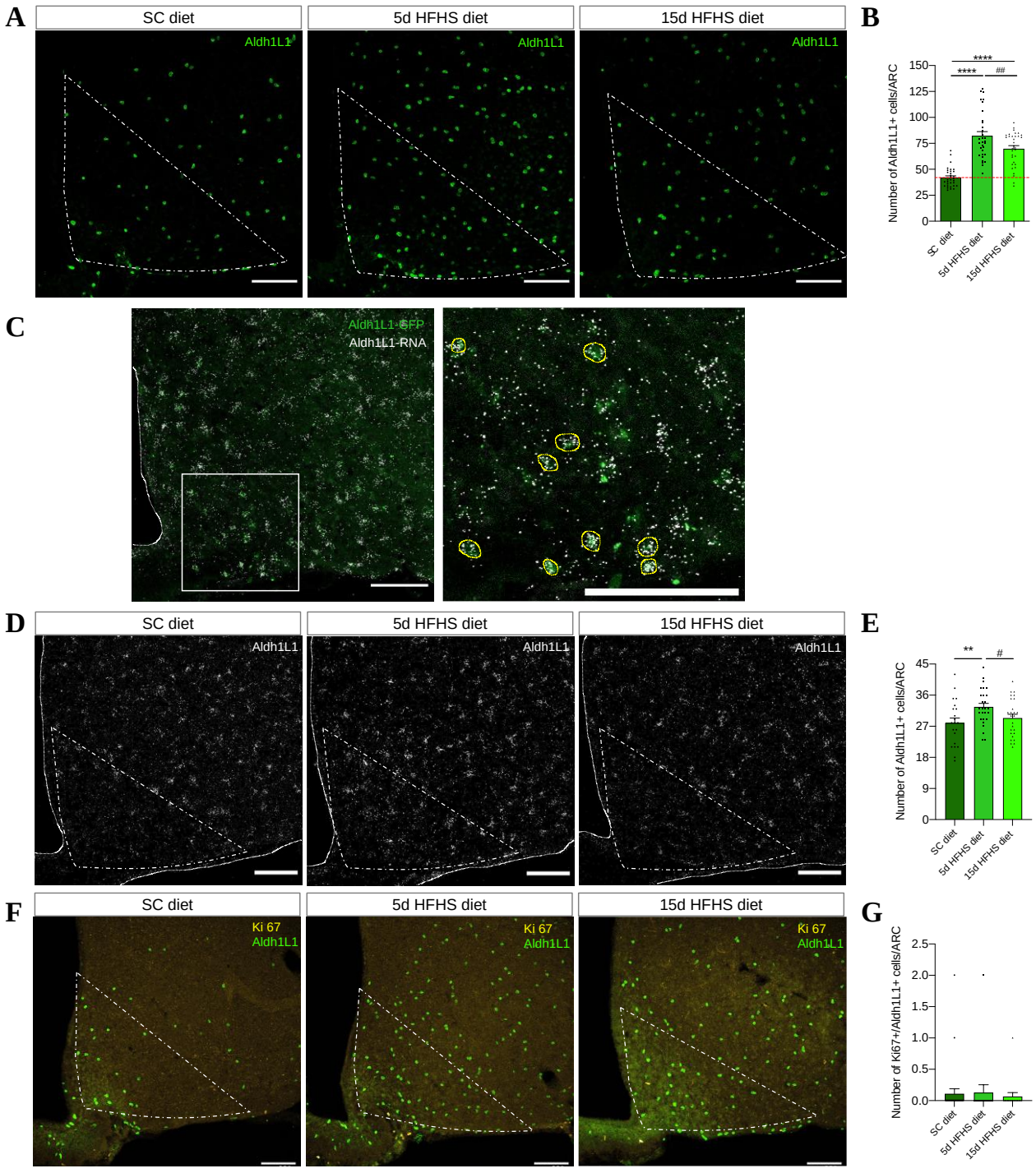

Figure 11: The number of Aldh1L1-expressing astrocytes in the ARC increases in a non-proliferative manner after the exposure to a HFHS diet. (A) Representative pictures of GFP-expressing nuclei in Aldh1L1^{+} cells (green) in the ARC (segmented triangle-shaped white line with an area of approximately 105350 µm^{2}) of Aldh1L1-CreER^{T2}::Sun1-sfGFP mice fed with a SC or a HFHS diet for 5 and 15 days. Scale bar: 100 µm. **(B)** Quantitative analysis of the number of Aldh1L1^{+} cells in the ARC of the Aldh1L1-CreER^{T2}::Sun1-sfGFP mice represented in **(A)** in each diet condition analyzed.

The segmented red line indicates the number of Aldh1L1$^+$ cells in SC diet-fed control mice. In each diet group, n = 32 (ARCs derived from 4 animals). ##p = 0.005; ****p < 0.0001. **(C)** Representative image (left) and detail enclosed in the white square enlarged (right) showing the co-localization (yellow circles) between the GFP (green) in the nuclei of Aldh1L1-expressing cells and the Aldh1L1-RNA (white) in SC diet-fed Aldh1L1-CreER^{T2}::Sun1-sfGFP mice. Scale bars = 100 μm. **(D)** Representative images of the Aldh1L1-RNA (white) expression in the ARC of wildtype mice fed with a SC or a HFHS diet for 5 and 15 days. The ARC is defined by a segmented white line and it has an area of approximately 105350 μm^2. Scale bar = 100 μm. **(E)** Bar plot depicting the 5d or 15d HFHS diet-induced changes in the number of cells positive for Aldh1L1-RNA in the ARC of the wildtype mice represented in **(D)**. N = 21 (SC diet; from 4 mice); n = 27 (5d HFHS diet; from 5 mice); n = 26 (15d HFHS diet; from 5 mice). **p = 0.0059; #p = 0.0355. **(F)** Representative pictures showing the co-localization between GFP expression (green) in the nuclei of Aldh1L1-expressing cells and anti-ki67 antibody (yellow) in the ARC (area of approximately 105350 μm^2 enclosed in the segmented triangle-shaped white line) of Aldh1L1-CreER^{T2}::Sun1-sfGFP mice fed with a SC or a HFHS diet for 5 and 15 days. Scale bar: 100 μm. **(G)** Bar plot indicating the number of Aldh1L1-expressing cells positive for ki67 in the ARC of the Aldh1L1-CreER^{T2}::Sun1-sfGFP mice represented in **(F)**. N = 28 (SC diet; from 7 animals); n = 16 (5d and 15d HFHS diet; from 4 animals per condition). 5d: 5 days; 15d: 15 days; Aldh1L1: Aldehyde Dehydrogenase 1 family member L1; ARC: Arcuate Nucleus of the Hypothalamus; GFAP: Glial Fibrillary Acidic Protein; GFP: Green Fluorescent Protein; HFHS: high-fat high-sugar; SC: standard chow. P values were assessed by using a generalized linear model. Results are expressed as mean ± the SEM.

Thereafter, in order to explore the effect of a HFHS diet on the expression pattern in the ARC of GFAP as well, a regular GFAP antibody staining was performed on the brain slices derived from the Aldh1L1-CreER^{T2}::Sun1-sfGFP mice described above. As a consequence, it was possible to quantitatively analyze the co-expression of Aldh1L1 and GFAP in the ARC of mice exposed to different diet regimes. In line with previous observations (Thaler *et al.*, 2012; Horvath *et al.*, 2010), the number of GFAP$^+$ astrocytes in the ARC significantly increased after the exposure to a HFHS diet for both 5d and 15d (**Figure 12A and B**). However, it was possible to observe that only a partial number of astrocytes in the ARC simultaneously co-expressed GFP and GFAP signals (**Figure 12C**), which suggests that the previously observed HFHS diet-induced increase in the number of Aldh1L1$^+$ and GFAP$^+$ cells in the ARC (**Figure 11A and B; Figure 12A and B**) might be influenced by the single or co-expression of the two molecular markers. For this reason, the number of astrocytes single- or co- expressing GFAP and/or GFP in the ARC of mice exposed to a SC or a HFHS diet was quantified, after distinguishing three astrocytic populations: Aldh1L1$^+$/GFAP$^-$ (indicated by white arrow in **Figure 12C**), Aldh1L1$^-$/GFAP$^+$ (indicated by white chevron in **Figure 12C**), and Aldh1L1$^+$/GFAP$^+$ (indicated by white pentagon in **Figure 12C**) cells. In a similar way described for Aldh1L1$^+$ and GFAP$^+$ cells (**Figure 11A and B; Figure 12A and B**), the number of Aldh1L1$^+$/GFAP$^-$ and Aldh1L1$^+$/GFAP$^+$ cells in the ARC significantly increased in response to a HFHS diet exposure for both 5d and 15d, when compared to the SC diet group (**Figure 12C and D**). Moreover, the

number of Aldh1L1^{+}/GFAP^{-} cells decreased in the ARC of mice fed with a HFHS diet for 15d, compared to 5d HFHS diet-fed mice (**Figure 12C and D**), similarly to Aldh1L1^{+} cells (**Figure 11A and B**). However, differently from GFAP^{+} cells (**Figure 12A and B**), the number of Aldh1L1^{-}/GFAP^{+} astrocytes in the ARC significantly increased after the exposure to a HFHS diet for 5d, but not 15d (**Figure 12C and D**). Furthermore, among the brain areas analyzed, the HFHS diet-induced increase in the number of Aldh1L1^{-}/GFAP^{+} astrocytes was selective to the ARC, as in the cortex (somatory-sensory region, layers 4-5) their number rather decreased after 15d HFHS diet feeding (**Figure 12E and F**), while in the hippocampus (CA1 region between stratum radiatum, stratum lacunosum-moleculare, and dentate gyrus) their number was unchanged after the exposure to a HFHS diet (**Figure 12G and H**). Contrarily, HFHS diet induced a significant increase in the number of Aldh1L1^{+}/GFAP^{-} cells in both the ARC, the cortex and the hippocampus (**Figure 12C-H**). Moreover, the HFHS diet-induced increase in the number of Aldh1L1^{+}/GFAP^{+} cells was present in both the ARC and the hippocampus, but not the cortex, which might be due to the very low number of cells stained with the anti-GFAP antibody in this brain region (**Figure 12C-H**). Together, these data indicate that HFHS diet induces rapid and brain region-specific molecular responses in astrocytes, such as an increase in the number of cells expressing Aldh1L1 and/or GFAP. In particular, among the brain areas studied, the increase in the number of Aldh1L1^{-}/GFAP^{+} astrocytes is selective to the ARC, while the increased number of Aldh1L1^{+}/GFAP^{-} cells can be observed in the cortex and in the hippocampus as well.

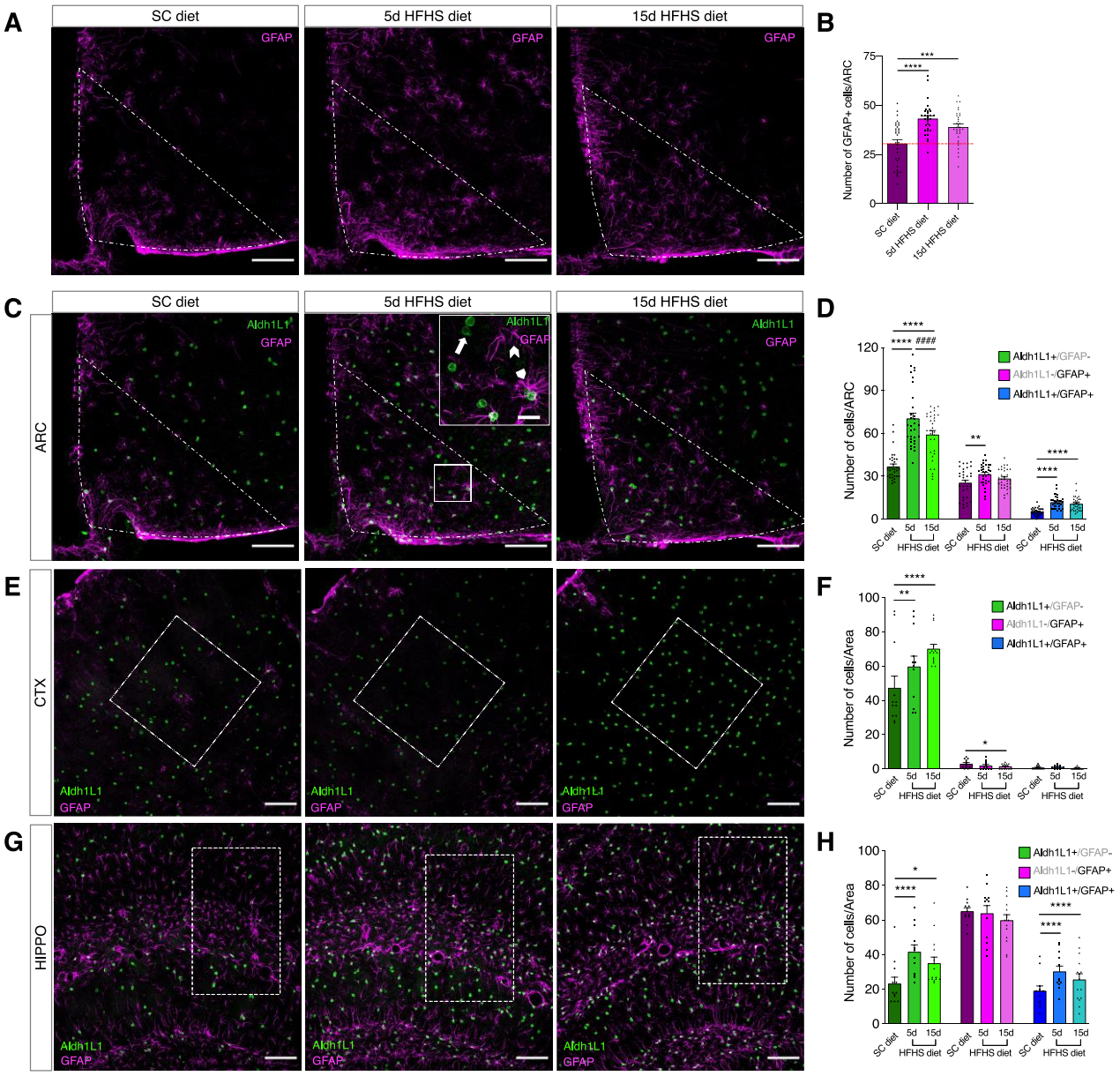

Figure 12: The effect of a HFHS diet on the number of astrocytes expressing Aldh1L1 and GFAP is brain-region specific. (A) Representative pictures of GFAP immunolabeling (magenta) in the ARC (segmented triangle-shaped white line with an area of approximately 105350 µm^2) of Aldh1L1-CreER^{T2}::Sun1-sfGFP mice fed with a SC or a HFHS diet for 5 and 15 days. Scale bar: 100 µm. **(B)** Quantitative analysis of the number of GFAP$^+$ cells in the ARC of the Aldh1L1-CreER^{T2}::Sun1-sfGFP mice represented in **(A)** in each diet condition analyzed. The segmented red line indicates the number of GFAP$^+$ cells in SC diet-fed control mice. In each diet group, n = 32 (ARCs derived from 4 animals). ***p = 0.0005; ****p < 0.0001. **(C)** Representative images showing the co-localization between Aldh1L1$^+$ (green) and GFAP$^+$ (magenta) cells in the ARC (segmented triangle-shaped white line with an area of approximately 105350 µm^2) of Aldh1L1-CreER^{T2}::Sun1-sfGFP mice exposed to different diets. Scale bar = 100 µm. In the top right corner of the middle picture, an enlargement of the detail enclosed in the white square below is shown (scale bar = 20 µm). The three astrocyte populations under analysis are pointed: Aldh1L1$^+$/GFAP$^-$ (white arrow), Aldh1L1$^-$/GFAP$^+$ (white chevron), and Aldh1L1$^+$/GFAP$^+$ (white pentagon). **(D)** The bar plot indicates the HFHS diet-induced changes in the number of Aldh1L1$^+$/GFAP$^-$ (green), Aldh1L1$^-$/GFAP$^+$ (magenta) and Aldh1L1$^+$/GFAP$^+$ (blue) cells in the ARC of the Aldh1L1-CreER^{T2}::Sun1-sfGFP mice represented in **(C)**. For each diet group, a n = 32 (ARCs from 4 mice) was used. **p = 0.0018; ****p and ####p < 0.0001. **(E)** Representative pictures

showing the co-localization between Aldh1L1$^+$ (green) and GFAP$^+$ (magenta) cells in the somatory sensory cortex (area analyzed enclosed in the segmented square of about 144334 μm^2) of Aldh1L1-CreER^{T2}::Sun1-sfGFP mice exposed to different diets. Scale bar = 100 μm. **(F)** The bar plot indicates the HFHS diet-induced changes in the number of Aldh1L1$^+$/GFAP$^-$ (green), Aldh1L1$^-$/GFAP$^+$ (magenta) and Aldh1L1$^+$/GFAP$^+$ (blue) cells in a selected region of the somatosensory cortex of the Aldh1L1-CreER^{T2}::Sun1-sfGFP mice represented in **(E)**. N = 12 (from 4 mice; SC diet and 5d HFHS diet); n = 15 (from 5 mice; 15d HFHS diet). **p = 0.0019; ****p < 0.0001; *p = 0.027. **(G)** Representative images showing the co-localization between Aldh1L1$^+$ (green) and GFAP$^+$ (magenta) cells in the hippocampal CA1 region (area analyzed enclosed in the segmented square of about 96138 μm^2) of Aldh1L1-CreER^{T2}::Sun1-sfGFP mice exposed to different diets. Scale bar = 100 μm. **(H)** The bar plot indicates the HFHS diet-induced changes in the number of Aldh1L1$^+$/GFAP$^-$ (green), Aldh1L1$^-$/GFAP$^+$ (magenta) and Aldh1L1$^+$/GFAP$^+$ (blue) cells in a selected region of the hippocampal CA1 area of the Aldh1L1-CreER^{T2}::Sun1-sfGFP mice represented in **(G)**. N = 12 (from 4 mice; SC diet and 5d HFHS diet); n = 15 (from 5 mice; 15d HFHS diet). ****p < 0.0001; *p = 0.012. 5d: 5 days; 15d: 15 days; Aldh1L1: Aldehyde Dehydrogenase 1 family member L1; ARC: Arcuate Nucleus of the Hypothalamus; GFAP: Glial Fibrillary Acidic Protein; GFP: Green Fluorescent Protein; HFHS: high-fat high-sugar; SC: standard chow. P values were assessed by using a generalized linear model. Results are indicated as mean ± the SEM.

4.2.4. Astrocytes expressing Aldh1L1 and GFAP in the ARC undergo a spatial reorganization in response to a HFHS diet

The results collected so far indicate that astrocytes in the ARC respond to a HFHS diet with transcriptional time-dependent changes, which include an alteration in the expression pattern of specific astrocyte-enriched proteins, such as Aldh1L1 and GFAP. Considering the HFHS diet-induced increase in the number of Aldh1L1- and GFAP- expressing astrocytes, the individual areas of such an increase within the ARC were further identified by performing a topographical analysis of those cells in the ARC of Aldh1L1-CreER^{T2}:: Sun1-sfGFP mice. To do so, a cartesian coordinate system was superimposed to the region of interest (ROI) matching the ARC, where the origin of axes coincided to the median eminence (ME), the x axis to the lower edge of the ARC, and the y axis to the vertical boundary of the third ventricle (**Figure 13A**). For each Aldh1L1$^+$/GFAP$^-$, Aldh1L1$^-$/GFAP$^+$, and Aldh1L1$^+$/GFAP$^+$ astrocyte, the cartesian coordinates indicating the distance in μm from the ME were found and used to measure the local density pattern of each astrocyte population (**Figure 13A and B**). Interestingly, these three astrocyte populations appeared to be concentrated in different areas of the ARC according to the molecular marker - Aldh1L1 and/or GFAP – expressed, in control mice fed with SC diet (**Figure 13B**). In particular, the highest density of Aldh1L1$^+$/GFAP$^-$ cells could be detected in an individual region close to the ME (x = 120 μm; y = 0 μm), while Aldh1L1$^-$/GFAP$^+$ cells highest concentration was found in two different points more distant from the ME than Aldh1L1$^+$/GFAP$^-$ cells (x = 250 μm; y = 50 μm and x = 0 μm; y = 400 μm) (**Figure 13B**). On the contrary, Aldh1L1$^+$/GFAP$^+$ cells were mostly concentrated in several

small areas throughout the ARC, with the maximal density peaks not overpassing the first 200 μm in the x direction from the ME (**Figure 13B**). Considering the differences existing between the three astrocyte populations in the ARC under physiological conditions, further divergences in their spatial distribution following the exposure to a HFHS diet were investigated by using a generalized linear model (**Figure 13C and D**). Specifically, the ARC was divided into equal squares with an area of 50 μm^2 each, and the variation in the number of cells between SC diet and HFHS diet groups was calculated in each square and overall the entire ARC (**Figure 13C**). Consistently with the previous results (see paragraph 4.2.3), the number of $Aldh1L1^+/GFAP^-$, $Aldh1L1^-/GFAP^+$, and $Aldh1L1^+/GFAP^+$ astrocytes increased in response to a HFHS diet in specific areas of the ARC, with 5d of a HFHS diet exposure inducing a greater effect on $Aldh1L1^+/GFAP^-$ and $Aldh1L1^+/GFAP^+$ cells than 15d of feeding with a HFHS diet (**Figure 13C and D**). Moreover, several small areas of the ARC were affected by a HFHS diet exposure, with the number of $Aldh1L1^+/GFAP^-$ and $Aldh1L1^+/GFAP^+$ cells increased uniformly and without a peculiar pattern, while the number of $Aldh1L1^-/GFAP^+$ cells increased in specific regions within 150 μm in the x direction from the ME (**Figure 13C and D**).

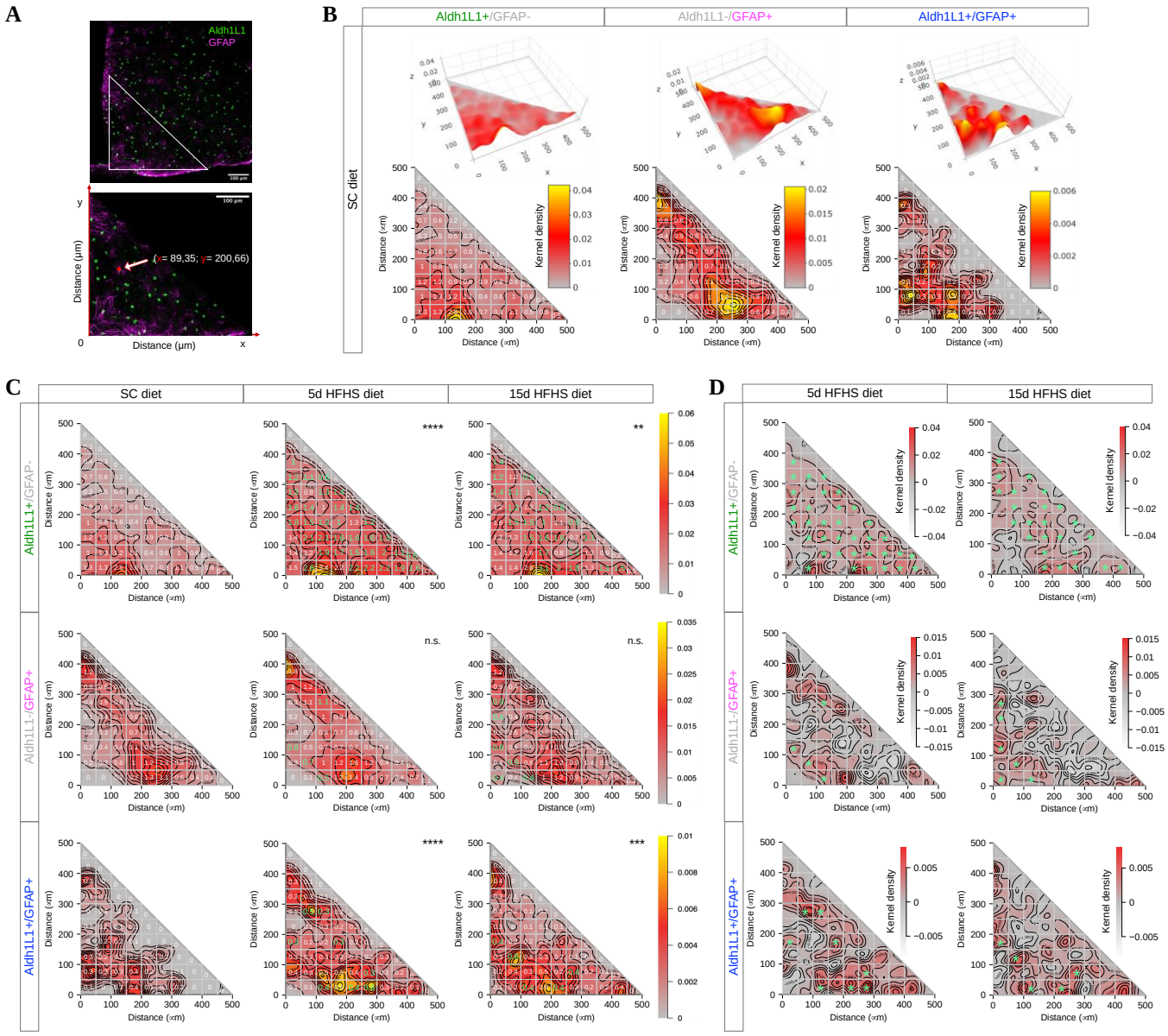

Figure 13: The spatial distribution of astrocytes expressing Aldh1L1 and GFAP in the ARC is influenced by the exposure to a HFHS diet. (A) Representative pictures of GFP-expressing nuclei in Aldh1L1^{+} cells (green) and GFAP immunolabeling (magenta) in the ARC (segmented triangle-shaped white line with an area of approximately 105350 µm^2) of Aldh1L1-CreER^{T2}::Sun1-sfGFP mice fed with a SC diet. The picture at the bottom is an enlargement of the top one, and represents the method used to define the cartesian coordinates for each astrocyte studied within the ARC. The position of the x/y axes (red) is indicated, and the cartesian coordinates of an example cell (red circle) are reported. Scale bars: 100 µm. **(B)** Spatial point patterns analysis of the kernel density in the ARC of the three astrocyte populations under study (Aldh1L1^{+}/GFAP^{-}, Aldh1L1^{-}/GFAP^{+}, and Aldh1L1^{+}/GFAP^{+}) in Aldh1L1-CreER^{T2}::Sun1-sfGFP mice fed with a SC diet. The plots are represented in 3D (upper figure) and 2D (lower figure), with a color-coded kernel density scale. In the 2D plots, a white grid formed by 50 µm^2 large areas is superimposed to the colormap, where the average number of astrocytes located in each square is indicated (white). N = 32 (ARCs from 4 mice). **(C)** Spatial point patterns analysis of the kernel density in the ARC of the three astrocyte populations under study (Aldh1L1^{+}/GFAP^{-}, Aldh1L1^{-}/GFAP^{+}, and Aldh1L1^{+}/GFAP^{+}) in Aldh1L1-CreER^{T2}::Sun1-sfGFP mice fed with a SC diet, and a HFHS diet for 5 or 15d. A color-coded kernel density scale is represented in each plot, where a white grid formed by 50 µm^2 large areas is superimposed. In each area, the average number of astrocytes there located is indicated in two different colors: white when the comparison between SC and HFHS diet is not

significant, and in green when it is significant ($p < 0.05$). N = 32 (ARCs from 4 mice). ****$p < 0.0001$; **$p = 0.0042$; ***$p = 0.00053$. **(D)** Subtraction plots generated by comparing the kernel density pattern in SC diet group to 5d or 15d HFHS diet groups, and subtracting the first from the last two groups, per each astrocyte population studied (Aldh1L1$^+$/GFAP$^-$, Aldh1L1$^-$/GFAP$^+$, and Aldh1L1$^+$/GFAP$^+$) in the ARC of Aldh1L1-CreER^{T2}::Sun1-sfGFP mice. The subtraction is applied in each 50 μm^2 large area by using a generalized linear model, and a significant result ($p < 0.05$) is reported with a green star. 5d: 5 days; 15d: 15 days; Aldh1L1: Aldehyde Dehydrogenase 1 family member L1; ARC: Arcuate Nucleus of the Hypothalamus; GFAP: Glial Fibrillary Acidic Protein; GFP: Green Fluorescent Protein; HFHS: high-fat high-sugar; n.s.: not significant; SC: standard chow. P values were assessed by using a generalized linear model.

Finally, the spatial organization into local clusters of Aldh1L1$^+$/GFAP$^-$, Aldh1L1$^-$/GFAP$^+$, and Aldh1L1$^+$/GFAP$^+$ astrocytes in the ARC and their behavior following an hypercaloric diet exposure was evaluated. To do so, the spatial dispersion and coherence of each astrocyte population in the ARC of SC diet, 5d and 15d HFHS diet fed mice were measured by determining the Moran I autocorrelation coefficient (Schmal *et al.*, 2017) (**Figure 14**). Interestingly, the spatial dispersion of Aldh1L1$^+$/GFAP$^-$, Aldh1L1$^-$/GFAP$^+$, and Aldh1L1$^+$/GFAP$^+$ astrocytes in the ARC gradually increased in response to a HFHS diet exposure, as indicated by the progressive decrease of the Moran I coefficient from SC diet to first 5d HFHS diet and then 15d HFHS diet conditions (**Figure 14**). Of note, the spatial domain occupied by Aldh1L1$^+$/GFAP$^-$ astrocytes in the ARC increased in response to a HFHS diet, populating the area previously occupied by Aldh1L1$^-$/GFAP$^+$ cells under standard conditions (**Figure 14**). Moreover, the spatial domain occupied by Aldh1L1$^+$/GFAP$^+$ astrocytes in the ARC represents less than the 1% of the total ARC region in all three diet conditions, when compared to the other astrocyte populations under study (**Figure 14**). Together, these data suggest that HFHS diet induces a topographical remodeling of Aldh1L1$^+$/GFAP$^-$, Aldh1L1$^-$/GFAP$^+$, and Aldh1L1$^+$/GFAP$^+$ astrocytes in the ARC, promoting their spatial dispersion over time.

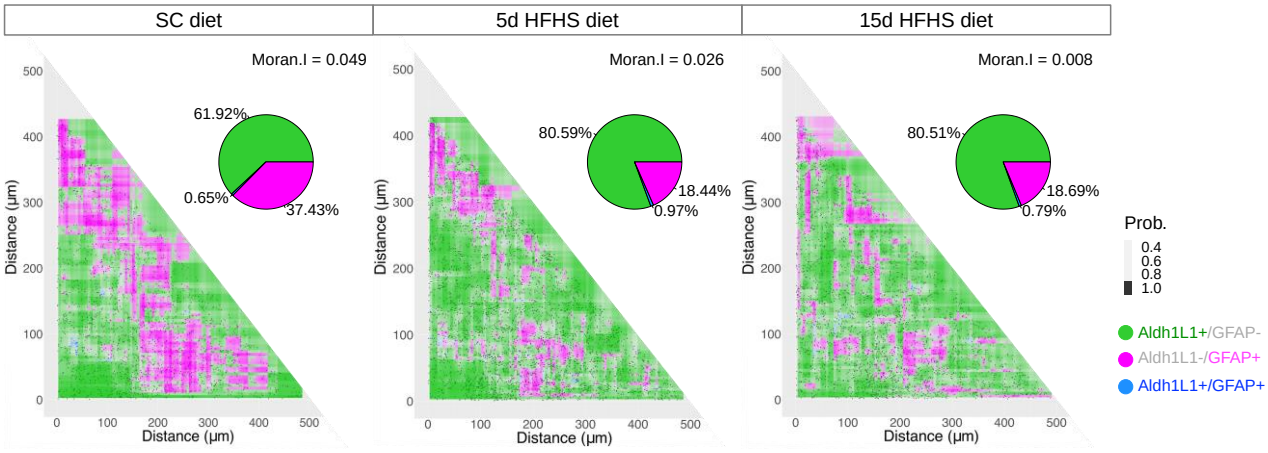

Figure 14: HFHS diet induces a gradual spatial dispersion of astrocytes expressing Aldh1L1 and GFAP in the ARC. In each experimental group, the random forest classifier is applied to determine the spatial domains occupied by Aldh1L1^{+}/GFAP^{-}, Aldh1L1^{-}/GFAP^{+}, and Aldh1L1^{+}/GFAP^{+} astrocytes in the ARC of Aldh1L1-CreER^{T2}::Sun1-sfGFP mice. In the top right corner of each plot, a pie chart indicates the percentage of spatial domain occupied by each astrocyte population analyzed in the ARC. The level of cellular spatial dispersion in each plot is indicated by the Moran I value (top right). SC diet: Moran I = 0.049, p-value <0.05; 5d HFHS diet: Moran I = 0.026, p-value <0.05; 15d HFHS diet: Moran I = 0.008, p-value <0.05. 5d: 5 days; 15d: 15 days; Aldh1L1: Aldehyde Dehydrogenase 1 family member L1; ARC: Arcuate Nucleus of the Hypothalamus; GFAP: Glial Fibrillary Acidic Protein; HFHS: high-fat high-sugar; SC: standard chow. P values were assessed by using a generalized linear model.

4.3. Hypercaloric diet-induced GFAP up-regulation in the ARC and body weight gain correlate with specific molecular pathways

4.3.1. HFHS diet-induced GFAP up-regulation in the ARC is mediated by Shh signaling pathway and IP$_3$R2-dependent calcium activity

As previously described along this thesis, an increase in GFAP expression can be observed in the ARC of mice exposed to a HFHS diet, although the molecular mechanisms behind this process, and its functional meaning are still largely unexplored. Therefore, the contribution of selected molecular pathways in HFHS diet-induced GFAP up-regulation in the ARC has been investigated. Considering evidences showing that astrocytes develop a reactive phenotype via Shh signaling in response to an acute brain injury (Sirko *et al.*, 2013), the effect of an astrocyte-specific postnatal ablation of the Shh downstream protein Smo on HFHS diet-induced increase in GFAP expression in the ARC has been investigated. For this reason, Smo deletion specifically in astrocytes has been first induced by tamoxifen injection, and successively Smo$^{fl/fl}$::hGFAP-CreER^{T2} mice and their littermate controls have been fed with a SC or a HFHS

diet for 5 or 15d, after which the number of $GFAP^+$ cells in the ARC was quantified **(Figure 15A and B**). As expected, HFHS diet feeding for both 5 and 15d induced a significant increase in the number of $GFAP^+$ cells in the ARC of wildtype control animals (**Figure 15A and B**). Interestingly, such an increase was maintained after 5d, and blunted after 15d of a HFHS diet exposure in the knockout (KO) animals, when compared to SC diet fed mice (**Figure 15A and B**). Indeed, the number of $GFAP^+$ cells in the ARC of KO mice fed with a SC diet or a 15d HFHS diet was comparable (**Figure 15A and B**). In addition, calcium-mediated signaling in hypothalamic astrocytes was identified as impacted by a HFHS diet (**Figure 7D**). For this reason, considering that IP_3R2 represents the major component of spontaneous and Gq-coupled receptor-induced Ca^{2+} signaling in astrocytes (Agulhon *et al.*, 2012), where it is highly enriched (Sharp *et al.*, 1999; Holtzclaw *et al.*, 2002), IP_3R2 KO mice have been used to investigate the effect of Ca^{2+} signaling on HFHS diet-induced GFAP up-regulation in the ARC. As before, IP_3R2 KO mice and their littermate controls received a SC diet or a HFHS diet for 5 or 15d, after which the number of $GFAP^+$ cells in the ARC was quantified (**Figure 15C and D**). Similarly to $Smo^{fl/fl}$::hGFAP-$CreER^{T2}$ mice, 15d HFHS diet fed IP_3R2 KO mice had blunted the increase in the number of $GFAP^+$ cells in the ARC, compared to SC diet fed animals, which was instead present in their littermate controls under the same diet (**Figure 15C and D**). However, in contrast to what reported above, 5d of a HFHS diet exposure were not sufficient to induce an increase in the number of $GFAP^+$ cells in the ARC of neither IP_3R2 KO mice or their wildtype littermates, which might be explained by differences in the genetic background of the mice (**Figure 15C and D**). Together, these results suggest that perturbations in the Shh signaling pathway in astrocytes and in the IP_3R2-dependent calcium activity restore the number of ARC GFAP-expressing astrocytes at 15d HFHS diet, as they play a time-dependent active role in the modulation of GFAP expression levels in the ARC.

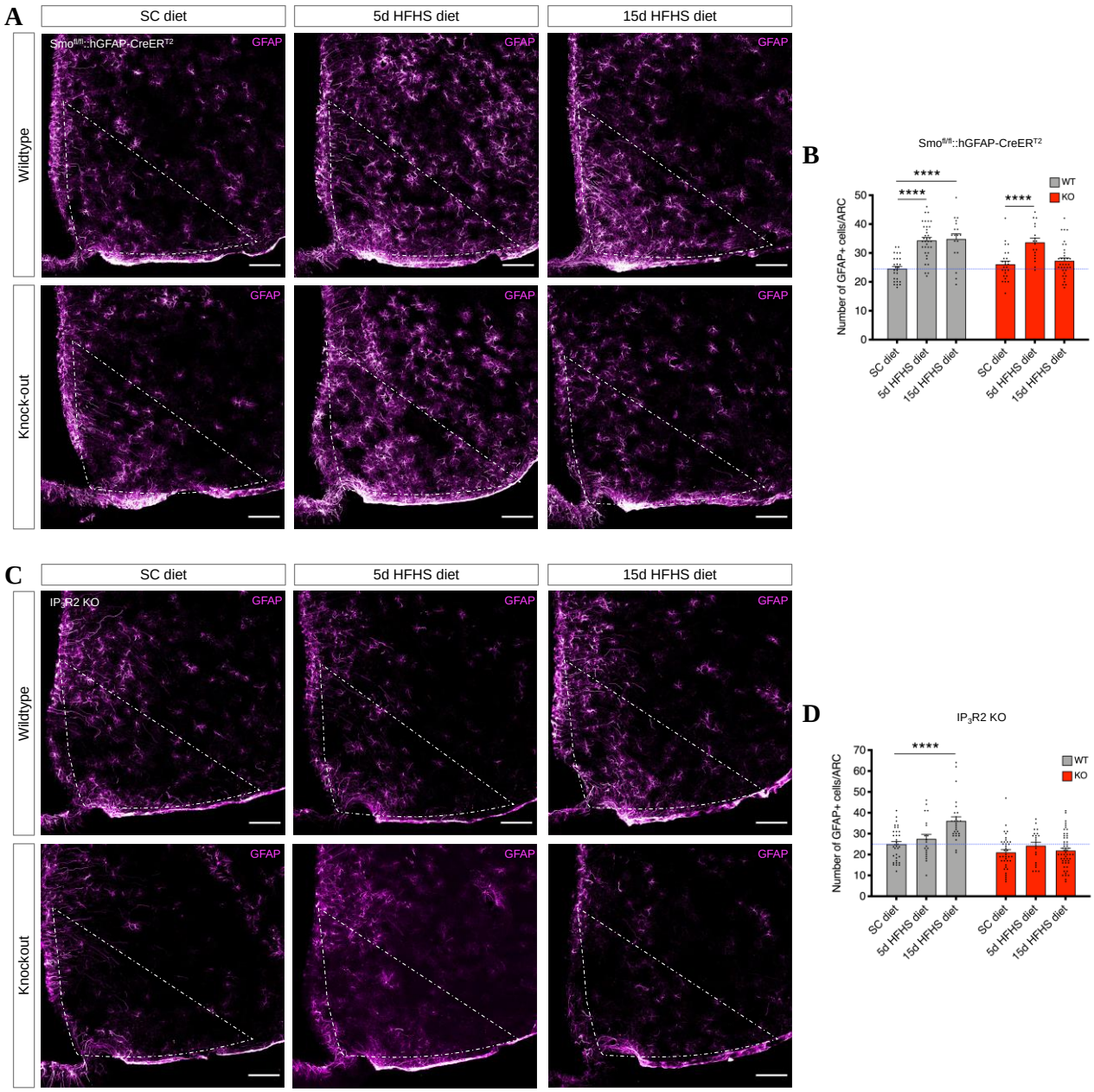

Figure 15: Perturbations in Shh signaling in astrocytes and IP_3R2 expression affect HFHS diet-induced increased number of $GFAP^+$ cells in the ARC. (A) Representative images of GFAP immunolabeling (magenta) in the ARC (segmented white line) of $Smo^{fl/fl}$::hGFAP-$CreER^{T2}$ mice and their littermate controls exposed to different diets. Scale bars = 100 µm. **(B)** The bar plot indicates the HFHS diet-induced changes in the number of $GFAP^+$ cells (magenta) in the ARC of the $Smo^{fl/fl}$::hGFAP-$CreER^{T2}$ mice represented in **(A)**. SC diet, wildtype mice: n = 26 (ARCs from 5 mice); 5d HFHS diet, wildtype mice: n = 35 (ARCs from 6 mice); 15d HFHS diet, wildtype mice: n = 18 (ARCs from 3 mice); SC diet, knockout mice: n = 26 (ARCs from 5 mice); 5d HFHS diet, knockout mice: n = 18 (ARCs from 3 mice); 15d HFHS diet, knockout mice: n = 34 (ARCs from 6 mice). ****p < 0.0001. **(C)** Representative pictures of GFAP immunolabeling (magenta) in the ARC (segmented white line) of IP_3R2 KO mice and their littermate controls exposed to different diets. Scale bars = 100 µm. **(D)** The bar plot indicates the HFHS diet-induced changes in the number of $GFAP^+$ cells (magenta) in the ARC of the IP_3R2 KO mice represented in **(C)**. SC diet, wildtype mice: n = 34 (ARCs from 6 mice); 5d HFHS diet, wildtype mice: n = 20 (ARCs from 4 mice); 15d HFHS diet, wildtype mice: n = 28 (ARCs from 6 mice); SC diet, knockout mice: n = 38 (ARCs from 7 mice); 5d HFHS diet, knockout mice: n = 22 (ARCs from 4 mice); 15d HFHS diet, knockout mice: n = 53 (ARCs from 10 mice). ****p < 0.0001.

5d: 5 days; 15d: 15 days; ARC: Arcuate Nucleus of the Hypothalamus; GFAP: Glial Fibrillary Acidic Protein; HFHS: high-fat high-sugar; IP_3R2: Inositol 1,4,5-Trisphosphate Receptor Type 2; KO: knockout; SC: standard chow; Smo: Smoothened; WT: wildtype. P values were assessed by using a generalized linear model.

4.3.2. Perturbations in Shh signaling pathway, IP_3R2-dependent calcium activity, and GFAP expression correlate with changes in the body weight gain

Although HFHS diet-induced increased number of $GFAP^+$ cells in the ARC has been widely described (Thaler *et al.*, 2012; Horvath *et al.*, 2010; González-García and García-Cáceres, 2021), the functional meaning of such a process and its correlation to HFHS diet-induced body weight gain has been poorly debated. Therefore, in order to assess whether altering selected mechanisms mediating GFAP up-regulation in the ARC might affect specific metabolic parameters, the body weight gain of mice with perturbations in the molecular pathways described above was measured. In particular, the body weight gain of the previously used $Smo^{fl/fl}$::hGFAP-$CreER^{T2}$, IP_3R2 KO mice, and their control littermates following a SC diet or a HFHS diet feeding for 5 or 15d was monitored. In line with previous evidences (Gruber *et al.*, 2021; Thaler *et al.*, 2012), the wildtype littermates of the $Smo^{fl/fl}$::hGFAP-$CreER^{T2}$ mice gained a significant body weight after the exposure to a HFHS diet for 15d, but not 5d, compared to SC diet fed mice (**Figure 16A**). A similar behavior was observed in the animals with an astrocyte-specific deletion of Smo, although the 15d HFHS diet-induced body weight gain was less evident than in their wildtype littermates (**Figure 16A**). Likewise, 5d of a HFHS diet exposure were not sufficient to induce a significant body weight gain in the wildtype littermates of IP_3R2 KO mice, while the last ones instead gained a considerable body weight, when compared to the same mice fed with a SC diet (**Figure 16B**). In addition, both IP_3R2 KO mice and their wildtype littermates similarly gained a substantial body weight in response to 15d HFHS diet feeding, in comparison to SC diet fed animals (**Figure 16B**). Finally, the effect of a GFAP deletion itself on the body weight gain following a HFHS diet exposure was assessed. In particular, the feeding with a HFHS diet for 15d, but not 5d, was sufficient to induce a considerable body weight gain in both GFAP KO mice and their wildtype controls, compared to the same mice fed with a SC diet (**Figure 16C**). However, such an increase was higher in the wildtype mice than in the GFAP KO animals (**Figure 16C**). Together, these evidences suggest that dysregulations in specific molecular pathways, which might mediate the HFHS-induced increased number of $GFAP^+$ cells in the ARC, differently affect the body weight

gain of mice exposed to an hypercaloric diet. In particular, perturbations in the astrocyte-specific Shh signaling pathway and in GFAP expression lead to a 15d HFHS diet-induced diminished body weight gain in comparison to wildtype mice, while interferences in calcium signaling are related to a significant body weight gain after only 5d of a HFHS diet feeding, diversely from wildtype mice.

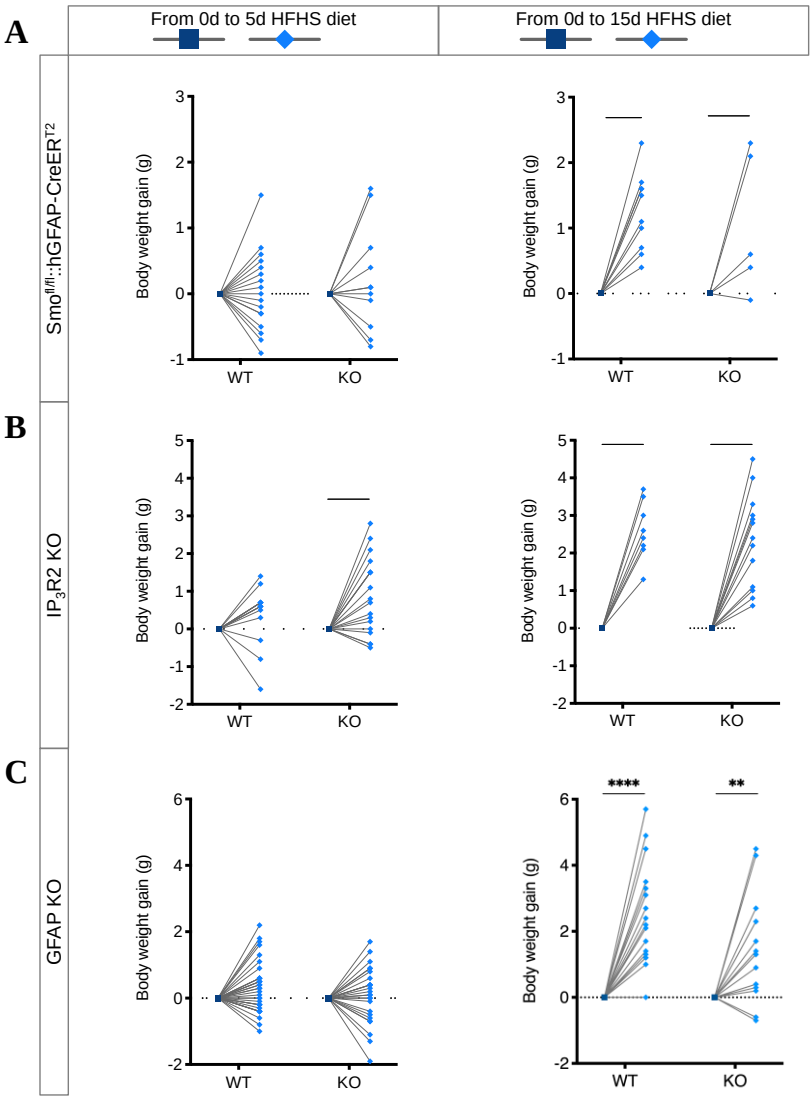

Figure 16: Alterations in specific molecular pathways associated to HFHS diet-induced GFAP up-regulation affect the body weight gain of mice fed with an hypercaloric diet. The plots show the body weight gain (grams) of $Smo^{fl/fl}$::hGFAP-$CreER^{T2}$ **(A)**, IP_3R2 KO **(B)**, and GFAP KO **(C)** mice and their littermate wildtype controls **(A-C)** exposed to a SC diet or a HFHS diet for 5 or 15 days. The plots on the left indicate the grams gained by the animals after 5d of a HFHS diet feeding (light blue) compared to a SC diet (dark blue), while the graphs on the right depict the grams gained by the mice after 15d of a HFHS diet exposure (light blue) compared to a SC diet (dark blue). **(A)** Wildtype mice, 5d HFHS diet: n = 17; wildtype mice, 15d HFHS diet: n = 10; knockout mice, 5d HFHS diet: n = 11; knockout mice, 15d HFHS diet: n = 5. ***p = 0.0004; *p = 0.018. **(B)** Wildtype mice, 5d HFHS diet: n = 14; wildtype mice, 15d HFHS diet: n = 8; knockout mice, 5d HFHS diet: n = 18; knockout mice, 15d HFHS diet: n = 13. ***p = 0.0007; ****p < 0.0001. **(C)** Wildtype mice, 5d HFHS diet: n = 33; wildtype mice, 15d HFHS diet: n = 19; knockout mice, 5d HFHS diet: n = 25; knockout mice, 15d HFHS diet: n

= 16. ****p < 0.0001; **p = 0.021. 5d: 5 days; 15d: 15 days; g: grams; GFAP: Glial Fibrillary Acidic Protein; HFHS: high-fat high-sugar; IP_3R2: Inositol 1,4,5-Trisphosphate Receptor Type 2; KO: knockout; SC: standard chow; Smo: Smoothened; WT: wildtype. P values were assessed by using a two-way ANOVA multiple comparison.

5. Discussion

Here I reported how hypercaloric diet triggers distinct changes in the molecular profile of astrocytes located in different brain regions. Moreover, ARC astrocytes exhibited a diverse transcriptional activity, number, and spatial arrangement depending on the expression of specific molecular markers and on the HFHS diet exposure time. Moreover, I explored putative molecular pathways which might mediate HFHS diet-induced GFAP up-regulation in the ARC, and their impact on the body weight gain which follows the exposure to an hypercaloric diet.

5.1. The HFHS diet-induced molecular response of astrocytes is encoded by their anatomical location in the brain

Based on previous evidences revealing as astrocytes play a specific role in the control of metabolism, e.g. showing opposing roles in appetite regulation, depending on the specific circuits they are embedded in (Chen *et al.*, 2016; Garcia-Caceres *et al.*, 2016; Varela *et al.*, 2021; Yang, Qi and Yang, 2015; Patel *et al.*, 2021; MacDonald *et al.*, 2020), it is important to always preserve the anatomical location of these glial cells, and thus their interactions with the local networks, while conducting astrocyte-centered studies. For this reason, the effect of an hypercaloric diet was evaluated on astrocytes isolated from three different brain regions (cortex, hypothalamus, hippocampus) in this study. In fact, the transcriptional and post-transcriptional profiles of astrocytes showed a remarkable inter-regional heterogeneity in both SC diet- and HFHS diet- fed mice, which might highlight a diversity in astrocyte functions according to the brain location and to their interaction with specific local circuits. This is in line with previous findings, demonstrating for example age-related differences in the transcriptome of astrocytes collected from cortex, cerebellum and hypothalamus (Boisvert *et al.*, 2018), or expression of unique sets of genes in astrocytes isolated from different brain regions (including thalamus, hypothalamus, hippocampus, cortex, nucleus accumbens, caudate putamen) (Morel *et al.*, 2017), such as differences in the transcriptome, proteome and morphology of astrocytes located in hippocampus and striatum (Chai *et al.*, 2017). Moreover, the results described in this thesis indicate that the similarities in the molecular phenotype among astrocytes were determined in a more substantial manner by the brain area they derived from, rather than by the effect of a HFHS diet. However, the chronic exposure to an hypercaloric diet induced remarkable changes at both RNA and protein levels in astrocytes within different brain regions. At transcriptional level, unlike astrocytes located in the hippocampus, both cortical and hypothalamic astrocytes

appeared to respond to a HFHS diet with changes in pathways related to hormonal and nutrient regulation, with a more pronounced involvement of cortical astrocytes in insulin response, and of hypothalamic astrocytes in glucose and lipid metabolism. However, at protein level, the hypothalamus emerged as the area with the highest astrocyte specialization in hormonal and nutrient regulative processes, in line with previous evidences describing the importance of hypothalamic astrocytes in sensing and responding to hormonal and nutritional cues for the regulation of feeding behavior and systemic metabolism (Kim *et al.*, 2014; Garcia-Caceres *et al.*, 2016; Gao *et al.*, 2017b). Of note, the down-regulation of pathways involved not only in neuronal and synaptic regulation, but also in calcium-mediated signaling in hypothalamic astrocytes, following a long-term exposure to a HFHS diet, might influence their inter-cellular communication with surrounding astrocytes, neurons and other cell types, contributing to the dysregulation of circuitries involved in the control of feeding behavior, and the subsequent obesity onset, as previously discussed (García-Cáceres, Yi and Tschöp, 2013; Kälin *et al.*, 2015; Harada, Kamiya and Tsuboi, 2016; Lee *et al.*, 2020; González-García and García-Cáceres, 2021). The different regulation and enrichment of the same molecular pathways in cortical, hypothalamic and hippocampal astrocytes in response to a HFHS diet supports the concept of the existence of specialized populations of astrocytes, characterized by different roles and interactions with the surrounding environment, depending on their physical location in the brain.

5.2. The highest transcriptional activity of astrocytes among other cell types in the ARC reveals their crucial role within the first 5 days of a HFHS diet feeding

Astrocytes have not only been described as characterized by a pronounced inter-regional heterogeneity, but also an intra-regional one, as shown by the differences in the expression of specific astrocyte-enriched proteins, and in the capability of regulating diverse neuronal circuits within the same brain area (Perea *et al.*, 2014; Martín *et al.*, 2015; Farmer *et al.*, 2016; Ben Haim and Rowitch, 2017). For this reason, the relevance of hypothalamic astrocytes in response to an hypercaloric diet was further confirmed by analyzing their transcriptional activity within the ARC, a crucial region of the hypothalamus, whose astrocyte involvement in response to a HFHS diet has been already described (Horvath *et al.*, 2010; Thaler *et al.*, 2012). In particular, the changes in the transcriptional activity of ARC astrocytes were assessed by sequencing the RNA at single-cell level in two critical timepoints of a HFHS diet feeding, before and after the arousal of significant changes in the body weight of mice. The analysis indicated that ARC

astrocytes are the fastest responders to 5d of exposure to a HFHS diet, as indicated by the highest number of DEGs among all ARC cell types, and the remarkable activation of their transcriptional activity, but this response was transient and reversed to a control-like pattern at 15d of a HFHS diet feeding, when animals gained a significant body weight. Moreover, such a time-dependent transcriptional responsive pattern was only observed in astrocytes, which supports the responsive distinction of these glial cells over other ARC cell types upon an hypercaloric diet. This might indicate that astrocytes in the ARC play a critical role in the initial days of an hypercaloric diet feeding, before any body weight change, while the surrounding cells might respond in a later time not only to a HFHS diet itself, but also to signals and molecules released by the previously activated astrocytes in the surrounding environment, when the body weight of the animals is already altered. Although hypothalamic astrocytes have been already reported as rapid responders to an hypercaloric diet (Thaler *et al.*, 2012), evidences indicate microglia to be concomitant fast responders, by rapidly producing and releasing inflammatory markers, which in turn affect the activity of neighboring cells, such as astrocytes and neurons (Valdearcos *et al.*, 2014). However, in this study it was not possible to observe such a picture after 5d of a HFHS diet exposure, which might derive by time-dependent fluctuations in microglia activation, not visualized at the selected timepoints. As the most remarkable changes in the transcriptional activity of ARC astrocytes were observed after 5d of a HFHS diet exposure, it was questioned how specific genes of interest might be affected by this response. Interestingly, particular genes involved in metabolic and astrocytic functions, such as *Aldoc*, *Pcsk1n*, *Clu*, *ApoE* and *Gfap*, were expressed at different levels between astrocytes in both physiological conditions and in response to an hypercaloric diet, with the cells presenting the highest expression being grouped accordingly to their transcriptional similarity. However, the limitations of this analysis prevent to question whether those cells might be considered a separated astrocytic population and form a specialized domain in the ARC, particularly sensitive to a HFHS diet feeding.

5.3. HFHS diet-induced changes in the Aldh1L1 and GFAP spatial expression levels in the ARC might be associated to different functional states of astrocytes

Considering the clear responsiveness of ARC astrocytes to a HFHS diet, highlighted by the scRNA-Seq study here described, the next question was to identify whether this response might concern particular subtypes of astrocytes defined according to the expression of well-known canonical markers. Two astrocyte-specific molecular markers were identified as selectively

responsive to an hypercaloric diet: Aldh1L1 and GFAP. Although GFAP has been extensively described as a main hallmark of reactive astrogliosis associated to a hypertrophic phenotype in both physiological and pathological conditions, including obesity (Horvath *et al.*, 2010; Thaler *et al.*, 2012; Pekny and Pekna, 2014; Sofroniew, 2014), the role of Aldh1L1 has never been deepened in this sense. Along this study, I showed for the first time that hypercaloric diet induces an increase in the number of cells expressing not only GFAP, but also Aldh1L1, in the ARC, before and after a significant body weight gain, and that this markers expression is differently distributed along the ARC. Although astrocytes have been reported to proliferate in certain pathological conditions, such as following a traumatic brain injury (Susarla *et al.*, 2014; Sirko *et al.*, 2013), astrocyte proliferation following a HFHS diet exposure has never been described. Accordingly, I could not find any evidence of astrocyte proliferation in the ARC following the exposure to a HFHS diet for 5 or 15 days, particularly in regards to Aldh1L1-expressing cells. This suggests that the HFHS diet-induced increase in the number of $Aldh1L1^{+}$ (and most probably also in $GFAP^{+}$) cells in the ARC does not derive from this cell type proliferation, but rather from a novel Aldh1L1 (or GFAP) expression in astrocytes, not expressing these molecular markers under physiological conditions. Of note, differences at cellular transcriptional and post-transcriptional levels, which existence has been already previously discussed (Liu, Beyer and Aebersold, 2016; Buccitelli and Selbach, 2020), were found here: the astrocyte response to an hypercaloric diet might lead to an increase in RNA levels of specific genes, successively translated into proteins, which amount might be high enough to sustain their function for a longer period of time on a HFHS diet, and thus explain the return of RNA to normal levels concomitant to a high protein level. Furthermore, astrocytes expressing GFAP and Aldh1L1 were found to occupy different territories in the ARC, suggestive of specific intra-regional functions, with the occupancy of Aldh1L1 particularly increased following the intake of an hypercaloric diet. So far, intra-regional molecular and physiological differences between astrocytes have been only observed within the cortex (Lanjakornsiripan *et al.*, 2018; Morel *et al.*, 2019; Bayraktar *et al.*, 2020), and the spinal cord (Molofsky *et al.*, 2014). However, the data here reported suggest the putative existence of an intra-regional heterogeneity between astrocytes in the ARC as well, as regards to their spatial organization, which changes according not only to the diet, but also to the concomitant or separate expression of Aldh1L1 and GFAP. The concept of astrocyte heterogeneity is further strengthened by the fact that Aldh1L1 and GFAP respond diversely to a HFHS diet across different brain areas, which might indicate a distinct involvement of these proteins in astrocyte-related functions. However, the impact of Aldh1L1 and GFAP expression on the specific

function of astrocytes, which might in turn affect the surrounding neuronal activity, is still unexplored. In this study, the expression of Aldh1L1 and GFAP in astrocytes is induced in response to an hypercaloric diet, with the latter one specifically observed in the ARC, without acting as specific markers of different astrocyte subpopulations. Therefore, the molecular diversity of ARC astrocytes could entail transient functional states of these glial cells required for synapse remodeling, for the switch between a resting/active state of local networks, and for the reorganization of circuits necessary for neuronal homeostasis; all this without altering the common basic cellular features, and without identifying different astrocyte subpopulations. Interestingly, HFHS diet leads to abnormal perturbations in the ARC neuronal circuits (Kälin *et al.*, 2015; Jais *et al.*, 2020; Jais and Brüning, 2021), which might lead to (or be caused by) the increase of GFAP and Aldh1L1 levels in the surrounding astrocytes, responding to the modifications in the local homeostasis.

5.4. HFHS diet-induced body weight gain might be prevented or strengthen by manipulating astrocyte-specific molecular pathways

Whether astrogliosis, which accompany several pathological conditions affecting the CNS, is a detrimental or beneficial astrocyte reaction for the brain and the whole-body correct functioning is still largely under debate (Pekny and Pekna, 2014; Sofroniew, 2014). Several independent studies tried to elucidate the functional role of GFAP, which over-expression denotates astrogliosis, by deleting this protein in mice and observing the effect on astrocyte phenotype and on the function of surrounding neurons (Pekny *et al.*, 1995; McCall *et al.*, 1996; Liedtke *et al.*, 1996; Otani *et al.*, 2006). However, the results reported were different, with the GFAP deletion leading to no abnormalities in the physiology and behavior of mice in one case (Pekny *et al.*, 1995), or to an impairment in the myelination and white matter vascularization in another study (Liedtke *et al.*, 1996), or to consequences on the function of surrounding neurons (McCall *et al.*, 1996; Otani *et al.*, 2006). Moreover, the functional meaning of HFHS diet-induced GFAP up-regulation in the hypothalamus, and particularly in the ARC, has never been explored up to date. For this reason, along this study, I evaluated whether GFAP ablation might affect a basic metabolic parameter, such as the body weight, which in normal conditions increases following a HFHS diet exposure. Although the body weight gain of GFAP KO animals exposed to a HFHS diet followed the trend of wildtype mice fed with the same diet, their gain was slower and less significant than the control mice one. This first evidence might suggest a more detrimental than beneficial role of HFHS diet-induced GFAP up-regulation in the ARC on the body weight of animals. However, this evidence alone is not solid enough to demonstrate the

role of HFHS diet-induced GFAP over-expression in the ARC, also considering the fact that mice globally lacking GFAP might develop compensatory mechanisms, such as the increase in the expression of other types of intermediate filaments, like vimentin, in line with previous studies (Kamphuis *et al.*, 2015; Galou *et al.*, 1996; Pekny *et al.*, 1999). Therefore, I targeted molecular pathways associated to HFHS diet-induced increased number of $GFAP^+$ cells, in addition to the global GFAP ablation, in order to find more evidences associated to the putative detrimental effect of ARC GFAP up-regulation on the body weight. Indeed, both IP_3R2 and astrocyte-specific Smo ablation led to an attenuated GFAP expression in the ARC following a HFHS diet exposure, especially in response to 15d of a HFHS diet feeding, compared to wildtype mice. Interestingly, while the effect of astrocyte-specific Smo ablation on the body weight was similar to GFAP deletion, IP_3R2 ablation seemed to mainly affect the body weight of mice exposed to a HFHS diet for 5 days, with a significant increase, contrarily to wildtype animals. This might indicate that, even though both molecular pathways are associated to HFHS diet-induced GFAP up-regulation in the ARC, their role in this process might be time-dependent. Moreover, the analysis of single molecular pathways associated to HFHS diet-induced GFAP over-expression in the ARC might not be sufficient to conclude whether this event might have a beneficial or detrimental connotation, considering as well possible and diverse compensatory mechanisms that each pathway might present.

5.5. Conclusion and outlook

Taken together, the data presented along this thesis indicate that astrocytes are molecularly different based on their anatomical location, and that their transcriptional and post-transcriptional changes might explain their functional role in the control of metabolism in health and obesity. Considering the increased prevalence of obesity and associated comorbidities in the modern world, a deeper understanding of the cellular and molecular mechanisms associated is urgently needed. This thesis suggests that further studies concerning astrocyte role in the development of obesity would be worth to pursue. In particular, the functional correlation between the spatial- and time- dependent expression of astrocyte-specific molecular markers and the activity of surrounding cells and neuronal circuitries would help to unravel the mechanisms behind the HFHS diet-induced perturbations in the systemic homeostasis. Moreover, the evidences showing Aldh1L1 to be particularly responsive to a HFHS diet, together with GFAP, indicate that the concept of astrogliosis might need to be reconsidered, by including this marker - and possibly others not analyzed in this work - over-expression as an additional possible hallmark of HFHS diet-induced astrogliosis. Finally, although the

understanding of the nature of HFHS diet-induced astrogliosis is of primary importance to have the possibility to develop target-specific drugs to prevent obesity, we are still far away from the complete knowledge of astrocyte role in such a process.

6. References

Aberg, F. and Kozlova, E. N. (2000) 'Metastasis-associated mts1 (S100A4) protein in the developing and adult central nervous system', *J Comp Neurol,* 424(2), pp. 269-82.

Agulhon, C., Boyt, K. M., Xie, A. X., Friocourt, F., Roth, B. L. and McCarthy, K. D. (2013) 'Modulation of the autonomic nervous system and behaviour by acute glial cell Gq protein-coupled receptor activation in vivo', *The Journal of physiology,* 591(22), pp. 5599-5609.

Agulhon, C., Fiacco, T. A. and McCarthy, K. D. (2010) 'Hippocampal short- and long-term plasticity are not modulated by astrocyte Ca2+ signaling', *Science,* 327(5970), pp. 1250-4.

Agulhon, C., Sun, M. Y., Murphy, T., Myers, T., Lauderdale, K. and Fiacco, T. A. (2012) 'Calcium Signaling and Gliotransmission in Normal vs. Reactive Astrocytes', *Front Pharmacol,* 3, pp. 139.

Alexander, G. M., Rogan, S. C., Abbas, A. I., Armbruster, B. N., Pei, Y., Allen, J. A., Nonneman, R. J., Hartmann, J., Moy, S. S., Nicolelis, M. A., McNamara, J. O. and Roth, B. L. (2009) 'Remote control of neuronal activity in transgenic mice expressing evolved G protein-coupled receptors', *Neuron,* 63(1), pp. 27-39.

Allard, C., Carneiro, L., Grall, S., Cline, B. H., Fioramonti, X., Chrétien, C., Baba-Aissa, F., Giaume, C., Pénicaud, L. and Leloup, C. (2014) 'Hypothalamic astroglial connexins are required for brain glucose sensing-induced insulin secretion', *J Cereb Blood Flow Metab,* 34(2), pp. 339-46.

Andrews, S. 2010. FastQC: a quality control tool for high throughput sequence data. Babraham Bioinformatics, Babraham Institute, Cambridge, United Kingdom.

Andriezen, W. L. (1893) 'The Neuroglia Elements in the Human Brain', *British medical journal,* 2(1700), pp. 227-230.

Anlauf, E. and Derouiche, A. (2013) 'Glutamine synthetase as an astrocytic marker: its cell type and vesicle localization', *Front Endocrinol (Lausanne),* 4, pp. 144.

Aponte, Y., Atasoy, D. and Sternson, S. M. (2011) 'AGRP neurons are sufficient to orchestrate feeding behavior rapidly and without training', *Nat Neurosci,* 14(3), pp. 351-5.

Araque, A., Carmignoto, G., Haydon, P. G., Oliet, S. H., Robitaille, R. and Volterra, A. (2014) 'Gliotransmitters travel in time and space', *Neuron*, 81(4), pp. 728-39.

Araque, A., Parpura, V., Sanzgiri, R. P. and Haydon, P. G. (1999) 'Tripartite synapses: glia, the unacknowledged partner', *Trends in Neurosciences*, 22(5), pp. 208-215.

Arriza, J. L., Fairman, W. A., Wadiche, J. I., Murdoch, G. H., Kavanaugh, M. P. and Amara, S. G. (1994) 'Functional comparisons of three glutamate transporter subtypes cloned from human motor cortex', *J Neurosci*, 14(9), pp. 5559-69.

Atlas, A. M. B. (2011) 'Seattle (WA): Allen Institute for Brain Science.© 2009', *World Wide Web (URL: http://mouse. brain-map. org).(Data retrieved October 2010)*.

Auestad, N., Korsak, R. A., Morrow, J. W. and Edmond, J. (1991) 'Fatty Acid Oxidation and Ketogenesis by Astrocytes in Primary Culture', *Journal of Neurochemistry*, 56(4), pp. 1376-1386.

Baddeley, A. and Turner, R. (2005) 'Spatstat: an R package for analyzing spatial point patterns: Journal of Statistical Software'.

Balthasar, N., Coppari, R., McMinn, J., Liu, S. M., Lee, C. E., Tang, V., Kenny, C. D., McGovern, R. A., Chua, S. C., Jr., Elmquist, J. K. and Lowell, B. B. (2004) 'Leptin receptor signaling in POMC neurons is required for normal body weight homeostasis', *Neuron*, 42(6), pp. 983-91.

Banks, W. A., Owen, J. B. and Erickson, M. A. (2012) 'Insulin in the brain: there and back again', *Pharmacology & therapeutics*, 136(1), pp. 82-93.

Barres, B. A. (2008) 'The Mystery and Magic of Glia: A Perspective on Their Roles in Health and Disease', *Neuron*, 60(3), pp. 430-440.

Batiuk, M. Y., de Vin, F., Duque, S. I., Li, C., Saito, T., Saido, T., Fiers, M., Belgard, T. G. and Holt, M. G. (2017) 'An immunoaffinity-based method for isolating ultrapure adult astrocytes based on ATP1B2 targeting by the ACSA-2 antibody', *J Biol Chem*, 292(21), pp. 8874-8891.

Bayraktar, O. A., Bartels, T., Holmqvist, S., Kleshchevnikov, V., Martirosyan, A., Polioudakis, D., Haim, L. B., Young, A. M., Batiuk, M. Y. and Prakash, K. (2020) 'Astrocyte layers in the mammalian cerebral cortex revealed by a single-cell in situ transcriptomic map', *Nature neuroscience*, 23(4), pp. 500-509.

Belgardt, B. F., Okamura, T. and Brüning, J. C. (2009) 'Hormone and glucose signalling in POMC and AgRP neurons', *The Journal of physiology*, 587(Pt 22), pp. 5305-5314.

Ben Haim, L. and Rowitch, D. H. (2017) 'Functional diversity of astrocytes in neural circuit regulation', *Nat Rev Neurosci*, 18(1), pp. 31-41.

Bergen, V., Lange, M., Peidli, S., Wolf, F. A. and Theis, F. J. (2020) 'Generalizing RNA velocity to transient cell states through dynamical modeling', *Nature Biotechnology*, 38(12), pp. 1408-1414.

Berkseth, K. E., Guyenet, S. J., Melhorn, S. J., Lee, D., Thaler, J. P., Schur, E. A. and Schwartz, M. W. (2014) 'Hypothalamic gliosis associated with high-fat diet feeding is reversible in mice: a combined immunohistochemical and magnetic resonance imaging study', *Endocrinology*, 155(8), pp. 2858-67.

Bernardis, L. L. and Bellinger, L. L. (1998) 'The Dorsomedial Hypothalamic Nucleus Revisited: 1998 Update', *Proceedings of the Society for Experimental Biology and Medicine*, 218(4), pp. 284-306.

Bindocci, E., Savtchouk, I., Liaudet, N., Becker, D., Carriero, G. and Volterra, A. (2017) 'Three-dimensional Ca(2+) imaging advances understanding of astrocyte biology', *Science*, 356(6339).

Blighe, K., Rana, S. and Lewis, M. 2021. EnhancedVolcano: publication-ready volcano plots with enhanced colouring and labeling. 2020. R package version 1.8. 0.

Boisvert, M. M., Erikson, G. A., Shokhirev, M. N. and Allen, N. J. (2018) 'The aging astrocyte transcriptome from multiple regions of the mouse brain', *Cell reports*, 22(1), pp. 269-285.

Borg, M. L., Omran, S. F., Weir, J., Meikle, P. J. and Watt, M. J. (2012) 'Consumption of a high-fat diet, but not regular endurance exercise training, regulates hypothalamic lipid accumulation in mice', *J Physiol*, 590(17), pp. 4377-89.

Boumezbeur, F., Mason, G. F., de Graaf, R. A., Behar, K. L., Cline, G. W., Shulman, G. I., Rothman, D. L. and Petersen, K. F. (2010) 'Altered brain mitochondrial metabolism in healthy aging as assessed by in vivo magnetic resonance spectroscopy', *J Cereb Blood Flow Metab*, 30(1), pp. 211-21.

Bouret, S. G., Draper, S. J. and Simerly, R. B. (2004) 'Formation of Projection Pathways from the Arcuate Nucleus of the Hypothalamus to Hypothalamic Regions Implicated in the Neural Control of Feeding Behavior in Mice', *The Journal of Neuroscience*, 24(11), pp. 2797-2805.

Bouzier-Sore, A. K., Voisin, P., Bouchaud, V., Bezancon, E., Franconi, J. M. and Pellerin, L. (2006) 'Competition between glucose and lactate as oxidative energy substrates in both neurons and astrocytes: a comparative NMR study', *European Journal of Neuroscience*, 24(6), pp. 1687-1694.

Brambilla, R., Bracchi-Ricard, V., Hu, W. H., Frydel, B., Bramwell, A., Karmally, S., Green, E. J. and Bethea, J. R. (2005) 'Inhibition of astroglial nuclear factor kappaB reduces inflammation and improves functional recovery after spinal cord injury', *J Exp Med*, 202(1), pp. 145-56.

Broberger, C., Johansen, J., Brismar, H., Johansson, C., Schalling, M. and Hökfelt, T. (1999) 'Changes in neuropeptide Y receptors and pro-opiomelanocortin in the anorexia (anx/anx) mouse hypothalamus', *The Journal of neuroscience : the official journal of the Society for Neuroscience*, 19(16), pp. 7130-7139.

Brown, A. M., Sickmann, H. M., Fosgerau, K., Lund, T. M., Schousboe, A., Waagepetersen, H. S. and Ransom, B. R. (2005) 'Astrocyte glycogen metabolism is required for neural activity during aglycemia or intense stimulation in mouse white matter', *J Neurosci Res*, 79(1-2), pp. 74-80.

Brozzi, F., Arcuri, C., Giambanco, I. and Donato, R. (2009) 'S100B Protein Regulates Astrocyte Shape and Migration via Interaction with Src Kinase: IMPLICATIONS FOR ASTROCYTE DEVELOPMENT, ACTIVATION, AND TUMOR GROWTH', *The Journal of biological chemistry*, 284(13), pp. 8797-8811.

Buccitelli, C. and Selbach, M. (2020) 'mRNAs, proteins and the emerging principles of gene expression control', *Nature Reviews Genetics*, 21(10), pp. 630-644.

Buckman, L. B., Hasty, A. H., Flaherty, D. K., Buckman, C. T., Thompson, M. M., Matlock, B. K., Weller, K. and Ellacott, K. L. (2014) 'Obesity induced by a high-fat diet is associated with increased immune cell entry into the central nervous system', *Brain Behav Immun*, 35, pp. 33-42.

Buckman, L. B., Thompson, M. M., Lippert, R. N., Blackwell, T. S., Yull, F. E. and Ellacott, K. L. (2015) 'Evidence for a novel functional role of astrocytes in the acute homeostatic response to high-fat diet intake in mice', *Mol Metab,* 4(1), pp. 58-63.

Buckman, L. B., Thompson, M. M., Moreno, H. N. and Ellacott, K. L. (2013) 'Regional astrogliosis in the mouse hypothalamus in response to obesity', *J Comp Neurol,* 521(6), pp. 1322-33.

Burda, J. E. and Sofroniew, M. V. (2014) 'Reactive gliosis and the multicellular response to CNS damage and disease', *Neuron,* 81(2), pp. 229-48.

Bushong, E. A., Martone, M. E., Jones, Y. Z. and Ellisman, M. H. (2002) 'Protoplasmic astrocytes in CA1 stratum radiatum occupy separate anatomical domains', *J Neurosci,* 22(1), pp. 183-92.

Butler, A. A., Kesterson, R. A., Khong, K., Cullen, M. J., Pelleymounter, M. A., Dekoning, J., Baetscher, M. and Cone, R. D. (2000) 'A unique metabolic syndrome causes obesity in the melanocortin-3 receptor-deficient mouse', *Endocrinology,* 141(9), pp. 3518-21.

Butt, A. M., Colquhoun, K., Tutton, M. and Berry, M. (1994) 'Three-dimensional morphology of astrocytes and oligodendrocytes in the intact mouse optic nerve', *J Neurocytol,* 23(8), pp. 469-85.

Cahoy, J. D., Emery, B., Kaushal, A., Foo, L. C., Zamanian, J. L., Christopherson, K. S., Xing, Y., Lubischer, J. L., Krieg, P. A., Krupenko, S. A., Thompson, W. J. and Barres, B. A. (2008) 'A transcriptome database for astrocytes, neurons, and oligodendrocytes: a new resource for understanding brain development and function', *J Neurosci,* 28(1), pp. 264-78.

Cai, W., Xue, C., Sakaguchi, M., Konishi, M., Shirazian, A., Ferris, H. A., Li, M. E., Yu, R., Kleinridders, A., Pothos, E. N. and Kahn, C. R. (2018) 'Insulin regulates astrocyte gliotransmission and modulates behavior', *J Clin Invest,* 128(7), pp. 2914-2926.

Cardona-Gómez, G. P., DonCarlos, L. and Garcia-Segura, L. M. (2000) 'Insulin-like growth factor I receptors and estrogen receptors colocalize in female rat brain', *Neuroscience,* 99(4), pp. 751-760.

Chaboub, L. S. and Deneen, B. (2012) 'Developmental origins of astrocyte heterogeneity: the final frontier of CNS development', *Developmental neuroscience,* 34(5), pp. 379-388.

Chai, H., Diaz-Castro, B., Shigetomi, E., Monte, E., Octeau, J. C., Yu, X., Cohn, W., Rajendran, P. S., Vondriska, T. M., Whitelegge, J. P., Coppola, G. and Khakh, B. S. (2017) 'Neural Circuit-Specialized Astrocytes: Transcriptomic, Proteomic, Morphological, and Functional Evidence', *Neuron,* 95(3), pp. 531-549 e9.

Chan-Ling, T. and Stone, J. (1991) 'Factors determining the morphology and distribution of astrocytes in the cat retina: A 'contact-spacing'model of astrocyte interaction', *Journal of comparative neurology,* 303(3), pp. 387-399.

Chen, H. and Boutros, P. C. (2011) 'VennDiagram: a package for the generation of highly-customizable Venn and Euler diagrams in R', *BMC bioinformatics,* 12(1), pp. 1-7.

Chen, N., Sugihara, H., Kim, J., Fu, Z., Barak, B., Sur, M., Feng, G. and Han, W. (2016) 'Direct modulation of GFAP-expressing glia in the arcuate nucleus bi-directionally regulates feeding', *Elife,* 5.

Chen, X. Q., He, J. R. and Wang, H. Y. (2012) 'Decreased expression of ALDH1L1 is associated with a poor prognosis in hepatocellular carcinoma', *Med Oncol,* 29(3), pp. 1843-9.

Chen, Y. and Struhl, G. (1998) 'In vivo evidence that Patched and Smoothened constitute distinct binding and transducing components of a Hedgehog receptor complex', *Development,* 125(24), pp. 4943-8.

Cheng, L., Yu, Y., Szabo, A., Wu, Y., Wang, H., Camer, D. and Huang, X. F. (2015a) 'Palmitic acid induces central leptin resistance and impairs hepatic glucose and lipid metabolism in male mice', *J Nutr Biochem,* 26(5), pp. 541-8.

Cheng, L., Yu, Y., Zhang, Q., Szabo, A., Wang, H. and Huang, X. F. (2015b) 'Arachidonic acid impairs hypothalamic leptin signaling and hepatic energy homeostasis in mice', *Mol Cell Endocrinol,* 412, pp. 12-8.

Cheunsuang, O. and Morris, R. (2005) 'Astrocytes in the arcuate nucleus and median eminence that take up a fluorescent dye from the circulation express leptin receptors and neuropeptide Y Y1 receptors', *Glia,* 52(3), pp. 228-233.

Chih, C. P. and Roberts, E. L., Jr. (2003) 'Energy substrates for neurons during neural activity: a critical review of the astrocyte-neuron lactate shuttle hypothesis', *J Cereb Blood Flow Metab,* 23(11), pp. 1263-81.

Chou, T. C., Scammell, T. E., Gooley, J. J., Gaus, S. E., Saper, C. B. and Lu, J. (2003) 'Critical role of dorsomedial hypothalamic nucleus in a wide range of behavioral circadian rhythms', *J Neurosci,* 23(33), pp. 10691-702.

Chowen, J. A., Argente-Arizón, P., Freire-Regatillo, A., Frago, L. M., Horvath, T. L. and Argente, J. (2016) 'The role of astrocytes in the hypothalamic response and adaptation to metabolic signals', *Prog Neurobiol,* 144, pp. 68-87.

Cone, R. D. (2005) 'Anatomy and regulation of the central melanocortin system', *Nature Neuroscience,* 8(5), pp. 571-578.

Cornell-Bell, A. H., Finkbeiner, S. M., Cooper, M. S. and Smith, S. J. (1990) 'Glutamate induces calcium waves in cultured astrocytes: long-range glial signaling', *Science,* 247(4941), pp. 470-473.

Coulter, D. A. and Steinhäuser, C. (2015) 'Role of astrocytes in epilepsy', *Cold Spring Harbor perspectives in medicine,* 5(3), pp. a022434-a022434.

Dafny, N. and Feldman, S. (1970) 'Unit responses and convergence of sensory stimuli in the hypothalamus', *Brain Research,* 17(2), pp. 243-257.

de Sousa Abreu, R., Penalva, L. O., Marcotte, E. M. and Vogel, C. (2009) 'Global signatures of protein and mRNA expression levels', *Mol Biosyst,* 5(12), pp. 1512-26.

De Souza, C. T., Araujo, E. P., Bordin, S., Ashimine, R., Zollner, R. L., Boschero, A. C., Saad, M. J. and Velloso, L. A. (2005) 'Consumption of a fat-rich diet activates a proinflammatory response and induces insulin resistance in the hypothalamus', *Endocrinology,* 146(10), pp. 4192-9.

Deiters, O. and Schultze, M. J. S. (1865) *Untersuchungen über Gehirn und Rückenmark des Menschen und der Säugethiere.* Braunschweig :: Vieweg.

Diano, S., Kalra, S. P. and Horvath, T. L. (1998) 'Leptin receptor immunoreactivity is associated with the Golgi apparatus of hypothalamic neurons and glial cells', *J Neuroendocrinol,* 10(9), pp. 647-50.

Dimicco, J. A. and Zaretsky, D. V. (2007) 'The dorsomedial hypothalamus: a new player in thermoregulation', *Am J Physiol Regul Integr Comp Physiol,* 292(1), pp. R47-63.

Dityatev, A. and Rusakov, D. A. (2011) 'Molecular signals of plasticity at the tetrapartite synapse', *Current Opinion in Neurobiology,* 21(2), pp. 353-359.

Donato, R., Cannon, B. R., Sorci, G., Riuzzi, F., Hsu, K., Weber, D. J. and Geczy, C. L. (2013) 'Functions of S100 proteins', *Curr Mol Med,* 13(1), pp. 24-57.

Dossi, E., Vasile, F. and Rouach, N. (2018) 'Human astrocytes in the diseased brain', *Brain research bulletin,* 136, pp. 139-156.

Douglass, J. D., Dorfman, M. D., Fasnacht, R., Shaffer, L. D. and Thaler, J. P. (2017) 'Astrocyte IKKβ/NF-κB signaling is required for diet-induced obesity and hypothalamic inflammation', *Mol Metab,* 6(4), pp. 366-373.

Dowell, J. A., Johnson, J. A. and Li, L. (2009) 'Identification of astrocyte secreted proteins with a combination of shotgun proteomics and bioinformatics', *J Proteome Res,* 8(8), pp. 4135-43.

Doyle, J. P., Dougherty, J. D., Heiman, M., Schmidt, E. F., Stevens, T. R., Ma, G., Bupp, S., Shrestha, P., Shah, R. D., Doughty, M. L., Gong, S., Greengard, P. and Heintz, N. (2008) 'Application of a translational profiling approach for the comparative analysis of CNS cell types', *Cell,* 135(4), pp. 749-62.

Drulis-Fajdasz, D., Wójtowicz, T., Wawrzyniak, M., Wlodarczyk, J., Mozrzymas, J. W. and Rakus, D. (2015) 'Involvement of cellular metabolism in age-related LTP modifications in rat hippocampal slices', *Oncotarget,* 6(16), pp. 14065-14081.

Elias, C. F., Lee, C., Kelly, J., Aschkenasi, C., Ahima, R. S., Couceyro, P. R., Kuhar, M. J., Saper, C. B. and Elmquist, J. K. (1998a) 'Leptin activates hypothalamic CART neurons projecting to the spinal cord', *Neuron,* 21(6), pp. 1375-85.

Elias, C. F., Saper, C. B., Maratos-Flier, E., Tritos, N. A., Lee, C., Kelly, J., Tatro, J. B., Hoffman, G. E., Ollmann, M. M., Barsh, G. S., Sakurai, T., Yanagisawa, M. and Elmquist, J. K. (1998b) 'Chemically defined projections linking the mediobasal hypothalamus and the lateral hypothalamic area', *Journal of Comparative Neurology,* 402(4), pp. 442-459.

Elmquist, J. K., Elias, C. F. and Saper, C. B. (1999) 'From Lesions to Leptin: Hypothalamic Control of Food Intake and Body Weight', *Neuron,* 22(2), pp. 221-232.

Eng, L. F. and Ghirnikar, R. S. (1994) 'GFAP and astrogliosis', *Brain Pathol,* 4(3), pp. 229-37.

Escartin, C., Galea, E., Lakatos, A., O'Callaghan, J. P., Petzold, G. C., Serrano-Pozo, A., Steinhäuser, C., Volterra, A., Carmignoto, G., Agarwal, A., Allen, N. J., Araque, A., Barbeito, L., Barzilai, A., Bergles, D. E., Bonvento, G., Butt, A. M., Chen, W. T., Cohen-Salmon, M., Cunningham, C., Deneen, B., De Strooper, B., Díaz-Castro, B., Farina, C., Freeman, M., Gallo, V., Goldman, J. E., Goldman, S. A., Götz, M., Gutiérrez, A., Haydon, P. G., Heiland, D. H., Hol, E. M., Holt, M. G., Iino, M., Kastanenka, K. V., Kettenmann, H., Khakh, B. S., Koizumi, S., Lee, C. J., Liddelow, S. A., MacVicar, B. A., Magistretti, P., Messing, A., Mishra, A., Molofsky, A. V., Murai, K. K., Norris, C. M., Okada, S., Oliet, S. H. R., Oliveira, J. F., Panatier, A., Parpura, V., Pekna, M., Pekny, M., Pellerin, L., Perea, G., Pérez-Nievas, B. G., Pfrieger, F. W., Poskanzer, K. E., Quintana, F. J., Ransohoff, R. M., Riquelme-Perez, M., Robel, S., Rose, C. R., Rothstein, J. D., Rouach, N., Rowitch, D. H., Semyanov, A., Sirko, S., Sontheimer, H., Swanson, R. A., Vitorica, J., Wanner, I. B., Wood, L. B., Wu, J., Zheng, B., Zimmer, E. R., Zorec, R., Sofroniew, M. V. and Verkhratsky, A. (2021) 'Reactive astrocyte nomenclature, definitions, and future directions', *Nat Neurosci,* 24(3), pp. 312-325.

Farmer, W. T., Abrahamsson, T., Chierzi, S., Lui, C., Zaelzer, C., Jones, E. V., Bally, B. P., Chen, G. G., Theroux, J. F., Peng, J., Bourque, C. W., Charron, F., Ernst, C., Sjostrom, P. J. and Murai, K. K. (2016) 'Neurons diversify astrocytes in the adult brain through sonic hedgehog signaling', *Science,* 351(6275), pp. 849-54.

Fenselau, H., Campbell, J. N., Verstegen, A. M. J., Madara, J. C., Xu, J., Shah, B. P., Resch, J. M., Yang, Z., Mandelblat-Cerf, Y., Livneh, Y. and Lowell, B. B. (2017) 'A rapidly acting glutamatergic ARC→PVH satiety circuit postsynaptically regulated by α-MSH', *Nature Neuroscience,* 20(1), pp. 42-51.

Ferguson, A. V., Latchford, K. J. and Samson, W. K. (2008) 'The paraventricular nucleus of the hypothalamus - a potential target for integrative treatment of autonomic dysfunction', *Expert Opin Ther Targets,* 12(6), pp. 717-27.

Freire-Regatillo, A., Fernández-Gómez, M. J., Díaz, F., Barrios, V., Sánchez-Jabonero, I., Frago, L. M., Argente, J., García-Segura, L. M. and Chowen, J. A. (2020) 'Sex differences in the peripubertal response to a short-term, high-fat diet intake', *J Neuroendocrinol,* 32(1), pp. e12756.

Fuccillo, M., Joyner, A. L. and Fishell, G. (2006) 'Morphogen to mitogen: the multiple roles of hedgehog signalling in vertebrate neural development', *Nat Rev Neurosci,* 7(10), pp. 772-83.

Fuente-Martin, E., Garcia-Caceres, C., Argente-Arizon, P., Diaz, F., Granado, M., Freire-Regatillo, A., Castro-Gonzalez, D., Ceballos, M. L., Frago, L. M., Dickson, S. L., Argente, J. and Chowen, J. A. (2016) 'Ghrelin Regulates Glucose and Glutamate Transporters in Hypothalamic Astrocytes', *Sci Rep,* 6, pp. 23673.

Fuente-Martin, E., Garcia-Caceres, C., Granado, M., de Ceballos, M. L., Sanchez-Garrido, M. A., Sarman, B., Liu, Z. W., Dietrich, M. O., Tena-Sempere, M., Argente-Arizon, P., Diaz, F., Argente, J., Horvath, T. L. and Chowen, J. A. (2012) 'Leptin regulates glutamate and glucose transporters in hypothalamic astrocytes', *J Clin Invest,* 122(11), pp. 3900-13.

Galou, M., Colucci-Guyon, E., Ensergueix, D., Ridet, J. L., Gimenez y Ribotta, M., Privat, A., Babinet, C. and Dupouey, P. (1996) 'Disrupted glial fibrillary acidic protein network in astrocytes from vimentin knockout mice', *J Cell Biol,* 133(4), pp. 853-63.

Ganat, Y. M., Silbereis, J., Cave, C., Ngu, H., Anderson, G. M., Ohkubo, Y., Ment, L. R. and Vaccarino, F. M. (2006) 'Early postnatal astroglial cells produce multilineage precursors and neural stem cells in vivo', *J Neurosci,* 26(33), pp. 8609-21.

Gandhi, G. K., Cruz, N. F., Ball, K. K. and Dienel, G. A. (2009) 'Astrocytes are poised for lactate trafficking and release from activated brain and for supply of glucose to neurons', *J Neurochem,* 111(2), pp. 522-36.

Gao, Q. and Horvath, T. L. (2007) 'Neurobiology of feeding and energy expenditure', *Annu Rev Neurosci,* 30, pp. 367-98.

Gao, Q. and Horvath, T. L. (2008) 'Neuronal control of energy homeostasis', *FEBS Lett,* 582(1), pp. 132-41.

Gao, Q., Mezei, G., Nie, Y., Rao, Y., Choi, C. S., Bechmann, I., Leranth, C., Toran-Allerand, D., Priest, C. A., Roberts, J. L., Gao, X. B., Mobbs, C., Shulman, G. I., Diano, S. and Horvath, T. L. (2007) 'Anorectic estrogen mimics leptin's effect on the rewiring of melanocortin cells and Stat3 signaling in obese animals', *Nat Med,* 13(1), pp. 89-94.

Gao, Y., Bielohuby, M., Fleming, T., Grabner, G. F., Foppen, E., Bernhard, W., Guzman-Ruiz, M., Layritz, C., Legutko, B., Zinser, E., Garcia-Caceres, C., Buijs, R. M., Woods, S. C., Kalsbeek, A., Seeley, R. J., Nawroth, P. P., Bidlingmaier, M., Tschop, M. H. and Yi, C. X. (2017a) 'Dietary sugars, not lipids, drive hypothalamic inflammation', *Mol Metab,* 6(8), pp. 897-908.

Gao, Y., Layritz, C., Legutko, B., Eichmann, T. O., Laperrousaz, E., Moullé, V. S., Cruciani-Guglielmacci, C., Magnan, C., Luquet, S., Woods, S. C., Eckel, R. H., Yi, C. X., Garcia-Caceres, C. and Tschöp, M. H. (2017b) 'Disruption of Lipid Uptake in Astroglia Exacerbates Diet-Induced Obesity', *Diabetes*, 66(10), pp. 2555-2563.

Gao, Y., Ottaway, N., Schriever, S. C., Legutko, B., Garcia-Caceres, C., de la Fuente, E., Mergen, C., Bour, S., Thaler, J. P., Seeley, R. J., Filosa, J., Stern, J. E., Perez-Tilve, D., Schwartz, M. W., Tschop, M. H. and Yi, C. X. (2014) 'Hormones and diet, but not body weight, control hypothalamic microglial activity', *Glia*, 62(1), pp. 17-25.

Garcia, A. D., Petrova, R., Eng, L. and Joyner, A. L. (2010) 'Sonic hedgehog regulates discrete populations of astrocytes in the adult mouse forebrain', *J Neurosci*, 30(41), pp. 13597-608.

Garcia-Caceres, C., Balland, E., Prevot, V., Luquet, S., Woods, S. C., Koch, M., Horvath, T. L., Yi, C. X., Chowen, J. A., Verkhratsky, A., Araque, A., Bechmann, I. and Tschop, M. H. (2019) 'Role of astrocytes, microglia, and tanycytes in brain control of systemic metabolism', *Nat Neurosci*, 22(1), pp. 7-14.

Garcia-Caceres, C., Fuente-Martin, E., Burgos-Ramos, E., Granado, M., Frago, L. M., Barrios, V., Horvath, T., Argente, J. and Chowen, J. A. (2011) 'Differential acute and chronic effects of leptin on hypothalamic astrocyte morphology and synaptic protein levels', *Endocrinology*, 152(5), pp. 1809-18.

Garcia-Caceres, C., Fuente-Martin, E., Diaz, F., Granado, M., Argente-Arizon, P., Frago, L. M., Freire-Regatillo, A., Barrios, V., Argente, J. and Chowen, J. A. (2014) 'The opposing effects of ghrelin on hypothalamic and systemic inflammatory processes are modulated by its acylation status and food intake in male rats', *Endocrinology*, 155(8), pp. 2868-80.

Garcia-Caceres, C., Quarta, C., Varela, L., Gao, Y., Gruber, T., Legutko, B., Jastroch, M., Johansson, P., Ninkovic, J., Yi, C. X., Le Thuc, O., Szigeti-Buck, K., Cai, W., Meyer, C. W., Pfluger, P. T., Fernandez, A. M., Luquet, S., Woods, S. C., Torres-Aleman, I., Kahn, C. R., Gotz, M., Horvath, T. L. and Tschop, M. H. (2016) 'Astrocytic Insulin Signaling Couples Brain Glucose Uptake with Nutrient Availability', *Cell*, 166(4), pp. 867-880.

García-Cáceres, C., Yi, C. X. and Tschöp, M. H. (2013) 'Hypothalamic astrocytes in obesity', *Endocrinol Metab Clin North Am*, 42(1), pp. 57-66.

Gazdzinski, S., Kornak, J., Weiner, M. W. and Meyerhoff, D. J. (2008) 'Body mass index and magnetic resonance markers of brain integrity in adults', *Ann Neurol,* 63(5), pp. 652-7.

Ge, W. P., Miyawaki, A., Gage, F. H., Jan, Y. N. and Jan, L. Y. (2012) 'Local generation of glia is a major astrocyte source in postnatal cortex', *Nature,* 484(7394), pp. 376-80.

Gerashchenko, D. and Shiromani, P. J. (2004) 'Different neuronal phenotypes in the lateral hypothalamus and their role in sleep and wakefulness', *Molecular neurobiology,* 29(1), pp. 41-59.

Giaume, C., Koulakoff, A., Roux, L., Holcman, D. and Rouach, N. (2010) 'Astroglial networks: a step further in neuroglial and gliovascular interactions', *Nature Reviews Neuroscience,* 11(2), pp. 87-99.

Golgi, C. (1903) *Opera omnia.* Milano: Ulrico Hoepli.

Gonçalves, C. A., Leite, M. C. and Nardin, P. (2008) 'Biological and methodological features of the measurement of S100B, a putative marker of brain injury', *Clin Biochem,* 41(10-11), pp. 755-63.

González-García, I. and García-Cáceres, C. (2021) 'Hypothalamic Astrocytes as a Specialized and Responsive Cell Population in Obesity', *International journal of molecular sciences,* 22(12), pp. 6176.

Gropp, E., Shanabrough, M., Borok, E., Xu, A. W., Janoschek, R., Buch, T., Plum, L., Balthasar, N., Hampel, B., Waisman, A., Barsh, G. S., Horvath, T. L. and Brüning, J. C. (2005) 'Agouti-related peptide-expressing neurons are mandatory for feeding', *Nat Neurosci,* 8(10), pp. 1289-91.

Gruber, T., Pan, C., Contreras, R. E., Wiedemann, T., Morgan, D. A., Skowronski, A. A., Lefort, S., De Bernardis Murat, C., Le Thuc, O., Legutko, B., Ruiz-Ojeda, F. J., Fuente-Fernández, M. d. l., García-Villalón, A. L., González-Hedström, D., Huber, M., Szigeti-Buck, K., Müller, T. D., Ussar, S., Pfluger, P., Woods, S. C., Ertürk, A., LeDuc, C. A., Rahmouni, K., Granado, M., Horvath, T. L., Tschöp, M. H. and García-Cáceres, C. (2021) 'Obesity-associated hyperleptinemia alters the gliovascular interface of the hypothalamus to promote hypertension', *Cell Metabolism,* 33(6), pp. 1155-1170.e10.

Gunstad, J., Paul, R. H., Cohen, R. A., Tate, D. F., Spitznagel, M. B., Grieve, S. and Gordon, E. (2008) 'Relationship Between Body Mass Index and Brain Volume in Healthy Adults', *International Journal of Neuroscience,* 118(11), pp. 1582-1593.

Gupta, S., Knight, A. G., Gupta, S., Keller, J. N. and Bruce-Keller, A. J. (2012) 'Saturated long-chain fatty acids activate inflammatory signaling in astrocytes', *J Neurochem,* 120(6), pp. 1060-71.

Guzmán, M. and Blázquez, C. (2004) 'Ketone body synthesis in the brain: possible neuroprotective effects', *Prostaglandins Leukot Essent Fatty Acids,* 70(3), pp. 287-92.

Gyengesi, E., Liu, Z. W., D'Agostino, G., Gan, G., Horvath, T. L., Gao, X. B. and Diano, S. (2010) 'Corticosterone regulates synaptic input organization of POMC and NPY/AgRP neurons in adult mice', *Endocrinology,* 151(11), pp. 5395-402.

Hahn, T. M., Breininger, J. F., Baskin, D. G. and Schwartz, M. W. (1998) 'Coexpression of Agrp and NPY in fasting-activated hypothalamic neurons', *Nat Neurosci,* 1(4), pp. 271-2.

Halassa, M. M., Fellin, T., Takano, H., Dong, J. H. and Haydon, P. G. (2007) 'Synaptic islands defined by the territory of a single astrocyte', *J Neurosci,* 27(24), pp. 6473-7.

Hales, C. M., Carroll, M. D., Fryar, C. D. and Ogden, C. L. (2017) 'Prevalence of Obesity Among Adults and Youth: United States, 2015-2016', *NCHS Data Brief,* (288), pp. 1-8.

Hamby, M. E. and Sofroniew, M. V. (2010) 'Reactive astrocytes as therapeutic targets for CNS disorders', *Neurotherapeutics,* 7(4), pp. 494-506.

Harada, K., Kamiya, T. and Tsuboi, T. (2016) 'Gliotransmitter release from astrocytes: functional, developmental and pathological implications in the brain', *Frontiers in Neuroscience,* 9(499).

Harwell, C. C., Parker, P. R., Gee, S. M., Okada, A., McConnell, S. K., Kreitzer, A. C. and Kriegstein, A. R. (2012) 'Sonic hedgehog expression in corticofugal projection neurons directs cortical microcircuit formation', *Neuron,* 73(6), pp. 1116-26.

Hayden, M. S. and Ghosh, S. (2008) 'Shared principles in NF-kappaB signaling', *Cell,* 132(3), pp. 344-62.

Heine, P. A., Taylor, J. A., Iwamoto, G. A., Lubahn, D. B. and Cooke, P. S. (2000) 'Increased adipose tissue in male and female estrogen receptor-alpha knockout mice', *Proc Natl Acad Sci U S A*, 97(23), pp. 12729-34.

Held, H. (1909) 'Ueber die Neuroglia marginalis der menschlichen Grosshirnrinde. pp. 360–374', *European Neurology*, 26(Suppl. 1), pp. 360-374.

Hernandez-Garzón, E., Fernandez, A. M., Perez-Alvarez, A., Genis, L., Bascuñana, P., Fernandez de la Rosa, R., Delgado, M., Angel Pozo, M., Moreno, E., McCormick, P. J., Santi, A., Trueba-Saiz, A., Garcia-Caceres, C., Tschöp, M. H., Araque, A., Martin, E. D. and Torres Aleman, I. (2016) 'The insulin-like growth factor I receptor regulates glucose transport by astrocytes', *Glia*, 64(11), pp. 1962-71.

Hill, J. W. (2012) 'PVN pathways controlling energy homeostasis', *Indian J Endocrinol Metab*, 16(Suppl 3), pp. S627-36.

Hinney, A. and Hebebrand, J. (2008) 'Polygenic Obesity in Humans', *Obesity Facts*, 1(1), pp. 35-42.

Holtzclaw, L. A., Pandhit, S., Bare, D. J., Mignery, G. A. and Russell, J. T. (2002) 'Astrocytes in adult rat brain express type 2 inositol 1,4,5-trisphosphate receptors', *Glia*, 39(1), pp. 69-84.

Horvath, T. L., Sarman, B., García-Cáceres, C., Enriori, P. J., Sotonyi, P., Shanabrough, M., Borok, E., Argente, J., Chowen, J. A., Perez-Tilve, D., Pfluger, P. T., Brönneke, H. S., Levin, B. E., Diano, S., Cowley, M. A. and Tschöp, M. H. (2010) 'Synaptic input organization of the melanocortin system predicts diet-induced hypothalamic reactive gliosis and obesity', *Proceedings of the National Academy of Sciences*, 107(33), pp. 14875-14880.

Hotamisligil, G. S., Arner, P., Caro, J. F., Atkinson, R. L. and Spiegelman, B. M. (1995) 'Increased adipose tissue expression of tumor necrosis factor-alpha in human obesity and insulin resistance', *The Journal of clinical investigation*, 95(5), pp. 2409-2415.

Howard, J. K., Cave, B. J., Oksanen, L. J., Tzameli, I., Bjørbaek, C. and Flier, J. S. (2004) 'Enhanced leptin sensitivity and attenuation of diet-induced obesity in mice with haploinsufficiency of Socs3', *Nat Med*, 10(7), pp. 734-8.

Hsuchou, H., He, Y., Kastin, A. J., Tu, H., Markadakis, E. N., Rogers, R. C., Fossier, P. B. and Pan, W. (2009) 'Obesity induces functional astrocytic leptin receptors in hypothalamus', *Brain*, 132(Pt 4), pp. 889-902.

Hubbard, J. A., Hsu, M. S., Seldin, M. M. and Binder, D. K. (2015) 'Expression of the Astrocyte Water Channel Aquaporin-4 in the Mouse Brain', *ASN neuro*, 7(5), pp. 1759091415605486.

Hunter, J. D. (2007) 'Matplotlib: A 2D graphics environment', *IEEE Annals of the History of Computing*, 9(03), pp. 90-95.

Iliff, J. J., Wang, M., Liao, Y., Plogg, B. A., Peng, W., Gundersen, G. A., Benveniste, H., Vates, G. E., Deane, R., Goldman, S. A., Nagelhus, E. A. and Nedergaard, M. (2012) 'A paravascular pathway facilitates CSF flow through the brain parenchyma and the clearance of interstitial solutes, including amyloid β', *Sci Transl Med*, 4(147), pp. 147ra111.

Jais, A. and Brüning, J. C. (2021) 'Arcuate nucleus-dependent regulation of metabolism - pathways to obesity and diabetes mellitus', *Endocr Rev*.

Jais, A., Paeger, L., Sotelo-Hitschfeld, T., Bremser, S., Prinzensteiner, M., Klemm, P., Mykytiuk, V., Widdershooven, P. J. M., Vesting, A. J., Grzelka, K., Minère, M., Cremer, A. L., Xu, J., Korotkova, T., Lowell, B. B., Zeilhofer, H. U., Backes, H., Fenselau, H., Wunderlich, F. T., Kloppenburg, P. and Brüning, J. C. (2020) 'PNOC(ARC) Neurons Promote Hyperphagia and Obesity upon High-Fat-Diet Feeding', *Neuron*, 106(6), pp. 1009-1025.e10.

John Lin, C. C., Yu, K., Hatcher, A., Huang, T. W., Lee, H. K., Carlson, J., Weston, M. C., Chen, F., Zhang, Y., Zhu, W., Mohila, C. A., Ahmed, N., Patel, A. J., Arenkiel, B. R., Noebels, J. L., Creighton, C. J. and Deneen, B. (2017) 'Identification of diverse astrocyte populations and their malignant analogs', *Nat Neurosci*, 20(3), pp. 396-405.

Kacem, K., Lacombe, P., Seylaz, J. and Bonvento, G. (1998) 'Structural organization of the perivascular astrocyte endfeet and their relationship with the endothelial glucose transporter: a confocal microscopy study', *Glia*, 23(1), pp. 1-10.

Kälin, S., Heppner, F. L., Bechmann, I., Prinz, M., Tschöp, M. H. and Yi, C. X. (2015) 'Hypothalamic innate immune reaction in obesity', *Nat Rev Endocrinol*, 11(6), pp. 339-51.

Kamphuis, W., Kooijman, L., Orre, M., Stassen, O., Pekny, M. and Hol, E. M. (2015) 'GFAP and vimentin deficiency alters gene expression in astrocytes and microglia in wild-type mice

and changes the transcriptional response of reactive glia in mouse model for Alzheimer's disease', *Glia,* 63(6), pp. 1036-56.

Kandel, E. R., Schwartz, J. H., Jessell, T. M., Siegelbaum, S., Hudspeth, A. J. and Mack, S. (2000) *Principles of neural science.* McGraw-hill New York.

Kanemaru, K., Kubota, J., Sekiya, H., Hirose, K., Okubo, Y. and Iino, M. (2013) 'Calcium-dependent N-cadherin up-regulation mediates reactive astrogliosis and neuroprotection after brain injury', *Proceedings of the National Academy of Sciences,* 110(28), pp. 11612-11617.

Kanemaru, K., Sekiya, H., Xu, M., Satoh, K., Kitajima, N., Yoshida, K., Okubo, Y., Sasaki, T., Moritoh, S., Hasuwa, H., Mimura, M., Horikawa, K., Matsui, K., Nagai, T., Iino, M. and Tanaka, K. F. (2014) 'In vivo visualization of subtle, transient, and local activity of astrocytes using an ultrasensitive Ca(2+) indicator', *Cell Rep,* 8(1), pp. 311-8.

Kantzer, C. G., Boutin, C., Herzig, I. D., Wittwer, C., Reiss, S., Tiveron, M. C., Drewes, J., Rockel, T. D., Ohlig, S., Ninkovic, J., Cremer, H., Pennartz, S., Jungblut, M. and Bosio, A. (2017) 'Anti-ACSA-2 defines a novel monoclonal antibody for prospective isolation of living neonatal and adult astrocytes', *Glia,* 65(6), pp. 990-1004.

Khaodhiar, L., McCowen, K. C. and Blackburn, G. L. (1999) 'Obesity and its comorbid conditions', *Clin Cornerstone,* 2(3), pp. 17-31.

Kim, J. G., Suyama, S., Koch, M., Jin, S., Argente-Arizon, P., Argente, J., Liu, Z. W., Zimmer, M. R., Jeong, J. K., Szigeti-Buck, K., Gao, Y., Garcia-Caceres, C., Yi, C. X., Salmaso, N., Vaccarino, F. M., Chowen, J., Diano, S., Dietrich, M. O., Tschop, M. H. and Horvath, T. L. (2014) 'Leptin signaling in astrocytes regulates hypothalamic neuronal circuits and feeding', *Nat Neurosci,* 17(7), pp. 908-10.

Kleinridders, A., Schenten, D., Könner, A. C., Belgardt, B. F., Mauer, J., Okamura, T., Wunderlich, F. T., Medzhitov, R. and Brüning, J. C. (2009) 'MyD88 signaling in the CNS is required for development of fatty acid-induced leptin resistance and diet-induced obesity', *Cell Metab,* 10(4), pp. 249-59.

Klöckener, T., Hess, S., Belgardt, B. F., Paeger, L., Verhagen, L. A. W., Husch, A., Sohn, J.-W., Hampel, B., Dhillon, H., Zigman, J. M., Lowell, B. B., Williams, K. W., Elmquist, J. K., Horvath, T. L., Kloppenburg, P. and Brüning, J. C. (2011) 'High-fat feeding promotes obesity

via insulin receptor/PI3K-dependent inhibition of SF-1 VMH neurons', *Nature Neuroscience*, 14(7), pp. 911-918.

Köhler, S., Winkler, U. and Hirrlinger, J. (2021) 'Heterogeneity of Astrocytes in Grey and White Matter', *Neurochemical Research*, 46(1), pp. 3-14.

Kolde, R. (2015) 'pheatmap: Pretty heatmaps [Software]', *URL https://CRAN. R-project. org/package= pheatmap*.

Kölliker, A. and Ebner, V. v. (1889) *Handbuch der Gewebelehre des Menschen.*

Krashes, M. J., Koda, S., Ye, C., Rogan, S. C., Adams, A. C., Cusher, D. S., Maratos-Flier, E., Roth, B. L. and Lowell, B. B. (2011) 'Rapid, reversible activation of AgRP neurons drives feeding behavior in mice', *J Clin Invest*, 121(4), pp. 1424-8.

Krashes, M. J., Shah, B. P., Koda, S. and Lowell, B. B. (2013) 'Rapid versus delayed stimulation of feeding by the endogenously released AgRP neuron mediators GABA, NPY, and AgRP', *Cell Metab*, 18(4), pp. 588-95.

Krashes, M. J., Shah, B. P., Madara, J. C., Olson, D. P., Strochlic, D. E., Garfield, A. S., Vong, L., Pei, H., Watabe-Uchida, M., Uchida, N., Liberles, S. D. and Lowell, B. B. (2014) 'An excitatory paraventricular nucleus to AgRP neuron circuit that drives hunger', *Nature*, 507(7491), pp. 238-242.

Kriegstein, A. and Alvarez-Buylla, A. (2009) 'The glial nature of embryonic and adult neural stem cells', *Annual review of neuroscience*, 32, pp. 149-184.

Krupenko, S. A. (2009) 'FDH: an aldehyde dehydrogenase fusion enzyme in folate metabolism', *Chem Biol Interact*, 178(1-3), pp. 84-93.

Kulak, N. A., Pichler, G., Paron, I., Nagaraj, N. and Mann, M. (2014) 'Minimal, encapsulated proteomic-sample processing applied to copy-number estimation in eukaryotic cells', *Nature Methods*, 11(3), pp. 319-324.

Kullmann, S., Valenta, V., Wagner, R., Tschritter, O., Machann, J., Häring, H. U., Preissl, H., Fritsche, A. and Heni, M. (2020) 'Brain insulin sensitivity is linked to adiposity and body fat distribution', *Nat Commun*, 11(1), pp. 1841.

La Manno, G., Soldatov, R., Zeisel, A., Braun, E., Hochgerner, H., Petukhov, V., Lidschreiber, K., Kastriti, M. E., Lönnerberg, P., Furlan, A., Fan, J., Borm, L. E., Liu, Z., van Bruggen, D., Guo, J., He, X., Barker, R., Sundström, E., Castelo-Branco, G., Cramer, P., Adameyko, I., Linnarsson, S. and Kharchenko, P. V. (2018) 'RNA velocity of single cells', *Nature,* 560(7719), pp. 494-498.

Lang, M., Binder, M., Richter, J., Schratz, P., Pfisterer, F., Coors, S., Au, Q., Casalicchio, G., Kotthoff, L. and Bischl, B. (2019) 'mlr3: A modern object-oriented machine learning framework in R', *Journal of Open Source Software,* 4(44), pp. 1903.

Langlet, F. (2014) 'Tanycytes: a gateway to the metabolic hypothalamus', *J Neuroendocrinol,* 26(11), pp. 753-60.

Lanjakornsiripan, D., Pior, B.-J., Kawaguchi, D., Furutachi, S., Tahara, T., Katsuyama, Y., Suzuki, Y., Fukazawa, Y. and Gotoh, Y. (2018) 'Layer-specific morphological and molecular differences in neocortical astrocytes and their dependence on neuronal layers', *Nature Communications,* 9(1), pp. 1623.

Lapato, A. S. and Tiwari-Woodruff, S. K. (2018) 'Connexins and pannexins: At the junction of neuro-glial homeostasis & disease', *J Neurosci Res,* 96(1), pp. 31-44.

Le Foll, C., Dunn-Meynell, A. A., Miziorko, H. M. and Levin, B. E. (2014) 'Regulation of hypothalamic neuronal sensing and food intake by ketone bodies and fatty acids', *Diabetes,* 63(4), pp. 1259-69.

Lee, A., Cardel, M. and Donahoo, W. T. (2000) 'Social and Environmental Factors Influencing Obesity', in Feingold, K.R., Anawalt, B., Boyce, A., Chrousos, G., de Herder, W.W., Dhatariya, K., Dungan, K., Grossman, A., Hershman, J.M., Hofland, J., Kalra, S., Kaltsas, G., Koch, C., Kopp, P., Korbonits, M., Kovacs, C.S., Kuohung, W., Laferrère, B., McGee, E.A., McLachlan, R., Morley, J.E., New, M., Purnell, J., Sahay, R., Singer, F., Stratakis, C.A., Trence, D.L. and Wilson, D.P. (eds.) *Endotext*. South Dartmouth (MA): MDText.com, Inc.
Copyright © 2000-2021, MDText.com, Inc.

Lee, C. H., Suk, K., Yu, R. and Kim, M. S. (2020) 'Cellular Contributors to Hypothalamic Inflammation in Obesity', *Mol Cells,* 43(5), pp. 431-437.

Leibowitz, S. F., Hammer, N. J. and Chang, K. (1981) 'Hypothalamic paraventricular nucleus lesions produce overeating and obesity in the rat', *Physiol Behav,* 27(6), pp. 1031-40.

Lein, E. S. and Hawrylycz, M. J. and Ao, N. and Ayres, M. and Bensinger, A. and Bernard, A. and Boe, A. F. and Boguski, M. S. and Brockway, K. S. and Byrnes, E. J. and Chen, L. and Chen, L. and Chen, T. M. and Chin, M. C. and Chong, J. and Crook, B. E. and Czaplinska, A. and Dang, C. N. and Datta, S. and Dee, N. R. and Desaki, A. L. and Desta, T. and Diep, E. and Dolbeare, T. A. and Donelan, M. J. and Dong, H. W. and Dougherty, J. G. and Duncan, B. J. and Ebbert, A. J. and Eichele, G. and Estin, L. K. and Faber, C. and Facer, B. A. and Fields, R. and Fischer, S. R. and Fliss, T. P. and Frensley, C. and Gates, S. N. and Glattfelder, K. J. and Halverson, K. R. and Hart, M. R. and Hohmann, J. G. and Howell, M. P. and Jeung, D. P. and Johnson, R. A. and Karr, P. T. and Kawal, R. and Kidney, J. M. and Knapik, R. H. and Kuan, C. L. and Lake, J. H. and Laramee, A. R. and Larsen, K. D. and Lau, C. and Lemon, T. A. and Liang, A. J. and Liu, Y. and Luong, L. T. and Michaels, J. and Morgan, J. J. and Morgan, R. J. and Mortrud, M. T. and Mosqueda, N. F. and Ng, L. L. and Ng, R. and Orta, G. J. and Overly, C. C. and Pak, T. H. and Parry, S. E. and Pathak, S. D. and Pearson, O. C. and Puchalski, R. B. and Riley, Z. L. and Rockett, H. R. and Rowland, S. A. and Royall, J. J. and Ruiz, M. J. and Sarno, N. R. and Schaffnit, K. and Shapovalova, N. V. and Sivisay, T. and Slaughterbeck, C. R. and Smith, S. C. and Smith, K. A. and Smith, B. I. and Sodt, A. J. and Stewart, N. N. and Stumpf, K. R. and Sunkin, S. M. and Sutram, M. and Tam, A. and Teemer, C. D. and Thaller, C. and Thompson, C. L. and Varnam, L. R. and Visel, A. and Whitlock, R. M. and Wohnoutka, P. E. and Wolkey, C. K. and Wong, V. Y. and Wood, M. and Yaylaoglu, M. B. and Young, R. C. and Youngstrom, B. L. and Yuan, X. F. and Zhang, B. and Zwingman, T. A. and Jones, A. R. (2007) 'Genome-wide atlas of gene expression in the adult mouse brain', *Nature,* 445(7124), pp. 168-76.

Lemus, M. B., Bayliss, J. A., Lockie, S. H., Santos, V. V., Reichenbach, A., Stark, R. and Andrews, Z. B. (2015) 'A stereological analysis of NPY, POMC, Orexin, GFAP astrocyte, and Iba1 microglia cell number and volume in diet-induced obese male mice', *Endocrinology,* 156(5), pp. 1701-13.

Lenhossék, M. (1893) *Der feinere Bau des Nervensystems im Lichte neuester Forschungen.* Fischer.

Li, H., Xie, Y., Zhang, N., Yu, Y., Zhang, Q. and Ding, S. (2015a) 'Disruption of IP_3R2-mediated Ca^{2+} signaling pathway in astrocytes ameliorates neuronal death and brain damage while reducing behavioral deficits after focal ischemic stroke', *Cell calcium,* 58(6), pp. 565-576.

Li, J. M., Ge, C. X., Xu, M. X., Wang, W., Yu, R., Fan, C. Y. and Kong, L. D. (2015b) 'Betaine recovers hypothalamic neural injury by inhibiting astrogliosis and inflammation in fructose-fed rats', *Mol Nutr Food Res,* 59(2), pp. 189-202.

Li, T., Giaume, C. and Xiao, L. (2014) 'Connexins-mediated glia networking impacts myelination and remyelination in the central nervous system', *Mol Neurobiol,* 49(3), pp. 1460-71.

Li, X., Zima, A. V., Sheikh, F., Blatter, L. A. and Chen, J. (2005) 'Endothelin-1-induced arrhythmogenic Ca2+ signaling is abolished in atrial myocytes of inositol-1,4,5-trisphosphate(IP3)-receptor type 2-deficient mice', *Circ Res,* 96(12), pp. 1274-81.

Liaw, A. and Wiener, M. (2002) 'Classification and regression by randomForest', *R news,* 2(3), pp. 18-22.

Liddelow, S. A., Guttenplan, K. A., Clarke, L. E., Bennett, F. C., Bohlen, C. J., Schirmer, L., Bennett, M. L., Münch, A. E., Chung, W. S., Peterson, T. C., Wilton, D. K., Frouin, A., Napier, B. A., Panicker, N., Kumar, M., Buckwalter, M. S., Rowitch, D. H., Dawson, V. L., Dawson, T. M., Stevens, B. and Barres, B. A. (2017) 'Neurotoxic reactive astrocytes are induced by activated microglia', *Nature,* 541(7638), pp. 481-487.

Liedtke, W., Edelmann, W., Bieri, P. L., Chiu, F. C., Cowan, N. J., Kucherlapati, R. and Raine, C. S. (1996) 'GFAP is necessary for the integrity of CNS white matter architecture and long-term maintenance of myelination', *Neuron,* 17(4), pp. 607-15.

Liu, Y., Beyer, A. and Aebersold, R. (2016) 'On the Dependency of Cellular Protein Levels on mRNA Abundance', *Cell,* 165(3), pp. 535-550.

Livet, J., Weissman, T. A., Kang, H., Draft, R. W., Lu, J., Bennis, R. A., Sanes, J. R. and Lichtman, J. W. (2007) 'Transgenic strategies for combinatorial expression of fluorescent proteins in the nervous system', *Nature,* 450(7166), pp. 56-62.

Locke, A. E. and Kahali, B. and Berndt, S. I. and Justice, A. E. and Pers, T. H. and Day, F. R. and Powell, C. and Vedantam, S. and Buchkovich, M. L. and Yang, J. and Croteau-Chonka, D. C. and Esko, T. and Fall, T. and Ferreira, T. and Gustafsson, S. and Kutalik, Z. and Luan, J. and Mägi, R. and Randall, J. C. and Winkler, T. W. and Wood, A. R. and Workalemahu, T. and Faul, J. D. and Smith, J. A. and Zhao, J. H. and Zhao, W. and Chen, J. and Fehrmann, R. and Hedman Å, K. and Karjalainen, J. and Schmidt, E. M. and Absher, D. and Amin, N. and

Anderson, D. and Beekman, M. and Bolton, J. L. and Bragg-Gresham, J. L. and Buyske, S. and Demirkan, A. and Deng, G. and Ehret, G. B. and Feenstra, B. and Feitosa, M. F. and Fischer, K. and Goel, A. and Gong, J. and Jackson, A. U. and Kanoni, S. and Kleber, M. E. and Kristiansson, K. and Lim, U. and Lotay, V. and Mangino, M. and Leach, I. M. and Medina-Gomez, C. and Medland, S. E. and Nalls, M. A. and Palmer, C. D. and Pasko, D. and Pechlivanis, S. and Peters, M. J. and Prokopenko, I. and Shungin, D. and Stančáková, A. and Strawbridge, R. J. and Sung, Y. J. and Tanaka, T. and Teumer, A. and Trompet, S. and van der Laan, S. W. and van Setten, J. and Van Vliet-Ostaptchouk, J. V. and Wang, Z. and Yengo, L. and Zhang, W. and Isaacs, A. and Albrecht, E. and Ärnlöv, J. and Arscott, G. M. and Attwood, A. P. and Bandinelli, S. and Barrett, A. and Bas, I. N. and Bellis, C. and Bennett, A. J. and Berne, C. and Blagieva, R. and Blüher, M. and Böhringer, S. and Bonnycastle, L. L. and Böttcher, Y. and Boyd, H. A. and Bruinenberg, M. and Caspersen, I. H. and Chen, Y. I. and Clarke, R. and Daw, E. W. and de Craen, A. J. M. and Delgado, G. and Dimitriou, M. and Doney, A. S. F. and Eklund, N. and Estrada, K. and Eury, E. and Folkersen, L. and Fraser, R. M. and Garcia, M. E. and Geller, F. and Giedraitis, V. and Gigante, B. and Go, A. S. and Golay, A. and Goodall, A. H. and Gordon, S. D. and Gorski, M. and Grabe, H. J. and Grallert, H. and Grammer, T. B. and Gräßler, J. and Grönberg, H. and Groves, C. J. and Gusto, G. and Haessler, J. and Hall, P. and Haller, T. and Hallmans, G. and Hartman, C. A. and Hassinen, M. and Hayward, C. and Heard-Costa, N. L. and Helmer, Q. and Hengstenberg, C. and Holmen, O. and Hottenga, J. J. and James, A. L. and Jeff, J. M. and Johansson, Å. and Jolley, J. and Juliusdottir, T. and Kinnunen, L. and Koenig, W. and Koskenvuo, M. and Kratzer, W. and Laitinen, J. and Lamina, C. and Leander, K. and Lee, N. R. and Lichtner, P. and Lind, L. and Lindström, J. and Lo, K. S. and Lobbens, S. and Lorbeer, R. and Lu, Y. and Mach, F. and Magnusson, P. K. E. and Mahajan, A. and McArdle, W. L. and McLachlan, S. and Menni, C. and Merger, S. and Mihailov, E. and Milani, L. and Moayyeri, A. and Monda, K. L. and Morken, M. A. and Mulas, A. and Müller, G. and Müller-Nurasyid, M. and Musk, A. W. and Nagaraja, R. and Nöthen, M. M. and Nolte, I. M. and Pilz, S. and Rayner, N. W. and Renstrom, F. and Rettig, R. and Ried, J. S. and Ripke, S. and Robertson, N. R. and Rose, L. M. and Sanna, S. and Scharnagl, H. and Scholtens, S. and Schumacher, F. R. and Scott, W. R. and Seufferlein, T. and Shi, J. and Smith, A. V. and Smolonska, J. and Stanton, A. V. and Steinthorsdottir, V. and Stirrups, K. and Stringham, H. M. and Sundström, J. and Swertz, M. A. and Swift, A. J. and Syvänen, A. C. and Tan, S. T. and Tayo, B. O. and Thorand, B. and Thorleifsson, G. and Tyrer, J. P. and Uh, H. W. and Vandenput, L. and Verhulst, F. C. and Vermeulen, S. H. and Verweij, N. and Vonk, J. M. and Waite, L. L. and Warren, H. R. and Waterworth, D. and Weedon, M. N. and Wilkens, L.

R. and Willenborg, C. and Wilsgaard, T. and Wojczynski, M. K. and Wong, A. and Wright, A. F. and Zhang, Q. and Brennan, E. P. and Choi, M. and Dastani, Z. and Drong, A. W. and Eriksson, P. and Franco-Cereceda, A. and Gådin, J. R. and Gharavi, A. G. and Goddard, M. E. and Handsaker, R. E. and Huang, J. and Karpe, F. and Kathiresan, S. and Keildson, S. and Kiryluk, K. and Kubo, M. and Lee, J. Y. and Liang, L. and Lifton, R. P. and Ma, B. and McCarroll, S. A. and McKnight, A. J. and Min, J. L. and Moffatt, M. F. and Montgomery, G. W. and Murabito, J. M. and Nicholson, G. and Nyholt, D. R. and Okada, Y. and Perry, J. R. B. and Dorajoo, R. and Reinmaa, E. and Salem, R. M. and Sandholm, N. and Scott, R. A. and Stolk, L. and Takahashi, A. and Tanaka, T. and van 't Hooft, F. M. and Vinkhuyzen, A. A. E. and Westra, H. J. and Zheng, W. and Zondervan, K. T. and Heath, A. C. and Arveiler, D. and Bakker, S. J. L. and Beilby, J. and Bergman, R. N. and Blangero, J. and Bovet, P. and Campbell, H. and Caulfield, M. J. and Cesana, G. and Chakravarti, A. and Chasman, D. I. and Chines, P. S. and Collins, F. S. and Crawford, D. C. and Cupples, L. A. and Cusi, D. and Danesh, J. and de Faire, U. and den Ruijter, H. M. and Dominiczak, A. F. and Erbel, R. and Erdmann, J. and Eriksson, J. G. and Farrall, M. and Felix, S. B. and Ferrannini, E. and Ferrières, J. and Ford, I. and Forouhi, N. G. and Forrester, T. and Franco, O. H. and Gansevoort, R. T. and Gejman, P. V. and Gieger, C. and Gottesman, O. and Gudnason, V. and Gyllensten, U. and Hall, A. S. and Harris, T. B. and Hattersley, A. T. and Hicks, A. A. and Hindorff, L. A. and Hingorani, A. D. and Hofman, A. and Homuth, G. and Hovingh, G. K. and Humphries, S. E. and Hunt, S. C. and Hyppönen, E. and Illig, T. and Jacobs, K. B. and Jarvelin, M. R. and Jöckel, K. H. and Johansen, B. and Jousilahti, P. and Jukema, J. W. and Jula, A. M. and Kaprio, J. and Kastelein, J. J. P. and Keinanen-Kiukaanniemi, S. M. and Kiemeney, L. A. and Knekt, P. and Kooner, J. S. and Kooperberg, C. and Kovacs, P. and Kraja, A. T. and Kumari, M. and Kuusisto, J. and Lakka, T. A. and Langenberg, C. and Marchand, L. L. and Lehtimäki, T. and Lyssenko, V. and Männistö, S. and Marette, A. and Matise, T. C. and McKenzie, C. A. and McKnight, B. and Moll, F. L. and Morris, A. D. and Morris, A. P. and Murray, J. C. and Nelis, M. and Ohlsson, C. and Oldehinkel, A. J. and Ong, K. K. and Madden, P. A. F. and Pasterkamp, G. and Peden, J. F. and Peters, A. and Postma, D. S. and Pramstaller, P. P. and Price, J. F. and Qi, L. and Raitakari, O. T. and Rankinen, T. and Rao, D. C. and Rice, T. K. and Ridker, P. M. and Rioux, J. D. and Ritchie, M. D. and Rudan, I. and Salomaa, V. and Samani, N. J. and Saramies, J. and Sarzynski, M. A. and Schunkert, H. and Schwarz, P. E. H. and Sever, P. and Shuldiner, A. R. and Sinisalo, J. and Stolk, R. P. and Strauch, K. and Tönjes, A. and Trégouët, D. A. and Tremblay, A. and Tremoli, E. and Virtamo, J. and Vohl, M. C. and Völker, U. and Waeber, G. and Willemsen, G. and Witteman, J. C. and Zillikens, M. C. and Adair, L. S. and Amouyel, P.

and Asselbergs, F. W. and Assimes, T. L. and Bochud, M. and Boehm, B. O. and Boerwinkle, E. and Bornstein, S. R. and Bottinger, E. P. and Bouchard, C. and Cauchi, S. and Chambers, J. C. and Chanock, S. J. and Cooper, R. S. and de Bakker, P. I. W. and Dedoussis, G. and Ferrucci, L. and Franks, P. W. and Froguel, P. and Groop, L. C. and Haiman, C. A. and Hamsten, A. and Hui, J. and Hunter, D. J. and Hveem, K. and Kaplan, R. C. and Kivimaki, M. and Kuh, D. and Laakso, M. and Liu, Y. and Martin, N. G. and März, W. and Melbye, M. and Metspalu, A. and Moebus, S. and Munroe, P. B. and Njølstad, I. and Oostra, B. A. and Palmer, C. N. A. and Pedersen, N. L. and Perola, M. and Pérusse, L. and Peters, U. and Power, C. and Quertermous, T. and Rauramaa, R. and Rivadeneira, F. and Saaristo, T. E. and Saleheen, D. and Sattar, N. and Schadt, E. E. and Schlessinger, D. and Slagboom, P. E. and Snieder, H. and Spector, T. D. and Thorsteinsdottir, U. and Stumvoll, M. and Tuomilehto, J. and Uitterlinden, A. G. and Uusitupa, M. and van der Harst, P. and Walker, M. and Wallaschofski, H. and Wareham, N. J. and Watkins, H. and Weir, D. R. and Wichmann, H. E. and Wilson, J. F. and Zanen, P. and Borecki, I. B. and Deloukas, P. and Fox, C. S. and Heid, I. M. and O'Connell, J. R. and Strachan, D. P. and Stefansson, K. and van Duijn, C. M. and Abecasis, G. R. and Franke, L. and Frayling, T. M. and McCarthy, M. I. and Visscher, P. M. and Scherag, A. and Willer, C. J. and Boehnke, M. and Mohlke, K. L. and Lindgren, C. M. and Beckmann, J. S. and Barroso, I. and North, K. E. and Ingelsson, E. and Hirschhorn, J. N. and Loos, R. J. F. and Speliotes, E. K. (2015) 'Genetic studies of body mass index yield new insights for obesity biology', *Nature,* 518(7538), pp. 197-206.

Long, F., Zhang, X. M., Karp, S., Yang, Y. and McMahon, A. P. (2001) 'Genetic manipulation of hedgehog signaling in the endochondral skeleton reveals a direct role in the regulation of chondrocyte proliferation', *Development,* 128(24), pp. 5099-108.

Love, M. I., Huber, W. and Anders, S. (2014) 'Moderated estimation of fold change and dispersion for RNA-seq data with DESeq2', *Genome Biol,* 15(12), pp. 550.

Love, M. I., Soneson, C., Hickey, P. F., Johnson, L. K., Pierce, N. T., Shepherd, L., Morgan, M. and Patro, R. (2020) 'Tximeta: Reference sequence checksums for provenance identification in RNA-seq', *PLoS computational biology,* 16(2), pp. e1007664-e1007664.

Luiten, P. G., ter Horst, G. J. and Steffens, A. B. (1987) 'The hypothalamus, intrinsic connections and outflow pathways to the endocrine system in relation to the control of feeding and metabolism', *Prog Neurobiol,* 28(1), pp. 1-54.

Lukaszevicz, A. C., Sampaïo, N., Guégan, C., Benchoua, A., Couriaud, C., Chevalier, E., Sola, B., Lacombe, P. and Onténiente, B. (2002) 'High sensitivity of protoplasmic cortical astroglia to focal ischemia', *J Cereb Blood Flow Metab,* 22(3), pp. 289-98.

Macauley, S. L., Pekny, M. and Sands, M. S. (2011) 'The role of attenuated astrocyte activation in infantile neuronal ceroid lipofuscinosis', *Journal of Neuroscience,* 31(43), pp. 15575-15585.

MacDonald, A. J., Holmes, F. E., Beall, C., Pickering, A. E. and Ellacott, K. L. J. (2020) 'Regulation of food intake by astrocytes in the brainstem dorsal vagal complex', *Glia,* 68(6), pp. 1241-1254.

Makar, T. K., Nedergaard, M., Preuss, A., Gelbard, A. S., Perumal, A. S. and Cooper, A. J. (1994) 'Vitamin E, ascorbate, glutathione, glutathione disulfide, and enzymes of glutathione metabolism in cultures of chick astrocytes and neurons: evidence that astrocytes play an important role in antioxidative processes in the brain', *J Neurochem,* 62(1), pp. 45-53.

Manley, G. T., Fujimura, M., Ma, T., Noshita, N., Filiz, F., Bollen, A. W., Chan, P. and Verkman, A. S. (2000) 'Aquaporin-4 deletion in mice reduces brain edema after acute water intoxication and ischemic stroke', *Nat Med,* 6(2), pp. 159-63.

Martín, R., Bajo-Grañeras, R., Moratalla, R., Perea, G. and Araque, A. (2015) 'Circuit-specific signaling in astrocyte-neuron networks in basal ganglia pathways', *Science,* 349(6249), pp. 730-4.

Marty, N., Dallaporta, M., Foretz, M., Emery, M., Tarussio, D., Bady, I., Binnert, C., Beermann, F. and Thorens, B. (2005) 'Regulation of glucagon secretion by glucose transporter type 2 (glut2) and astrocyte-dependent glucose sensors', *J Clin Invest,* 115(12), pp. 3545-53.

Mathiisen, T. M., Lehre, K. P., Danbolt, N. C. and Ottersen, O. P. (2010) 'The perivascular astroglial sheath provides a complete covering of the brain microvessels: an electron microscopic 3D reconstruction', *Glia,* 58(9), pp. 1094-1103.

Matias, I., Morgado, J. and Gomes, F. C. A. (2019) 'Astrocyte Heterogeneity: Impact to Brain Aging and Disease', *Frontiers in Aging Neuroscience,* 11(59).

Matsugami, T. R., Tanemura, K., Mieda, M., Nakatomi, R., Yamada, K., Kondo, T., Ogawa, M., Obata, K., Watanabe, M., Hashikawa, T. and Tanaka, K. (2006) 'From the Cover:

Indispensability of the glutamate transporters GLAST and GLT1 to brain development', *Proc Natl Acad Sci U S A*, 103(32), pp. 12161-6.

Matthias, K., Kirchhoff, F., Seifert, G., Hüttmann, K., Matyash, M., Kettenmann, H. and Steinhäuser, C. (2003) 'Segregated expression of AMPA-type glutamate receptors and glutamate transporters defines distinct astrocyte populations in the mouse hippocampus', *J Neurosci*, 23(5), pp. 1750-8.

Mayer, J. and Thomas, D. W. (1967) 'Regulation of food intake and obesity', *Science*, 156(3773), pp. 328-37.

McCall, M. A., Gregg, R. G., Behringer, R. R., Brenner, M., Delaney, C. L., Galbreath, E. J., Zhang, C. L., Pearce, R. A., Chiu, S. Y. and Messing, A. (1996) 'Targeted deletion in astrocyte intermediate filament (Gfap) alters neuronal physiology', *Proc Natl Acad Sci U S A*, 93(13), pp. 6361-6.

McClellan, K. M., Parker, K. L. and Tobet, S. (2006) 'Development of the ventromedial nucleus of the hypothalamus', *Front Neuroendocrinol*, 27(2), pp. 193-209.

Milanski, M., Arruda, A. P., Coope, A., Ignacio-Souza, L. M., Nunez, C. E., Roman, E. A., Romanatto, T., Pascoal, L. B., Caricilli, A. M., Torsoni, M. A., Prada, P. O., Saad, M. J. and Velloso, L. A. (2012) 'Inhibition of hypothalamic inflammation reverses diet-induced insulin resistance in the liver', *Diabetes*, 61(6), pp. 1455-62.

Milanski, M., Degasperi, G., Coope, A., Morari, J., Denis, R., Cintra, D. E., Tsukumo, D. M., Anhe, G., Amaral, M. E., Takahashi, H. K., Curi, R., Oliveira, H. C., Carvalheira, J. B., Bordin, S., Saad, M. J. and Velloso, L. A. (2009) 'Saturated fatty acids produce an inflammatory response predominantly through the activation of TLR4 signaling in hypothalamus: implications for the pathogenesis of obesity', *J Neurosci*, 29(2), pp. 359-70.

Miller, R. H. and Raff, M. C. (1984) 'Fibrous and protoplasmic astrocytes are biochemically and developmentally distinct', *J Neurosci*, 4(2), pp. 585-92.

Mo, A., Mukamel, E. A., Davis, F. P., Luo, C., Henry, G. L., Picard, S., Urich, M. A., Nery, J. R., Sejnowski, T. J., Lister, R., Eddy, S. R., Ecker, J. R. and Nathans, J. (2015) 'Epigenomic Signatures of Neuronal Diversity in the Mammalian Brain', *Neuron*, 86(6), pp. 1369-84.

Molofsky, A. V., Kelley, K. W., Tsai, H.-H., Redmond, S. A., Chang, S. M., Madireddy, L., Chan, J. R., Baranzini, S. E., Ullian, E. M. and Rowitch, D. H. (2014) 'Astrocyte-encoded positional cues maintain sensorimotor circuit integrity', *Nature*, 509(7499), pp. 189-194.

Moraes, J. C., Coope, A., Morari, J., Cintra, D. E., Roman, E. A., Pauli, J. R., Romanatto, T., Carvalheira, J. B., Oliveira, A. L., Saad, M. J. and Velloso, L. A. (2009) 'High-fat diet induces apoptosis of hypothalamic neurons', *PLoS One*, 4(4), pp. e5045.

Morel, L., Chiang, M. S. R., Higashimori, H., Shoneye, T., Iyer, L. K., Yelick, J., Tai, A. and Yang, Y. (2017) 'Molecular and functional properties of regional astrocytes in the adult brain', *Journal of Neuroscience*, 37(36), pp. 8706-8717.

Morel, L., Men, Y., Chiang, M. S., Tian, Y., Jin, S., Yelick, J., Higashimori, H. and Yang, Y. (2019) 'Intracortical astrocyte subpopulations defined by astrocyte reporter mice in the adult brain', *Glia*, 67(1), pp. 171-181.

Morgello, S., Uson, R. R., Schwartz, E. J. and Haber, R. S. (1995) 'The human blood-brain barrier glucose transporter (GLUT1) is a glucose transporter of gray matter astrocytes', *Glia*, 14(1), pp. 43-54.

Mori, H., Hanada, R., Hanada, T., Aki, D., Mashima, R., Nishinakamura, H., Torisu, T., Chien, K. R., Yasukawa, H. and Yoshimura, A. (2004) 'Socs3 deficiency in the brain elevates leptin sensitivity and confers resistance to diet-induced obesity', *Nat Med*, 10(7), pp. 739-43.

Morrison, E. and Castro, M. G. (1997) 'Post-Translational Processing of Proopiomelanocortin in the Pituitary and in the Brain', 11(1), pp. 35-57.

Morselli, E., Fuente-Martin, E., Finan, B., Kim, M., Frank, A., Garcia-Caceres, C., Navas, C. R., Gordillo, R., Neinast, M., Kalainayakan, S. P., Li, D. L., Gao, Y., Yi, C. X., Hahner, L., Palmer, B. F., Tschop, M. H. and Clegg, D. J. (2014) 'Hypothalamic PGC-1alpha protects against high-fat diet exposure by regulating ERalpha', *Cell Rep*, 9(2), pp. 633-45.

Moulson, A. J., Squair, J. W., Franklin, R. J. M., Tetzlaff, W. and Assinck, P. (2021) 'Diversity of Reactive Astrogliosis in CNS Pathology: Heterogeneity or Plasticity?', *Frontiers in cellular neuroscience*, 15, pp. 703810-703810.

Mountjoy, K. G. (2015) 'Pro-Opiomelanocortin (POMC) Neurones, POMC-Derived Peptides, Melanocortin Receptors and Obesity: How Understanding of this System has Changed Over the Last Decade', *Journal of Neuroendocrinology*, 27(6), pp. 406-418.

Mountjoy, K. G., Mortrud, M. T., Low, M. J., Simerly, R. B. and Cone, R. D. (1994) 'Localization of the melanocortin-4 receptor (MC4-R) in neuroendocrine and autonomic control circuits in the brain', *Mol Endocrinol*, 8(10), pp. 1298-308.

Münzberg, H., Flier, J. S. and Bjørbaek, C. (2004) 'Region-specific leptin resistance within the hypothalamus of diet-induced obese mice', *Endocrinology*, 145(11), pp. 4880-9.

Muoio, V., Persson, P. B. and Sendeski, M. M. (2014) 'The neurovascular unit - concept review', *Acta Physiol (Oxf)*, 210(4), pp. 790-8.

Murat, C. B. and García-Cáceres, C. (2021) 'Astrocyte Gliotransmission in the Regulation of Systemic Metabolism', *Metabolites*, 11(11).

Musatov, S., Chen, W., Pfaff, D. W., Mobbs, C. V., Yang, X. J., Clegg, D. J., Kaplitt, M. G. and Ogawa, S. (2007) 'Silencing of estrogen receptor alpha in the ventromedial nucleus of hypothalamus leads to metabolic syndrome', *Proc Natl Acad Sci U S A*, 104(7), pp. 2501-6.

Nagelhus, E. A. and Ottersen, O. P. (2013) 'Physiological roles of aquaporin-4 in brain', *Physiol Rev*, 93(4), pp. 1543-62.

Nagy, J. I., Patel, D., Ochalski, P. A. and Stelmack, G. L. (1999) 'Connexin30 in rodent, cat and human brain: selective expression in gray matter astrocytes, co-localization with connexin43 at gap junctions and late developmental appearance', *Neuroscience*, 88(2), pp. 447-68.

Navarrete, M., Perea, G., Fernandez de Sevilla, D., Gómez-Gonzalo, M., Núñez, A., Martín, E. D. and Araque, A. (2012) 'Astrocytes mediate in vivo cholinergic-induced synaptic plasticity', *PLoS Biol*, 10(2), pp. e1001259.

Nestor, C. C., Qiu, J., Padilla, S. L., Zhang, C., Bosch, M. A., Fan, W., Aicher, S. A., Palmiter, R. D., Rønnekleiv, O. K. and Kelly, M. J. (2016) 'Optogenetic Stimulation of Arcuate Nucleus Kiss1 Neurons Reveals a Steroid-Dependent Glutamatergic Input to POMC and AgRP Neurons in Male Mice', *Mol Endocrinol*, 30(6), pp. 630-44.

Nishiyama, A., Boshans, L., Goncalves, C. M., Wegrzyn, J. and Patel, K. D. (2016) 'Lineage, fate, and fate potential of NG2-glia', *Brain Res,* 1638(Pt B), pp. 116-128.

Norenberg, M. D. and Martinez-Hernandez, A. (1979) 'Fine structural localization of glutamine synthetase in astrocytes of rat brain', *Brain Res,* 161(2), pp. 303-10.

Nwaobi, S. E., Cuddapah, V. A., Patterson, K. C., Randolph, A. C. and Olsen, M. L. (2016) 'The role of glial-specific Kir4.1 in normal and pathological states of the CNS', *Acta Neuropathologica,* 132(1), pp. 1-21.

Oberheim, N. A., Goldman, S. A. and Nedergaard, M. (2012) 'Heterogeneity of astrocytic form and function', *Methods in molecular biology (Clifton, N.J.),* 814, pp. 23-45.

Ogata, K. and Kosaka, T. (2002) 'Structural and quantitative analysis of astrocytes in the mouse hippocampus', *Neuroscience,* 113(1), pp. 221-233.

Ohno, Y., Tokudome, K., Kunisawa, N., Iha, H. A., Kinboshi, M., Mukai, T., Serikawa, T. and Shimizu, S. (2015) 'Role of astroglial Kir4. 1 channels in the pathogenesis and treatment of epilepsy', *Therapeutic Targets for Neurological Diseases,* 2.

Ollmann, M. M., Wilson, B. D., Yang, Y. K., Kerns, J. A., Chen, Y., Gantz, I. and Barsh, G. S. (1997) 'Antagonism of central melanocortin receptors in vitro and in vivo by agouti-related protein', *Science,* 278(5335), pp. 135-8.

Olney, J. W. (1969) 'Brain lesions, obesity, and other disturbances in mice treated with monosodium glutamate', *Science,* 164(3880), pp. 719-21.

Otani, N., Nawashiro, H., Fukui, S., Ooigawa, H., Ohsumi, A., Toyooka, T., Shima, K., Gomi, H. and Brenner, M. (2006) 'Enhanced hippocampal neurodegeneration after traumatic or kainate excitotoxicity in GFAP-null mice', *J Clin Neurosci,* 13(9), pp. 934-8.

Padilla, S. L., Qiu, J., Nestor, C. C., Zhang, C., Smith, A. W., Whiddon, B. B., Rønnekleiv, O. K., Kelly, M. J. and Palmiter, R. D. (2017) 'AgRP to Kiss1 neuron signaling links nutritional state and fertility', *Proc Natl Acad Sci U S A,* 114(9), pp. 2413-2418.

Paeger, L., Karakasilioti, I., Altmüller, J., Frommolt, P., Brüning, J. and Kloppenburg, P. (2017) 'Antagonistic modulation of NPY/AgRP and POMC neurons in the arcuate nucleus by noradrenalin', *Elife,* 6.

Pan, W., Hsuchou, H., He, Y., Sakharkar, A., Cain, C., Yu, C. and Kastin, A. J. (2008) 'Astrocyte leptin receptor (ObR) and leptin transport in adult-onset obese mice', *Endocrinology*, 149(6), pp. 2798-806.

Pan, W., Hsuchou, H., Xu, C., Wu, X., Bouret, S. G. and Kastin, A. J. (2011) 'Astrocytes modulate distribution and neuronal signaling of leptin in the hypothalamus of obese A vy mice', *J Mol Neurosci*, 43(3), pp. 478-84.

Pappalardo, L. W., Black, J. A. and Waxman, S. G. (2016) 'Sodium channels in astroglia and microglia', *Glia*, 64(10), pp. 1628-45.

Paradis, E. and Schliep, K. (2019) 'ape 5.0: an environment for modern phylogenetics and evolutionary analyses in R', *Bioinformatics*, 35(3), pp. 526-528.

Park, E. J., Lee, J. H., Yu, G. Y., He, G., Ali, S. R., Holzer, R. G., Osterreicher, C. H., Takahashi, H. and Karin, M. (2010) 'Dietary and genetic obesity promote liver inflammation and tumorigenesis by enhancing IL-6 and TNF expression', *Cell*, 140(2), pp. 197-208.

Parpura, V., Heneka, M. T., Montana, V., Oliet, S. H., Schousboe, A., Haydon, P. G., Stout, R. F., Jr., Spray, D. C., Reichenbach, A., Pannicke, T., Pekny, M., Pekna, M., Zorec, R. and Verkhratsky, A. (2012) 'Glial cells in (patho)physiology', *J Neurochem*, 121(1), pp. 4-27.

Pascual, O., Casper, K. B., Kubera, C., Zhang, J., Revilla-Sanchez, R., Sul, J.-Y., Takano, H., Moss, S. J., McCarthy, K. and Haydon, P. G. (2005) 'Astrocytic Purinergic Signaling Coordinates Synaptic Networks', *Science*, 310(5745), pp. 113-116.

Patel, B., New, L. E., Griffiths, J. C., Deuchars, J. and Filippi, B. M. (2021) 'Inhibition of mitochondrial fission and iNOS in the dorsal vagal complex protects from overeating and weight gain', *Mol Metab*, 43, pp. 101123.

Patro, R., Duggal, G., Love, M. I., Irizarry, R. A. and Kingsford, C. (2017) 'Salmon provides fast and bias-aware quantification of transcript expression', *Nature Methods*, 14(4), pp. 417-419.

Payne, S. H. (2015) 'The utility of protein and mRNA correlation', *Trends Biochem Sci*, 40(1), pp. 1-3.

Pekny, M., Johansson, C. B., Eliasson, C., Stakeberg, J., Wallén, A., Perlmann, T., Lendahl, U., Betsholtz, C., Berthold, C. H. and Frisén, J. (1999) 'Abnormal reaction to central nervous

system injury in mice lacking glial fibrillary acidic protein and vimentin', *J Cell Biol*, 145(3), pp. 503-14.

Pekny, M., Levéen, P., Pekna, M., Eliasson, C., Berthold, C. H., Westermark, B. and Betsholtz, C. (1995) 'Mice lacking glial fibrillary acidic protein display astrocytes devoid of intermediate filaments but develop and reproduce normally', *Embo j*, 14(8), pp. 1590-8.

Pekny, M. and Pekna, M. (2004) 'Astrocyte intermediate filaments in CNS pathologies and regeneration', *J Pathol*, 204(4), pp. 428-37.

Pekny, M. and Pekna, M. (2014) 'Astrocyte reactivity and reactive astrogliosis: costs and benefits', *Physiol Rev*, 94(4), pp. 1077-98.

Pellerin, L. and Magistretti, P. J. (1994) 'Glutamate uptake into astrocytes stimulates aerobic glycolysis: a mechanism coupling neuronal activity to glucose utilization', *Proceedings of the National Academy of Sciences*, 91(22), pp. 10625-10629.

Pellerin, L., Pellegri, G., Bittar, P. G., Charnay, Y., Bouras, C., Martin, J. L., Stella, N. and Magistretti, P. J. (1998) 'Evidence supporting the existence of an activity-dependent astrocyte-neuron lactate shuttle', *Dev Neurosci*, 20(4-5), pp. 291-9.

Perea, G., Yang, A., Boyden, E. S. and Sur, M. (2014) 'Optogenetic astrocyte activation modulates response selectivity of visual cortex neurons in vivo', *Nat Commun*, 5, pp. 3262.

Perez-Alvarez, A., Navarrete, M., Covelo, A., Martin, E. D. and Araque, A. (2014) 'Structural and functional plasticity of astrocyte processes and dendritic spine interactions', *J Neurosci*, 34(38), pp. 12738-44.

Pestana, F., Edwards-Faret, G., Belgard, T. G., Martirosyan, A. and Holt, M. G. (2020) 'No Longer Underappreciated: The Emerging Concept of Astrocyte Heterogeneity in Neuroscience', *Brain Sciences*, 10(3), pp. 168.

Petravicz, J., Boyt, K. M. and McCarthy, K. D. (2014) 'Astrocyte IP3R2-dependent Ca(2+) signaling is not a major modulator of neuronal pathways governing behavior', *Frontiers in behavioral neuroscience*, 8, pp. 384-384.

Petravicz, J., Fiacco, T. A. and McCarthy, K. D. (2008) 'Loss of IP3 receptor-dependent Ca2+ increases in hippocampal astrocytes does not affect baseline CA1 pyramidal neuron synaptic activity', *J Neurosci*, 28(19), pp. 4967-73.

Petrovich, G. D. (2018) 'Lateral Hypothalamus as a Motivation-Cognition Interface in the Control of Feeding Behavior', *Frontiers in Systems Neuroscience,* 12(14).

Piet, R., Vargová, L., Syková, E., Poulain, D. A. and Oliet, S. H. R. (2004) 'Physiological contribution of the astrocytic environment of neurons to intersynaptic crosstalk', *Proceedings of the National Academy of Sciences,* 101(7), pp. 2151-2155.

Pigeyre, M., Yazdi, F. T., Kaur, Y. and Meyre, D. (2016) 'Recent progress in genetics, epigenetics and metagenomics unveils the pathophysiology of human obesity', *Clin Sci (Lond),* 130(12), pp. 943-86.

Pinto, S., Roseberry, A. G., Liu, H., Diano, S., Shanabrough, M., Cai, X., Friedman, J. M. and Horvath, T. L. (2004) 'Rapid rewiring of arcuate nucleus feeding circuits by leptin', *Science,* 304(5667), pp. 110-5.

Pitter, K. L., Tamagno, I., Feng, X., Ghosal, K., Amankulor, N., Holland, E. C. and Hambardzumyan, D. (2014) 'The SHH/Gli pathway is reactivated in reactive glia and drives proliferation in response to neurodegeneration-induced lesions', *Glia,* 62(10), pp. 1595-607.

Posey, K. A., Clegg, D. J., Printz, R. L., Byun, J., Morton, G. J., Vivekanandan-Giri, A., Pennathur, S., Baskin, D. G., Heinecke, J. W., Woods, S. C., Schwartz, M. W. and Niswender, K. D. (2009) 'Hypothalamic proinflammatory lipid accumulation, inflammation, and insulin resistance in rats fed a high-fat diet', *Am J Physiol Endocrinol Metab,* 296(5), pp. E1003-12.

Pritchard, L. E., Turnbull, A. V. and White, A. (2002) 'Pro-opiomelanocortin processing in the hypothalamus: impact on melanocortin signalling and obesity', *J Endocrinol,* 172(3), pp. 411-21.

Rakers, C. and Petzold, G. C. (2017) 'Astrocytic calcium release mediates peri-infarct depolarizations in a rodent stroke model', *The Journal of clinical investigation,* 127(2), pp. 511-516.

Ramón y Cajal, S. (1909) *Histologie du système nerveux de l'homme & des vertébrés.* Ed. française rev. & mise à jour par l'auteur, tr. de l'espagnol par L. Azoulay. edn. Paris :: Maloine.

Rash, J. E., Yasumura, T., Dudek, F. E. and Nagy, J. I. (2001) 'Cell-specific expression of connexins and evidence of restricted gap junctional coupling between glial cells and between neurons', *Journal of Neuroscience,* 21(6), pp. 1983-2000.

Ravussin, E. and Bogardus, C. (2000) 'Energy balance and weight regulation: genetics versus environment', *Br J Nutr*, 83 Suppl 1, pp. S17-20.

Retzius, G. (1894) *Die neuroglia des Gehirns beim Menschen und bei Saeugethieren.* von Gustav Fischer.

Rodriguez, F. J., Giannini, C., Asmann, Y. W., Sharma, M. K., Perry, A., Tibbetts, K. M., Jenkins, R. B., Scheithauer, B. W., Anant, S., Jenkins, S., Eberhart, C. G., Sarkaria, J. N. and Gutmann, D. H. (2008) 'Gene expression profiling of NF-1-associated and sporadic pilocytic astrocytoma identifies aldehyde dehydrogenase 1 family member L1 (ALDH1L1) as an underexpressed candidate biomarker in aggressive subtypes', *J Neuropathol Exp Neurol*, 67(12), pp. 1194-204.

Rothstein, J. D., Dykes-Hoberg, M., Pardo, C. A., Bristol, L. A., Jin, L., Kuncl, R. W., Kanai, Y., Hediger, M. A., Wang, Y., Schielke, J. P. and Welty, D. F. (1996) 'Knockout of glutamate transporters reveals a major role for astroglial transport in excitotoxicity and clearance of glutamate', *Neuron*, 16(3), pp. 675-86.

Rungta, R. L., Bernier, L. P., Dissing-Olesen, L., Groten, C. J., LeDue, J. M., Ko, R., Drissler, S. and MacVicar, B. A. (2016) 'Ca(2+) transients in astrocyte fine processes occur via Ca(2+) influx in the adult mouse hippocampus', *Glia*, 64(12), pp. 2093-2103.

Rusakov, D. A. (2015) 'Disentangling calcium-driven astrocyte physiology', *Nat Rev Neurosci*, 16(4), pp. 226-33.

Rusakov, D. A. and Fine, A. (2003) 'Extracellular Ca2+ depletion contributes to fast activity-dependent modulation of synaptic transmission in the brain', *Neuron*, 37(2), pp. 287-97.

Saito, K., Shigetomi, E., Yasuda, R., Sato, R., Nakano, M., Tashiro, K., Tanaka, K. F., Ikenaka, K., Mikoshiba, K., Mizuta, I., Yoshida, T., Nakagawa, M., Mizuno, T. and Koizumi, S. (2018) 'Aberrant astrocyte Ca(2+) signals "AxCa signals" exacerbate pathological alterations in an Alexander disease model', *Glia*, 66(5), pp. 1053-1067.

Santello, M. and Volterra, A. (2009) 'Synaptic modulation by astrocytes via Ca2+-dependent glutamate release', *Neuroscience*, 158(1), pp. 253-259.

Sartorius, T., Lutz, S. Z., Hoene, M., Waak, J., Peter, A., Weigert, C., Rammensee, H. G., Kahle, P. J., Häring, H. U. and Hennige, A. M. (2012) 'Toll-like receptors 2 and 4 impair

insulin-mediated brain activity by interleukin-6 and osteopontin and alter sleep architecture', *Faseb j*, 26(5), pp. 1799-809.

Savtchouk, I. and Volterra, A. (2018) 'Gliotransmission: Beyond Black-and-White', *J Neurosci*, 38(1), pp. 14-25.

Saxena, A., Wagatsuma, A., Noro, Y., Kuji, T., Asaka-Oba, A., Watahiki, A., Gurnot, C., Fagiolini, M., Hensch, T. K. and Carninci, P. (2012) 'Trehalose-enhanced isolation of neuronal sub-types from adult mouse brain', *Biotechniques*, 52(6), pp. 381-5.

Schmal, C., Myung, J., Herzel, H. and Bordyugov, G. (2017) 'Moran's I quantifies spatio-temporal pattern formation in neural imaging data', *Bioinformatics*, 33(19), pp. 3072-3079.

Schneeberger, M., Gomis, R. and Claret, M. (2014) 'Hypothalamic and brainstem neuronal circuits controlling homeostatic energy balance', *Journal of Endocrinology*, 220(2), pp. T25-T46.

Schousboe, A., Scafidi, S., Bak, L. K., Waagepetersen, H. S. and McKenna, M. C. (2014) 'Glutamate metabolism in the brain focusing on astrocytes', *Adv Neurobiol*, 11, pp. 13-30.

Seoane-Collazo, P., Fernø, J., Gonzalez, F., Diéguez, C., Leis, R., Nogueiras, R. and López, M. (2015) 'Hypothalamic-autonomic control of energy homeostasis', *Endocrine*, 50(2), pp. 276-91.

Shannon, C., Salter, M. and Fern, R. (2007) 'GFP imaging of live astrocytes: regional differences in the effects of ischaemia upon astrocytes', *Journal of Anatomy*, 210(6), pp. 684-692.

Sharp, A. H., Nucifora, F. C., Jr., Blondel, O., Sheppard, C. A., Zhang, C., Snyder, S. H., Russell, J. T., Ryugo, D. K. and Ross, C. A. (1999) 'Differential cellular expression of isoforms of inositol 1,4,5-triphosphate receptors in neurons and glia in brain', *J Comp Neurol*, 406(2), pp. 207-20.

Shen, L., Tso, P., Wang, D. Q. H., Woods, S. C., Davidson, W. S., Sakai, R. and Liu, M. (2009) 'Up-regulation of apolipoprotein E by leptin in the hypothalamus of mice and rats', *Physiology & behavior*, 98(1-2), pp. 223-228.

Shen, L., Tso, P., Woods, S. C., Clegg, D. J., Barber, K. L., Carey, K. and Liu, M. (2008) 'Brain apolipoprotein E: an important regulator of food intake in rats', *Diabetes*, 57(8), pp. 2092-2098.

Sherwood, M. W., Arizono, M., Hisatsune, C., Bannai, H., Ebisui, E., Sherwood, J. L., Panatier, A., Oliet, S. H. and Mikoshiba, K. (2017) 'Astrocytic IP(3) Rs: Contribution to Ca(2+) signalling and hippocampal LTP', *Glia,* 65(3), pp. 502-513.

Shin, A. C., Filatova, N., Lindtner, C., Chi, T., Degann, S., Oberlin, D. and Buettner, C. (2017) 'Insulin Receptor Signaling in POMC, but Not AgRP, Neurons Controls Adipose Tissue Insulin Action', *Diabetes,* 66(6), pp. 1560-1571.

Sievert, C. (2020) *Interactive web-based data visualization with R, plotly, and shiny.* CRC Press.

Silver, J. and Miller, J. H. (2004) 'Regeneration beyond the glial scar', *Nature Reviews Neuroscience,* 5(2), pp. 146-156.

Simonds, S. E., Pryor, J. T., Ravussin, E., Greenway, F. L., Dileone, R., Allen, A. M., Bassi, J., Elmquist, J. K., Keogh, J. M., Henning, E., Myers, M. G., Jr., Licinio, J., Brown, R. D., Enriori, P. J., O'Rahilly, S., Sternson, S. M., Grove, K. L., Spanswick, D. C., Farooqi, I. S. and Cowley, M. A. (2014) 'Leptin mediates the increase in blood pressure associated with obesity', *Cell,* 159(6), pp. 1404-16.

Sirko, S., Behrendt, G., Johansson, P. A., Tripathi, P., Costa, M., Bek, S., Heinrich, C., Tiedt, S., Colak, D., Dichgans, M., Fischer, I. R., Plesnila, N., Staufenbiel, M., Haass, C., Snapyan, M., Saghatelyan, A., Tsai, L. H., Fischer, A., Grobe, K., Dimou, L. and Gotz, M. (2013) 'Reactive glia in the injured brain acquire stem cell properties in response to sonic hedgehog. [corrected]', *Cell Stem Cell,* 12(4), pp. 426-39.

Sofroniew, M. V. (2009) 'Molecular dissection of reactive astrogliosis and glial scar formation', *Trends Neurosci,* 32(12), pp. 638-47.

Sofroniew, M. V. (2014) 'Astrogliosis', *Cold Spring Harb Perspect Biol,* 7(2), pp. a020420.

Sofroniew, M. V. (2015) 'Astrocyte barriers to neurotoxic inflammation', *Nat Rev Neurosci,* 16(5), pp. 249-63.

Sofroniew, M. V. and Vinters, H. V. (2010) 'Astrocytes: biology and pathology', *Acta Neuropathol,* 119(1), pp. 7-35.

Sohn, J.-W., Elmquist, J. K. and Williams, K. W. (2013) 'Neuronal circuits that regulate feeding behavior and metabolism', *Trends in neurosciences,* 36(9), pp. 504-512.

Spence, R. D., Hamby, M. E., Umeda, E., Itoh, N., Du, S., Wisdom, A. J., Cao, Y., Bondar, G., Lam, J., Ao, Y., Sandoval, F., Suriany, S., Sofroniew, M. V. and Voskuhl, R. R. (2011) 'Neuroprotection mediated through estrogen receptor-alpha in astrocytes', *Proc Natl Acad Sci U S A*, 108(21), pp. 8867-72.

Srinivasan, R., Huang, B. S., Venugopal, S., Johnston, A. D., Chai, H., Zeng, H., Golshani, P. and Khakh, B. S. (2015) 'Ca(2+) signaling in astrocytes from Ip3r2(-/-) mice in brain slices and during startle responses in vivo', *Nature neuroscience*, 18(5), pp. 708-717.

Sternson, S. M., Shepherd, G. M. G. and Friedman, J. M. (2005) 'Topographic mapping of VMH → arcuate nucleus microcircuits and their reorganization by fasting', *Nature Neuroscience*, 8(10), pp. 1356-1363.

Suh, S. W., Bergher, J. P., Anderson, C. M., Treadway, J. L., Fosgerau, K. and Swanson, R. A. (2007) 'Astrocyte glycogen sustains neuronal activity during hypoglycemia: studies with the glycogen phosphorylase inhibitor CP-316,819 ([R-R*,S*]-5-chloro-N-[2-hydroxy-3-(methoxymethylamino)-3-oxo-1-(phenylmethyl)propyl]-1H-indole-2-carboxamide)', *J Pharmacol Exp Ther*, 321(1), pp. 45-50.

Sun, W., Cornwell, A., Li, J., Peng, S., Osorio, M. J., Aalling, N., Wang, S., Benraiss, A., Lou, N., Goldman, S. A. and Nedergaard, M. (2017) 'SOX9 Is an Astrocyte-Specific Nuclear Marker in the Adult Brain Outside the Neurogenic Regions', *J Neurosci*, 37(17), pp. 4493-4507.

Susarla, B. T., Villapol, S., Yi, J. H., Geller, H. M. and Symes, A. J. (2014) 'Temporal patterns of cortical proliferation of glial cell populations after traumatic brain injury in mice', *ASN Neuro*, 6(3), pp. 159-70.

Takata, N. and Hirase, H. (2008) 'Cortical layer 1 and layer 2/3 astrocytes exhibit distinct calcium dynamics in vivo', *PloS one*, 3(6), pp. e2525-e2525.

Takata, N., Mishima, T., Hisatsune, C., Nagai, T., Ebisui, E., Mikoshiba, K. and Hirase, H. (2011) 'Astrocyte calcium signaling transforms cholinergic modulation to cortical plasticity in vivo', *J Neurosci*, 31(49), pp. 18155-65.

Thaler, J. P., Yi, C. X., Schur, E. A., Guyenet, S. J., Hwang, B. H., Dietrich, M. O., Zhao, X., Sarruf, D. A., Izgur, V., Maravilla, K. R., Nguyen, H. T., Fischer, J. D., Matsen, M. E., Wisse, B. E., Morton, G. J., Horvath, T. L., Baskin, D. G., Tschop, M. H. and Schwartz, M. W. (2012)

'Obesity is associated with hypothalamic injury in rodents and humans', *J Clin Invest*, 122(1), pp. 153-62.

Timper, K. and Brüning, J. C. (2017) 'Hypothalamic circuits regulating appetite and energy homeostasis: pathways to obesity', *Dis Model Mech*, 10(6), pp. 679-689.

Traiffort, E., Angot, E. and Ruat, M. (2010) 'Sonic Hedgehog signaling in the mammalian brain', *J Neurochem*, 113(3), pp. 576-90.

Tsai, H. H., Li, H., Fuentealba, L. C., Molofsky, A. V., Taveira-Marques, R., Zhuang, H., Tenney, A., Murnen, A. T., Fancy, S. P., Merkle, F., Kessaris, N., Alvarez-Buylla, A., Richardson, W. D. and Rowitch, D. H. (2012) 'Regional astrocyte allocation regulates CNS synaptogenesis and repair', *Science*, 337(6092), pp. 358-62.

Tyanova, S., Temu, T., Sinitcyn, P., Carlson, A., Hein, M. Y., Geiger, T., Mann, M. and Cox, J. (2016) 'The Perseus computational platform for comprehensive analysis of (prote)omics data', *Nature Methods*, 13(9), pp. 731-740.

Valdearcos, M., Robblee, M. M., Benjamin, D. I., Nomura, D. K., Xu, A. W. and Koliwad, S. K. (2014) 'Microglia dictate the impact of saturated fat consumption on hypothalamic inflammation and neuronal function', *Cell reports*, 9(6), pp. 2124-2138.

Vannucci, S. J., Maher, F. and Simpson, I. A. (1997) 'Glucose transporter proteins in brain: delivery of glucose to neurons and glia', *Glia*, 21(1), pp. 2-21.

Varela, L., Stutz, B., Song, J. E., Kim, J. G., Liu, Z. W., Gao, X. B. and Horvath, T. L. (2021) 'Hunger-promoting AgRP neurons trigger an astrocyte-mediated feed-forward autoactivation loop in mice', *J Clin Invest*, 131(10).

Velloso, L. A., Araújo, E. P. and de Souza, C. T. (2008) 'Diet-induced inflammation of the hypothalamus in obesity', *Neuroimmunomodulation*, 15(3), pp. 189-93.

Verkhratsky, A. and Nedergaard, M. (2014) 'Astroglial cradle in the life of the synapse', *Philosophical transactions of the Royal Society of London. Series B, Biological sciences*, 369(1654), pp. 20130595-20130595.

Verkhratsky, A. and Nedergaard, M. (2016) 'The homeostatic astroglia emerges from evolutionary specialization of neural cells', *Philosophical Transactions of the Royal Society B: Biological Sciences*, 371(1700), pp. 20150428.

Verkhratsky, A. and Nedergaard, M. (2018) 'Physiology of Astroglia', *Physiological reviews,* 98(1), pp. 239-389.

Verkhratsky, A., Rodríguez, J. J. and Parpura, V. (2012) 'Calcium signalling in astroglia', *Mol Cell Endocrinol,* 353(1-2), pp. 45-56.

Verstynen, T. D., Weinstein, A. M., Schneider, W. W., Jakicic, J. M., Rofey, D. L. and Erickson, K. I. (2012) 'Increased body mass index is associated with a global and distributed decrease in white matter microstructural integrity', *Psychosom Med,* 74(7), pp. 682-90.

Virchow, R. (1846) 'Über das granulierte Ansehen der Wandungen der Gerhirnventrikel', *Allg Z Psychiatr,* 3, pp. 242.

Volterra, A. and Meldolesi, J. (2005) 'Astrocytes, from brain glue to communication elements: the revolution continues', *Nature Reviews Neuroscience,* 6(8), pp. 626-640.

Wakefield, J. (2004) 'Fighting obesity through the built environment', *Environmental health perspectives,* 112(11), pp. A616-A618.

Walz, W. (2000) 'Role of astrocytes in the clearance of excess extracellular potassium', *Neurochemistry International,* 36(4), pp. 291-300.

Walz, W. and Lang, M. K. (1998) 'Immunocytochemical evidence for a distinct GFAP-negative subpopulation of astrocytes in the adult rat hippocampus', *Neurosci Lett,* 257(3), pp. 127-30.

Wang, Y., Hsuchou, H., He, Y., Kastin, A. J. and Pan, W. (2015) 'Role of Astrocytes in Leptin Signaling', *Journal of molecular neuroscience : MN,* 56(4), pp. 829-839.

Wanner, I. B., Anderson, M. A., Song, B., Levine, J., Fernandez, A., Gray-Thompson, Z., Ao, Y. and Sofroniew, M. V. (2013) 'Glial scar borders are formed by newly proliferated, elongated astrocytes that interact to corral inflammatory and fibrotic cells via STAT3-dependent mechanisms after spinal cord injury', *J Neurosci,* 33(31), pp. 12870-86.

Ward, M. A., Carlsson, C. M., Trivedi, M. A., Sager, M. A. and Johnson, S. C. (2005) 'The effect of body mass index on global brain volume in middle-aged adults: a cross sectional study', *BMC Neurology,* 5(1), pp. 23.

Wickham, H. (2016) 'ggplot2-Elegant Graphics for Data Analysis. Springer International Publishing', *Cham, Switzerland*.

Wilcox, G. (2005) 'Insulin and insulin resistance', *The Clinical biochemist. Reviews,* 26(2), pp. 19-39.

Williams, S. M., Sullivan, R. K., Scott, H. L., Finkelstein, D. I., Colditz, P. B., Lingwood, B. E., Dodd, P. R. and Pow, D. V. (2005) 'Glial glutamate transporter expression patterns in brains from multiple mammalian species', *Glia,* 49(4), pp. 520-41.

Winchenbach, J., Düking, T., Berghoff, S. A., Stumpf, S. K., Hülsmann, S., Nave, K. A. and Saher, G. (2016) 'Inducible targeting of CNS astrocytes in Aldh1l1-CreERT2 BAC transgenic mice', *F1000Res,* 5, pp. 2934.

Wolf, F. A., Angerer, P. and Theis, F. J. (2018) 'SCANPY: large-scale single-cell gene expression data analysis', *Genome biology,* 19(1), pp. 1-5.

Xia, Y.-p., He, Q.-w., Li, Y.-n., Chen, S.-c., Huang, M., Wang, Y., Gao, Y., Huang, Y., Wang, M.-d., Mao, L. and Hu, B. (2013) 'Recombinant Human Sonic Hedgehog Protein Regulates the Expression of ZO-1 and Occludin by Activating Angiopoietin-1 in Stroke Damage', *PLOS ONE,* 8(7), pp. e68891.

y Cajal, S. R. (1913) *Un nuevo proceder para la impregnación de la neuroglía.*

Yang, L., Qi, Y. and Yang, Y. (2015) 'Astrocytes control food intake by inhibiting AGRP neuron activity via adenosine A1 receptors', *Cell Rep,* 11(5), pp. 798-807.

Yang, Y. and Jackson, R. (2019) 'Astrocyte identity: evolutionary perspectives on astrocyte functions and heterogeneity', *Current opinion in neurobiology,* 56, pp. 40-46.

Yang, Y., Jorstad, N. L., Shiao, C., Cherne, M. K., Khademi, S. B., Montine, K. S., Montine, T. J. and Keene, C. D. (2013) 'Perivascular, but not parenchymal, cerebral engraftment of donor cells after non-myeloablative bone marrow transplantation', *Experimental and molecular pathology,* 95(1), pp. 7-17.

Yaswen, L., Diehl, N., Brennan, M. B. and Hochgeschwender, U. (1999) 'Obesity in the mouse model of pro-opiomelanocortin deficiency responds to peripheral melanocortin', *Nat Med,* 5(9), pp. 1066-70.

Yi, C. X., Gericke, M., Krüger, M., Alkemade, A., Kabra, D. G., Hanske, S., Filosa, J., Pfluger, P., Bingham, N., Woods, S. C., Herman, J., Kalsbeek, A., Baumann, M., Lang, R., Stern, J. E.,

Bechmann, I. and Tschöp, M. H. (2012) 'High calorie diet triggers hypothalamic angiopathy', *Mol Metab,* 1(1-2), pp. 95-100.

Yu, G., Wang, L.-G., Han, Y. and He, Q.-Y. (2012) 'clusterProfiler: an R package for comparing biological themes among gene clusters', *Omics : a journal of integrative biology,* 16(5), pp. 284-287.

Zamanian, J. L., Xu, L., Foo, L. C., Nouri, N., Zhou, L., Giffard, R. G. and Barres, B. A. (2012) 'Genomic analysis of reactive astrogliosis', *J Neurosci,* 32(18), pp. 6391-410.

Zhan, C., Zhou, J., Feng, Q., Zhang, J.-e., Lin, S., Bao, J., Wu, P. and Luo, M. (2013) 'Acute and Long-Term Suppression of Feeding Behavior by POMC Neurons in the Brainstem and Hypothalamus, Respectively', *The Journal of Neuroscience,* 33(8), pp. 3624-3632.

Zhang, X. and van den Pol, A. N. (2016) 'Hypothalamic arcuate nucleus tyrosine hydroxylase neurons play orexigenic role in energy homeostasis', *Nat Neurosci,* 19(10), pp. 1341-7.

Zhang, X., Zhang, G., Zhang, H., Karin, M., Bai, H. and Cai, D. (2008) 'Hypothalamic IKKbeta/NF-kappaB and ER stress link overnutrition to energy imbalance and obesity', *Cell,* 135(1), pp. 61-73.

Zhang, Y. and Barres, B. A. (2010) 'Astrocyte heterogeneity: an underappreciated topic in neurobiology', *Curr Opin Neurobiol,* 20(5), pp. 588-94.

Zhang, Y., Chen, K., Sloan, S. A., Bennett, M. L., Scholze, A. R., O'Keeffe, S., Phatnani, H. P., Guarnieri, P., Caneda, C., Ruderisch, N., Deng, S., Liddelow, S. A., Zhang, C., Daneman, R., Maniatis, T., Barres, B. A. and Wu, J. Q. (2014) 'An RNA-sequencing transcriptome and splicing database of glia, neurons, and vascular cells of the cerebral cortex', *J Neurosci,* 34(36), pp. 11929-47.

Zhang, Y., Proenca, R., Maffei, M., Barone, M., Leopold, L. and Friedman, J. M. (1994) 'Positional cloning of the mouse obese gene and its human homologue', *Nature,* 372(6505), pp. 425-32.

Zhang, Y., Reichel, J. M., Han, C., Zuniga-Hertz, J. P. and Cai, D. (2017) 'Astrocytic Process Plasticity and IKKβ/NF-κB in Central Control of Blood Glucose, Blood Pressure, and Body Weight', *Cell Metab,* 25(5), pp. 1091-1102.e4.

Zhou, Y. D. (2018) 'Glial Regulation of Energy Metabolism', *Adv Exp Med Biol*, 1090, pp. 105-121.

Zhuo, L., Sun, B., Zhang, C. L., Fine, A., Chiu, S. Y. and Messing, A. (1997) 'Live astrocytes visualized by green fluorescent protein in transgenic mice', *Dev Biol*, 187(1), pp. 36-42.

Zorec, R., Araque, A., Carmignoto, G., Haydon, P. G., Verkhratsky, A. and Parpura, V. (2012) 'Astroglial excitability and gliotransmission: an appraisal of Ca2+ as a signalling route', *ASN neuro*, 4(2), pp. e00080.

7. Abbreviations

15d	15 days
3V	Third Ventricle
5d	5 days
ACN	Acetonitrile
ACSA2	Astrocyte Cell Surface Antigen 2
ACTH	Adrenocorticotrophin
Adm	Adrenomedullin
AGC	Automatic Gain Control
Aif1	Allograft inflammatory factor 1
Agrp	Agouti-Related Protein
Aldh1L1	Aldehyde Dehydrogenase 1 Family Member L1
Aldoc	Fructose-bisphosphate aldolase C
ALKO	Astrocyte-specific LepR Knockout
ANLS	Astrocyte-to-Neuron Lactate Shuttle
ApoE	Apolipoprotein E
AQP4	Aquaporin 4
ARC	Arcuate Nucleus of the Hypothalamus
ATP	Adenosine Triphosphate
ATP1B2	ATPase Na^+/K^+ Transporting Subunit Beta 2
Avy	Agouti viable yellow
BAT	Brown Adipose Tissue
BBB	Blood Brain Barrier
BCA	Bicinchoninic Acid
BMI	Body Mass Index
BSA	Bovine Serum Albumin
BW	Body Weight
Ca^{2+}	Calcium ion
CAA	2-Chloroacetamide

CART	Cocaine- and Amphetamine- Regulated Transcript
Ccdc153	Coiled-Coil Domain Containing 153
Cldn5	Claudin 5
Clu	Clusterin
CNS	Central Nervous System
Col1a1	Collagen Type I Alpha 1 Chain
Col23a1	Collagen Type XXIII Alpha 1 Chain
Col3a1	Collagen Type III Alpha 1 Chain
Crym	Crystallin Mu
Csf1r	Colony stimulating factor 1 receptor
CTX	Cortex
Cx30	Connexin 30
Cx3cr1	C-X3-C Motif Chemokine Receptor 1
Cx43	Connexin 43
DAPI	4′,6-diamidino-2-phenylindole
DEGs	Differentially Expressed Genes
DEPs	Differentially Expressed Proteins
Des	Desmin
DMEM	Dulbecco's Modified Eagle Media
DMEM/F12	Dulbecco's Modified Eagle Media/Nutrient Mixture F12
DMH	Dorsomedial Hypothalamus
dNTP	Deoxynucleotide Triphosphate
D-PBS	Dulbecco's Phosphate Buffered Saline
DREADD	Designer Receptors Exclusively Activated by Designer Drugs
ECM	Extracellular Matrix
EDTA	Ethylenediaminetetraacetic Acid
eGFP	Enhanced Green Fluorescent Protein
ER	Endoplasmic Reticulum
ERα	Estrogen Receptor alpha
FACS	Fluorescent-Activated Cell Sorting

FC	Fold Change
FISH	Fluorescence in Situ Hybridization
GABA	Gamma-Aminobutyric Acid
GFAP	Glial Fibrillary Acidic Protein
GFP	Green Fluorescent Protein
Gja1	Gap Junction Protein Alpha 1
Gjb6	Gap Junction Protein Beta 6
GLAST	Glutamate/Aspartate Transporter
GLT-1	Glutamate transporter 1
GLUT	Glucose Transporter
GLUT-1	Glucose Transporter 1
GLUT-2	Glucose Transporter 2
GO	Gene Ontology
GPCR	G-Protein Coupled Receptor
GS	Glutamine Synthetase
GWAS	Genome-Wide Association Studies
HCD	Higher-Energy Collisional Dissociation
Hdc	Histidine Decarboxylase
HFHS	High-Fat High-Sugar
hGFAP	Human Glial Fibrillary Acidic Protein
HIPPO	Hippocampus
HPLC	High Performance Liquid Chromatography
HPT	Hypothalamus
HRP	Horseradish peroxidase
Icv	Intracerebroventricular
Ift43	Intraflagellar Transport 43
IgG	Immunoglobulin G
IHC	Immunohistochemistry
IKK	IkB Kinase
IL	Interleukin

i.p.	Intraperitoneal
IP_3	Inositol Triphosphate
IP_3R2	Inositol Triphosphate type 2 Receptor
IR	Insulin Receptor
Itgam	Integrin Subunit Alpha M
IVC	Individually Ventilated Cages
JNK	c-Jun N-terminal Kinase
Kir4.1	Inwardly rectifying potassium 4.1 channel
Kiss1	Kisspeptin
kNN	k-Nearest Neighbor
KO	Knockout
LC	Locus Coeruleus
LepR	Leptin Receptor
LH	Lateral Hypothalamus
Lhx2	LIM Homeobox 2
LPL	Lipoprotein Lipase
Lum	Lumican
MACS	Magnetic-Activated Cell Sorting
Mag	Myelin Associated Glycoprotein
MBH	Medio-Basal Hypothalamus
MC	Melanocortin
MC3R	Melanocortin Receptor 3
MC4R	Melanocortin Receptor 4
MCR	Melanocortin Receptor
MCT1	Monocarboxylate Transporter 1
ME	Median Eminence
mG	Cell membrane localized eGFP
$MgCl_2$	Magnesium Chloride
Mog	Myelin Oligodendrocyte Glycoprotein
MRI	Magnetic Resonance Imaging

MS	Mass Spectrometry
MSH	γ-Melanocyte Stimulating Hormone
Mustn1	Musculoskeletal, Embryonic Nuclear Protein 1
NaCl	Sodium Chloride
Na_2HPO_4	Sodium Phosphate Dibasic
NaH_2PO_4	Sodium Phosphate Monobasic
NaOH	Sodium Hydroxide
NF-kB	Nuclear Factor-kB
NG2	Neuron Glial 2
NPY	Neuropeptide Y
NS	Not Significant
NTS	Nucleus Tractus Solitarius
Olig1	Oligodendrocyte Transcription Factor 1
P2ry12	Purinergic Receptor P2Y12
PBS	Phosphate Buffered Saline
PC	Principal Component
PCA	Principal Component Analysis
PCR	Polymerase Chain Reaction
Pcsk1n	Proprotein Convertase Subtilisin/Kexin Type 1 Inhibitor
Pdgfrb	Platelet Derived Growth Factor Receptor Beta
Pecam1	Platelet and Endothelial Cell Adhesion Molecule 1
PFA	Paraformaldehyde
PLC	Phospholipase C
PMSF	Phenylmethylsulfonyl Fluoride
POMC	Pro-Opiomelanocortin
pSTAT3	Phosphorylated Signal Transducer and Activator of Transcription 3
Ptc	Patched
PVN	Paraventricular Nucleus of the Hypothalamus
QC	Quality Control
Rarres2	Retinoic Acid Receptor Responder 2

Rax	Retina and Anterior Neural Fold Homeobox
Rbfox3	RNA Binding Fox-1 Homolog 3
RIPA	Radio-Immunoprecipitation Assay
RN	Raphe Nucleus
RNA-seq	RNA sequencing
ROI	Region of Interest
ROS	Reactive Oxygen Species
RT	Room Temperature
RTL	RNA Lysis Buffer
S100β	S100 calcium binding protein beta
SC	Standard Chow
scRNA-Seq	Single cell RNA sequencing
SDB-RPS	Styrenedivinylbenzene–Reversed Phase Sulfonated
SDC	Sodium Deoxycholate
SEM	Standard Error of the Mean
SFO	Subfornical Organ
Shh	Sonic hedgehog
Slc16a2	Solute Carrier Family 16 Member 2
Slc1a2	Solute Carrier Family 1 Member 2
Slc1a3	Solute Carrier Family 1 Member 3
Slco1c1	Solute Carrier Organic Anion Transporter Family Member 1 C1
Smo	Smoothened
Snap25	Synaptosome Associated Protein 25
SNARE	Soluble NSF Attachment Protein Receptor
SNP	Single Nucleotide Polymorphism
SOCS-3	Suppressor of Cytokine Signaling 3
SOX9	SRY-Box Transcription Factor 9
Syp	Synaptophysin
Syt1	Synaptotagmin 1
TBS	Tris-Buffered Saline

TCEP	Tris (2-carboxyethyl) phosphine hydrochloride
TFA	Trifluoroacetic Acid
TH	Tyrosine Hydroxylase
TLR	Toll-Like Receptor
TLR4	Toll-Like Receptor 4
Tm4sf1	Transmembrane 4 L Six Family Member 1
Tmem119	Transmembrane Protein 119
TRAP	Translating Ribosome Affinity Purification
Tubb3	Tubulin Beta 3 Class III
Ucp2	Uncoupling Protein 2
UMAP	Uniform Manifold Approximation and Projection
UMI	Unique Molecular Identifier
Vamp5	Vesicle Associated Membrane Protein 5
VGluT2	Glutamate Vesicular Transporter 2
VLMCs	Vascular and Leptomeningeal Cells
VMH	Ventromedial Hypothalamic Nucleus
WHO	World Health Organization
WT	Wildtype
w/v	Weight per Volume
Y1R	Neuropeptide Y Receptor type 1

8. List of figures

9. List of tables

10. Acknowledgments

Being a PhD student has been a great adventure, which would not have been possible without the help of amazing people.

First of all, I would like to truly thank Cristina, who gave me the opportunity to join an incredible group of people, and an exceptional research environment. Her positive, energetic, understanding, and brilliant attitude was an inspiration to me, and gave me the motivation to pursue my objectives and to never give up. Her lead and supervision were crucial for the successful completion of my project. Thank you, Cristina!!!

I would like to extend my gratitude to Prof. Pfluger and to Dr. Krumsiek, as my thesis advisors, who followed my project progress from the beginning, sharing important feedbacks and advices, which helped me in the construction of the thesis.

I am very grateful to Dominik as well, who advised me with the bioinformatics-related part of my thesis, and who was always available to discuss mistakes and next steps. His help was crucial to generate high-level data.

An enormous and heartfelt thanks to all the former and current members of the Astrocyte-Neuron Networks group is imperative. Since the very beginning (when I looked like a baby bird out of place) until the end (when this bird became able to fly), I was never left alone. In the "Astro" group, it is always possible to find a hand to help you with experiments, a brain for finding solutions together, an eye for supervising difficult procedures, a shoulder to cry on in hard moments, and a smile to celebrate your successes with you.
Between these people, I need to thank in a special way Viktorian, whose collaboration was essential for this project, and who shared a lot of time with me, patiently listening to my crazy ideas and accepting my perfectionist needs. Beata, who taught me the majority of things I currently know, and who always found the time to help me, often sacrificing her own. With her incredible technical skills and with her sincerity, she taught me not only how to pursue the excellence and satisfaction in the professional life, but also how to become a better person. Isma and Cahuê, always available to help me, to give me feedbacks, and to support me through my PhD journey. I will never forget our fruitful lunch breaks! Cassie, who often acted as my second hand, and gave me the strength to continue my PhD project. The difficult situations became

less tough thanks to her joyful nature! Ophélia, whose good heart, intelligence, and patience were important for me to move on when I felt stuck. Tim, who has always encouraged me to become a better version of myself. Last but not least, Nicole, Clarita, Elisa, Melanie, Franzi, Yan, Elena, Alex, each of them played an important role in my PhD adventure.

Furthermore, I would like to thank all the people who had a role in the completion of my PhD project, by helping with experiments or giving important advices. In particular, Dr. Krahmer, Dr. Sterr, Dr. Saher, Prof. Lickert, Dr. Müller, Dr. Ussar, Prof. Tschöp, Dr. Walzthoeni, Dr. De Rosa, M.D. Doege, and Kunze.

A special thanks to all IDO people, with who I shared not only the floor, lab, and office, but also instructive seminars and good moments!

Moreover, I would like to express my gratitude to my mom and Luigi, who always had my back and supported me with my studies. Without them, I would have never started this German adventure, and I would have never been the person I currently am. Another person who pushed me to start my PhD journey is my little sister Elena, for who I have always tried to be a good example to follow.

And finally, I need to thank my lovely husband, who stayed at my side during this complicate period, always supporting me and dealing with my ups and downs with extreme patience and understanding.

Thank you all.